AFM-Raman/TERS

Real-time and Direct Correlative Nanoscopy

HORIBA Scientific

Introduction to AFM-Raman/TERS

Raman and AFM (Atomic Force Microscope) analysis can be combined on a single microscope system, opening interesting new capabilities.

What is co-localized AFM-Raman?

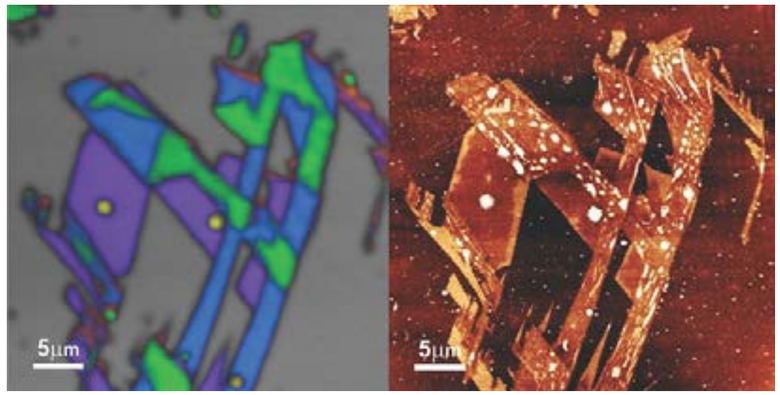

Raman and AFM (Atomic Force Microscope) analysis can be combined on a single microscope system, opening interesting new capabilities and providing enhanced information on a sample's composition and structure by collecting physical and chemical information on the same sample area. Co-localized AFM-Raman measurement is the sequential or simultaneous acquisition of overlapped SPM (Scanning Probe Microscope) and Raman maps with pixel-to-pixel correspondence in the images.

On one hand, AFM and other SPM techniques like STM, Shear-Force, or Normal-Force, provide topographic, mechanical, thermal, electrical, and magnetic properties down to the molecular resolution (~ nm, over µm^2 area), on the other hand, confocal Raman spectroscopy and imaging provides specific chemical information about the material, with diffraction-limited spatial resolution (sub-micron).

What is Tip Enhanced Raman Spectroscopy?

Tip Enhanced Raman Spectroscopy (TERS) brings Raman spectroscopy into nanoscale resolution imaging. TERS is a super-resolution chemical technique. Better yet, it is a label-free super-resolution imaging technique that has been extended by our novel technology into an important new imaging technology.

TERS imaging is performed with an AFM-Raman system, where a Scanning Probe Microscope (SPM that can be used in atomic force, scanning tunneling, or normal/shear force mode) is integrated with a confocal Raman spectrometer through an optomechanical coupling. The scanning probe microscope allows for nanoscale imaging, the optical coupling brings the excitation laser to the functionalized tip (or probe), and the spectrometer analyzes the Raman (or otherwise scattered) light providing a hyperspectral image with nanometer-scale chemical contrast.

A TERS system is based on a metallic tip (generally made of gold or silver) employed to concentrate the incident light field at the apex.

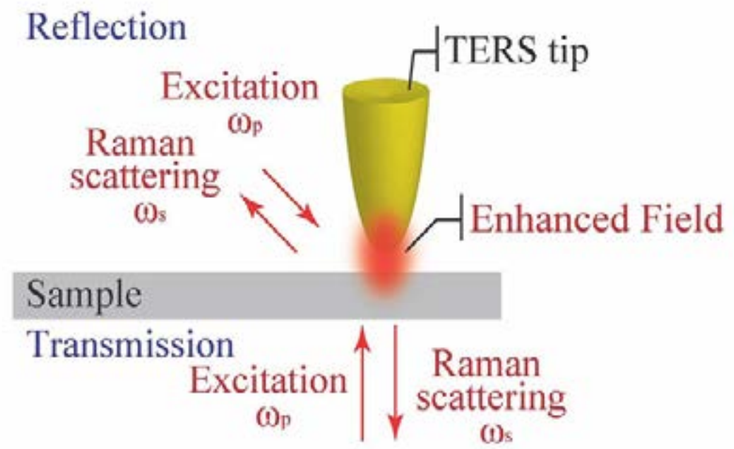

The transmission configuration allows the use of the highest numerical aperture (NA) objectives, but can only be used for transparent samples. The reflection configuration can be used for any kind of sample (opaque and transparent) but is limited to lower NA objectives.

The tip acts as a nano-source of light and local field enhancer, greatly improving the Raman sensitivity (by a factor of 103 -107) and reducing the probed volume to the “nano” region immediately below the tip. The optical coupling that combines the two instruments uses a confocal scheme. Two different configurations exist for this coupling: One in transmission and one in reflection, having their own advantages and drawbacks.

The transmission configuration allows the use of the highest numerical aperture (NA) objectives (including immersion objectives) giving high power density at the focus point and enabling the collection of high signal levels, but it can only be used for transparent samples. The reflection configuration can be used for any kind of sample (opaque and transparent) but is limited to lower NA objectives. By combining point-by-point scanning with simultaneous spectrum acquisition, near-field Raman mappings can be performed with lateral resolution down to ten nanometers or less.

Computers will act and perform a lot differently by 2032.

Understanding two-dimensional material interfaces with AFM-Raman/TERS will transform computing

Computers will act and perform a lot differently by 2032. Those differences will revolutionize the efficiency, size, and speed of these devices. Getting there is a long road.

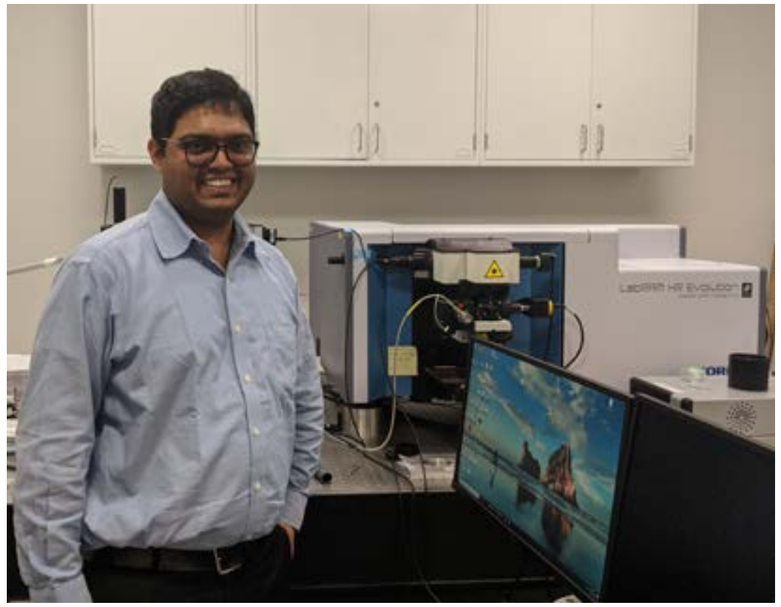

Prof. Deep Jariwala with a HORIBA LabRAM HR Evolution Raman microscope with TERS

Deep Jariwala, Ph.D., is an Assistant Professor of Electrical and Systems Engineering at the University of Pennsylvania's Device Research and Engineering Laboratory. The lab focuses on the study, design, and development of nanometer and atomic-scale devices, materials, and interfaces for applications in computing, sensing, information technology, and renewable energy.

His role has evolved over the years.

"I'm a materials engineer by training and then I have slowly ventured into applied physics and then electrical engineering and device research," he said. "I'm materials agnostic. So, I like to investigate any and all interesting nanoscale materials that appear on the research horizon."

Much of these nanoscale materials have features embedded within them or are themselves of dimensions that are just one to a few hundred nanometers. So, investigating the local, atomic structure, electronic structure, optical properties, and vibrational structure, is quite interesting to him. And these materials are important for our devices as well.

It is fairly well known at this point that Atomic Force Microscopy with Tip Enhanced Raman Scattering (AFM-Raman/TERS) is the easiest and most versatile technique that allows us to visualize nanoscale structures in a few minutes.

It's even more powerful than electron microscopy in some respect, especially if you're trying to image something on a surface. AFM-Raman/TERS has also evolved to a point that it can help visualize local optical properties. We tend to use a combination of all these techniques to integrate all kinds of nanomaterials, starting from quantum dots, which are polarly synthesized to carbon nanotubes to two-dimensional materials.

"One area of research where we use AFM-Raman/TERS heavily is the investigation of two-dimensional materials and its heterojunctions within them," he said. "One of the reasons we want to investigate that is two-dimensional materials are extremely promising. They are poised to be the semiconductors of the future that drive our microelectronics and various other things."

But one of the challenges with these materials is that, because it is so thin, it has many inhomogeneities in it from time to time. There could be defects in certain regions, which are oxidized or come from other defects. Looking at those regions, which are nanoscale in their dimensions is quite important. Defects in particular have different optical properties, and also have different vibrational properties. And so, if you were to use TERS or tip enhanced photoluminescence (PL) to probe these materials, it becomes visible.

NEXT »

Understanding two-dimensional material interfaces with AFM-Raman/TERS will transform computing, cont.

"You would be able to see how spatially localized or delocalized the defects are. What is the density of defects? You can also do other interesting things like you can make interfaces of these semiconductors with metal, and probe how good these interfaces are. As many of us know in modern semiconductor microelectronics, the interface between the metal and the semiconductor is one of the hardest to optimize and is the source of most losses. This interface has yet not been optimized for two-dimensional semiconductors. And so, by using Tip Enhanced Raman Scattering, we can look at how good these interfaces are that you're forming and what are the ways you can understand the defects or other deformations to make these interfaces better."

How does knowing these defects advance the materials characterization?

"Because we are dealing with semiconductor materials, it is important that semiconductors are produced at the highest quality and purity. That's because they need to perform at a very high level when they are inserted into devices. So, quantifying the defect structure both visually, as well as in terms of numbers, is quite important. When you are making devices out of these semiconductors or materials, or when you are growing them and then evaluating them after growth, having this kind of characterization tool lets you rapidly evaluate at the nanoscale what the defect types, properties, and densities are. And Tip Enhanced Raman Scattering and AFM-Raman are some of the most powerful techniques in that regard."

How does this bridge technology into applied engineering?

There are a few ways. ***Semiconductors made from two-dimensional materials are being looked at by various industries, including the biggest semiconductor companies as a potential replacement for silicon. If we want to replace silicon with some of these emerging materials, we want to understand everything about it and need standard characterization routes for it, too.***

"This is where these semiconductors are extremely powerful, and I don't think they will just impact the semiconductor industry or the mainstream semiconductor electronics industry. The two-dimensional material's optical properties are so fascinating that they will also impact electronics industries, such as, for example, displays or LEDs, lasers and optical modulators, telecom, and things like that. So, in all of these places understanding the material, property, understanding its interfaces with other materials is very, very important. And, this is where these characterization techniques are paramount in understanding the fundamental nature of these materials and their structure."

What beneficial optical and electrical properties do two-dimensional materials possess?

"The optical properties are mainly their ability to luminesce. When you shine light on these semiconductors, they absorb some of the light and then fluoresce or send out light again. This can also be done in a different way, where if you send in electrons and emit light, this is the principle of LEDs as we know it...or light-emitting diodes. And so many of these two-dimensional materials that we're investigating, emit light very efficiently, which means that you could use them for a display or lasers. The other interesting thing about them is that because they are so thin, it is also easy to modulate their optical properties, which means you can change the amount of light going through them as a function of some electric field that you can apply to them."

This has potentially transformative applications for optical modulation, which is the basis of light-based communication, which is also the basis of our internet and all our communication technology.

Those are the interesting optical properties on the electronic property side. The ability to modulate current flow in these semiconductors as a function of electric field allows you to do electrical switching. And that is the basis of all of computing.

"These are the two central properties, on the optical side, on the electronic side that makes these semiconductors so exciting for the future," Jariwala said.

With all this innovation, where are we going to be in 10 years, 2032, when it comes to 2D materials?

"I would say that I was not very optimistic about (two-dimensional materials) just a couple of years ago, because of the pandemic effects, but I was also slowly believing that people will keep making silicon just better and better. I didn't think these materials would ever have the potential to replace silicon."

« *PREVIOUS*

NEXT »

Understanding two-dimensional material interfaces with AFM-Raman/TERS will transform computing, cont.

“But what has happened in the past two to three years is people have really figured out ways to grow these materials over large areas or wafers with very high quality. And at the same time, people like myself and others have also figured out a way to make devices out of them that are really good, even beating some of the silicon devices.”

Now many companies, including some of the biggest semiconductor chipmakers, are seriously thinking about two-dimensional materials as a next-generation semiconductor, either for doing the computational logic or for storing data, such as memory applications. He predicts it might happen in about eight to 10 years from now.

“There are research pipelines or development programs, and we are starting several pilot projects. If successful, these companies will launch research projects worth multi-hundreds of millions of dollars to drive these materials and devices towards commercial technology.”

So, things are looking more and more promising now, and Jariwala has been interacting closely with some of the biggest semiconductor groups in this regard.

What does that mean? He predicts that by 2032, we can expect to see the beginnings of nanotechnology computing. Although, one could say that computing already reached the nanoscale years before 2010, with all of the transistors nanoscopic in dimensions.

« *PREVIOUS*

“I think the key question to ask is when would bottom-up grown nanomaterials actually enter computing hardware? And I think the answer to that is yes, I think in 10 years, in one or the other layer in the microprocessor, some of these bottom-up grown nanoscale materials would have been added as functional units in computing hardware.” That would add essential properties to the microprocessor or storage medium – efficiency and speed.

“You know, it's a trillion-dollar industry, and when things are at those scales, profits, and certainly the turnover in the business, matters the most,” he said. ***“What is driving our computing industry to make better and better chips now is the energy efficiency in computing and the speed. These are the two most important things.”***

“Energy efficiency has become a huge problem because we are making so many tiny devices, all crammed onto a single chip. So, energy efficiency is the key thing, and once energy efficiency kicks in, to some extent, speed also is sort of related. Efficiency helps out with some of the speed too since it reduces heating up of the components.’

The push behind this research, besides energy efficiency and speed, is size, and the drive to make smaller devices. Two-dimensional materials can be so well tuned with an electrostatic field that we can keep shrinking the dimensions while not driving up energy consumption.

With silicon, as manufacturers are designing devices shorter and shorter, it is also leading to more steady-state energy consumption, which means the processors heat up a lot more. In other words, **a metric that is important is how many numbers of computations you can do per Joule of energy or per watt of power.**

“This number has flattened out with silicon, and we *somehow need to get this number up again. And that is only possible if at an individual device level, you drive down the power consumed per computation, and that is possible when you shrink these devices further and make them even thinner, which is what you naturally get from two-dimensional semiconductors.”*

Research occupies almost 70 percent of Jariwala’s time at the University of Pennsylvania. He uses a HORIBA LabRAM HR Evolution with an attached TERS microscope, along with a variety of lasers to hit the TERS system to investigate his samples.

“We have a 633-nanometer laser and a 785-nanometer laser, both of which can do TERS. We are hoping to add one more laser to the system. It's been working very nicely for us, and we have been publishing some really good papers using the system. So, we are very happy about it overall.”

These tools, along with the ingenuity to apply the results into tangible technologies, will undoubtedly contribute to the next generation of computing.

"You have a nanoscopic chemical eye that can tell you where the stuff is and what it is."

Researcher developing (non) linear nano-optical methods to characterize heterogenous interfaces

The Great Barrier Reef covers 133,000 square miles off the coast of Queensland, Australia, in the Coral Sea. It is the largest living structure in the world, formed by tiny creatures called polyps, with nearly endless heterogeneous peaks, dips, micro basins, and other rich topological features.

Patrick El-Khoury
Senior Research Scientist
Pacific Northwest National Laboratory

Now, take that and shrink it down to 10 nanometers. For reference, a square mile equals 2.59 x 1024 square nanometers. That's what life looks like to Patrick El-Khoury, Ph.D, a senior research scientist at Pacific Northwest National Laboratory in Richland, Washington.

El-Khoury spends his time examining heterogeneous interfaces on the nanoscale, where chemical, physical, and biological properties change over tiny length scales.

His job is to conduct basic chemical physics research on heterogeneous interfaces encountered in the chemical, biological, and energy sciences. To do that, he predominantly uses Tip Enhanced Raman Spectroscopy (TERS), which allows him to see and identify (bio) molecular and (bio) material systems with few-nanometer precision. He also adapts and actively develops novel nano-imaging and nano-spectroscopy approaches that can be used to visualize matter over the length (nanometers) and time scales (femtoseconds) of relevance to chemical transformations.

"You look at these nano-basins, or local environments, and they each feature unique physical and chemical properties," he said. "It makes the local properties of nearby (bio) molecular systems even more complex than they naturally are."

El-Khoury sees heterogeneity to be the rule rather than the exception. The properties of most realistic interfaces encountered in biology, chemistry, and materials sciences vary over the nanoscale. This is a far cry from the idealized systems that are described in textbooks. Embracing and understanding this exquisite complexity is a pre-requisite to the development of more efficient functional materials that can be deployed, e.g., in modern photovoltaic and optoelectronic devices.

"We image things with very high spatial resolution, and because we are using different tools of optical spectroscopy, such as Raman scattering, we're also able to identify them. In effect, you have a nanoscopic chemical eye that can tell you where the stuff is, and what it is."

The high spatial resolution that is attainable with the techniques used by El-Khoury necessitates that the signals are nascent from no more than a handful of molecules. In this regime of ultrasensitive optical spectroscopy, the rules of the game are different.

"Part of our work involves using well-known molecules to characterize the complex local environments in which they reside. In TERS, this means looking at different properties of nano-localized optical fields with ultrahigh spatial resolution. This requires a detailed fundamental understanding of the operative physics in TERS."

Biology and energy researchers are often interested in processes taking place at solid/liquid interfaces. This poses a challenge from the measurement science perspective, since chemical visualization of such interfaces under ambient laboratory conditions is not trivial with existing technologies.

NEXT »

Researcher developing (non) linear nano-optical methods to characterize heterogenous interfaces, cont.

“You have methods that yield nanometer spatial resolution with no chemical information. You also have methods that have been developed for about a century now that give you ample chemical information and selectivity, but that lack the required spatial resolution. This is particularly true when the goal is to visualize biological and energy processes as they happen, or in situ / in operando.”

Though there is tremendous value in conducting fundamental research in controlled environments – after all, that’s where much of our knowledge of physics has stemmed from, at some point, this idealized knowledge doesn't transfer over to real life because of the above-mentioned nanoscale heterogeneity, particularly at solid-liquid interfaces.

“The best example I can give you is that of a catalyst,” he said. “You have a catalytic surface that operates at a certain efficiency. The question then becomes why isn’t it 100 percent efficient? Answering that question requires finding and characterizing the so-called active sites and comparing them to inactive catalytic sites, which are generally much more prevalent in a device. Do active sites feature unique properties compared to the rest of the surface? Do successful catalytic conversion events occur at topographically distinct sites? Is the unique topography accompanied by unique physical (e.g. electric fields) and chemical (e.g. oxidation states) properties? These are the kinds of questions that need to be asked. Answering these questions with an eye on the nanoscale requires multimodal nano-topographic and nano-chemical characterization tools, such as TERS.“

« *PREVIOUS*

That, he describes, is seeing something that’s (in)efficient, like a solar cell, zooming in and trying to ask the basic question of why it is or isn’t it working at specific sites. The fundamental chemical physics studies that he performs are meant to inform device makers that, for example, have trouble with local oxidation sites in particular devices.

El-Khoury also explained how he is constantly deploying and developing novel nano-spectroscopic tools by combining different optical spectroscopy methods with tools of nano-optics.

“The Raman-based approach can be generalized if you have an optical setup that is flexible– and enough lasers, of course. At this point, we successfully performed not just nano-Raman, but also nano-PL, nano-extinction, and multimodal nonlinear optical measurements like nano-CARS, nano-SHG/SFG, and nano-TPPL. Some of these are published, others are on the way out.”

El-Khoury ended by stressing that biological/energy science/material science applications of these unique nano-optical technologies are important, but it is equally important to further develop the existing basic understanding of the optical signatures of (bio) molecules and (bio) materials on the nanoscale.

“I’m not the guy that makes wafer-scale devices. But I can probably generate enough useful information about existing and prototypical devices to inform — or just annoy device scientists.”

He also emphasized the importance of not taking anything for granted, e.g., spectroscopic selection rules on the nanoscale. He joked that “rules are meant to be broken” in referring to the differences between conventional/nano-optical measurements that track many/few molecules.

Instrumentation

El-Khoury takes advantage of several HORIBA instruments, including every AFM-optical system offered by the company, the EvoNano. That said, his optical setups are highly customized to enable multimodal linear and nonlinear optical nano-imaging and nano-spectroscopy. The combination of nano-optical measurements that can be performed in a single optical setup that he calls “our own trios” is unique to his PNNL lab. His group also uses the LabRAM HR Evolution for routine micro-Raman and ultra-low frequency Raman measurements. All his setups are described in recent publications from his group.

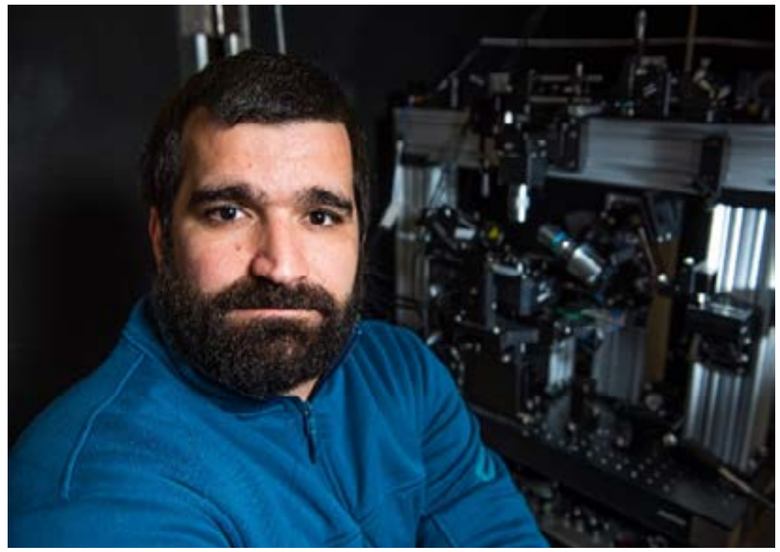

Your next long-distance flight might be on an aircraft made almost entirely of plastic

Nanoscale research and technology leads to advanced materials development

Your next long-distance flight might be on an aircraft made almost entirely of plastic.

Yes, it's true. But before you begin booking your next trip on a train, consider the science that's gone into materials development and the role spectroscopy has played.

Models confirmed by Tip Enhanced Raman Spectroscopy (TERS) and Atomic Force Raman Microscopy (AFM-Raman) explorations helped to confirm key models and hypotheses with innovative research techniques, sophisticated instrumentation, and inventive minds.

Alexei Sokolov, Ph.D, holds a Governor's Chair position at the University of Tennessee and Oak Ridge National Laboratory (ORNL), where he leads the Soft Materials and Membranes group. ORNL is close to Knoxville, Tennessee.

He noted conventional TERS technology can easily investigate a material from the bottom, and this was the direction taken by most groups in the world. But this technology works only if the sample and its substrate are transparent.

"We said, well, for most nanostructures, you usually have a non-transparent substrate like silicon, or some metal substrate, and samples might not be transparent either. So, looking from below will not work, and looking from above, you cannot see what happened under the tip," Sokolov said.

It was a matter of turning the problem on its side.

"The only way to look effectively in this case is to look from the side," he said. "At that time, when we did it in the early 2000s, people were very skeptical because it's very unusual optics. With a normal microscope, you have to look from below or from the top, and we said, 'no, let's look from the side.' We did some simulations and we did some analysis and we demonstrated that, yes, you can work like that. And after that technology started to emerge, companies like HORIBA and others developed the technology. So in that respect, I believe we took a risk, and we got funding from the National Science Foundation for that. We took a risk, we put in our efforts and we demonstrated that, yes, that's a way to go."

NEXT »

Nanoscale research and technology leads to advanced materials development, cont.

Material Heterogeneity

When you look at the materials on the nanoscale level from the side, you can see the chemistry, crystallographic structures, and many other parameters, which Raman and fluorescence spectroscopy can reveal.

He and his team looked at solid electrolyte interfaces (SEI) in Li ion batteries. When you cycle all our batteries, they will form very thin layers of electrochemical reactions on electrodes. This was the key to protect a battery against failure later, because this thin layer stops the electrochemical reaction, and then the battery is stable. Researchers suspected that this SEI is formed from heterogeneous regions with different chemistries, but the size of this heterogeneity was not clear, and no technique could analyze this length scale.

“And that's what we did,” Sokolov said. “With the AFM-Raman experiment, we had to prepare every sample and do all the TERS measurements in a glove box, because once the samples are exposed to air, the SEI layer will be damaged.

These were challenging measurements, but for the first time, researchers demonstrated the SEI heterogeneity with the scale of ~ 20 - 30 nanometers, consisting of different chemistry.”

Why is that important? Well, for one thing, it informs engineers what happens at the electrode-electrolyte interface, and how to design this interface better.

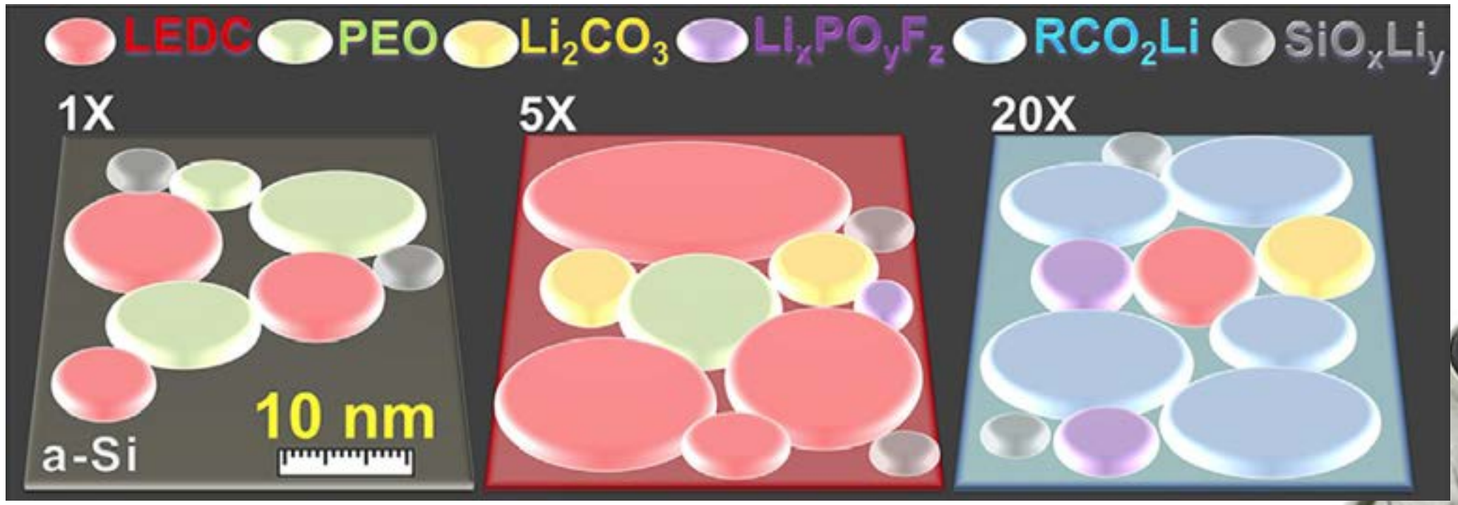

Figure1: Mosaic structure of various chemical compositions in the SEI layer after first, fifth and twentieth charge/discharge cycles. Clear evolution of chemistry and size of heterogeneities was demonstrated.

And that leads to better battery efficiency.

His paper published in 2019 clearly revealed heterogeneous chemistry in SEI layer with characteristic size ~10-30 nm. “Earlier researchers have seen mixtures of different chemistries in the SEI. And the suspicion was from the beginning that it's not a homogeneous mixture for these chemistries. There will be one chemistry here, another chemistry there, but there was no experimental technique that could resolve this nanoscale heterogeneity. Using TERS enabled us to reveal this heterogeneity and to estimate its characteristic length scale.”

This example demonstrates the power of AFM-Raman/TERS technology in analysis of chemistry in a tiny location, and in nanoscale heterogeneity in this chemistry.

« PREVIOUS

NEXT »

Nanoscale research and technology leads to advanced materials development, cont.

Battery Design

How does the knowledge of that heterogeneity extend to better design? His group didn't go in that direction. His arena was basic research, and he achieved that mission.

"As you know, in the United States, to do science you need funding. So, because I don't have specific funding for these kinds of research, we did not go any further, except that we analyzed some silicon-based electrodes also, when we discovered some totally new kinds of chemistry, which people did not expect existed. But with this particular SEI layer analysis, we just demonstrated that we can do it. The next logical step would be to use different electrolytes and analyze these to show how layers are formed, or what is formed by using different electrolytes."

And that will help to develop better batteries in the sense that makers can focus on forming most efficient SEI layers. If they know how this layer is formed and what this layer is, it will inform design.

In fact, researchers in Sokolov's group are working on electrolytes and developing solid state batteries. There's been a good amount of success in this endeavor. Sokolov believes that we will soon have commercial solid state batteries. Prototypes already exists. He says it will store twice more energy per kilogram, meaning that your electrical car can two times longer per single charge.

And this is very timely development for Tennessee, because the electric Ford F150 Lightning will be produced here, in addition to the already existing Volkswagen. Also Microvast is looking to build a "Giga-factory" not far from Knoxville.

What's the significance of a solid state battery? It's different than conventional batteries because it doesn't have liquids. Instead, it features solid electrolytes. All these liquid electrolytes are flammable, toxic and can leak, leading to many safety concerns with conventional batteries. Replacing liquid electrolytes with solid electrolytes will provide a much safer battery with higher energy density.

Nanocomposite Materials

Sokolov also uses AFM-Raman also to analyze nanostructures and heterogeneity in nano-composite materials. "We use a lot of plastics polymers and to make them strong we usually put some nanoparticles in them. You want to see how all these particles are arranged and how they change properties of the polymeric materials around them. And they usually change properties only on a scale of a few nanometers. And that's what we are also trying to analyze," Sokolov said.

"For long time, there was a discussion that this interfacial layer propagates for one hundred nanometers, or even more, into the polymer matrix. Our studies clearly demonstrate that this interfacial layer is only a few nanometers thick."

« *PREVIOUS*

NEXT »

Nanoscale research and technology leads to advanced materials development, cont.

These nanocomposite materials surround us in everyday life, starting with car tires and many interior and exterior parts. “We are working now, for example, on doing carbon fiber reinforced plastics. And we are trying to make them also recyclable to minimize the effect of the planet pollution by plastics.“ Adding nanoparticles to a polymer strongly improves its mechanical properties. They become comparable to traditional metal strength while significantly reducing the weight.

A good example is the Boeing 787 Dreamliner. Eighty percent of it by volume is constructed with nanocomposite plastics. The wings and body of this airplane are plastic and much lighter than if they will be done using should be much lighter than if it was made using aluminum, but are as strong as aluminum alloys. That means the airplane is much lighter. It consumes less fuel, a significant cost savings. And it will travel farther, and carry more cargo and passengers.

Wind turbines serve as another example of nanocomposite polymers. If the blades of the turbines were made of metal, they would be much heavier, and less efficient in producing electricity. Blades made of plastic reinforced with nanomaterials are lighter and produce energy more efficiently. It adds strength to the blades.

“For nanocomposites, we now know well how to predict what will happen with materials properties when I put particular nano-fillers in a particular polymer,” Sokolov said.

Figure 2: “Plastic airplane” Boeing 787 Dreamliner

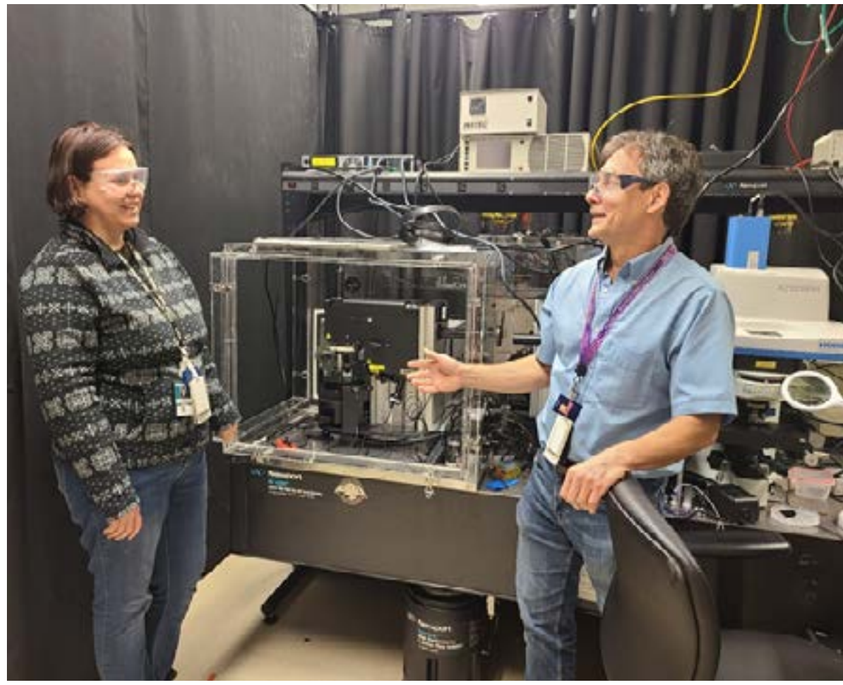

Figure 3: Dr. Bocharova (left) and Dr. Sokolov (right) discussing the next TERS experiments in front of the AFM-Raman system from HORIBA.

« PREVIOUS

Scientific Papers

This 2016 study was the first time TERS was used to image transition-metal dicalgogenides (TMDs).

Improving resolution in quantum subnanometre-gap tip enhanced Raman nanoimaging

Yingchao Zhang, Dmitri V.Voronine, Shangran Qiu, Alexander M. Sinyukov, MaryHamilton, Zachary Liege, Alexei V. Sokolov, Zhenrong Zhang & Marlan O.Scully. May 25, 2016.

This 2016 study was the first time TERS was used to image transition-metal dicalgogenides (TMDs). This broadly explored class of two-dimensional semiconductors is like a sandwich. A layer of transition-metal atoms separates two layers of chalcogen atoms, like sulfur, selenium or tellurium, forming an atomically thin semiconductor sheet.

The beauty of these two-dimensional semiconductors to the research community is that the optical band gap is within the visible range and near IR; this imparts a huge number of fascinating electronic properties. The band gap defines the energy of a light photon that can be absorbed by the sheet to generate a charge separation, which creates mobile electrons and holes in the structure.

These materials can absorb energy, and that energy can then be transferred by some other means to other parts of the sheet, which is exactly what you want in an electronic device — e.g., something that's absorbing energy from sunlight, transferring that energy to a reactive site where hydrogen gas can be released from water.

These materials present a new physics, depending on the particular atoms which are in the layers. The electronic properties can be tuned so that this band gap is wider or narrower. That is exactly what you do with silicon when you're doping it in a semiconductor to control the properties of the materials that will form transistors and other electronic devices in an integrated circuit.

These materials are not yet used in electronics, but people are starting to investigate how these would be incorporated; their useful properties and can be precisely tuned in a variety of ways.

These materials feature the optical properties of the materials. These are governed by so-called excitons. Excitons are a coupled electron and hole; unlike in standard semiconductors, they are bound together as a quasi-particle instead of moving independently. In prior years, generating these sorts of quasi-particles was extremely difficult; researchers had to create complicated and expensive superlattices and operate at liquid helium temperatures, because of the two-dimensional nature of those materials.

These new materials are stable at room temperature. The energy that holds this together is huge compared to the energy of the lattice vibrations at room temperature. These materials demonstrate the physical phenomena that are only accessible to researchers with TERS and AFM Raman, which see materials at the nanoscale.

In addition, these materials can be synthesized side-by-side when you have two adjacent materials within the same layer, with different band gaps. In effect, you can form atomically sharp N or P junctions. And, if you stack these vertically and twist it a tiny bit, then other electronic structures are formed, with their own peculiar properties, e.g., creating materials with superconducting properties at low temperatures.

For optical spectroscopy, confocal Raman microscopy is limited by physical optics, operating in the far-field optical regime. A lens cannot create a spot of light that's smaller than about half the wavelength of that light. So we're limited in resolution to about a half of a micron.

Tip Enhanced Raman Spectroscopy extends what you can see to the nanometer scale, or by a factor of a couple of hundred times better in lateral resolution than you can get with far-field optics. Tip Enhanced Raman Spectroscopy illuminates such a much smaller volume as it operates in what’s called the near-field optical regime. A wealth of new physics is being exposed through the properties of these two-dimensional materials. In the future when we look back, the first part of the 21st century will have been dominated by the elucidation and application of the physics of such two-dimensional materials. It’s a real revolution.

Scientific Papers

When we have graphene sandwiched between the tip and the plasmonic substrate, the electric field is perpendicular to the plane of the material...

Tip Enhanced Raman Scattering from nanopatterned graphene and graphene oxide

Ashish Bhattarai, Andrey Krayev, Alexey Temiryazev, Dmitry Evplov, Kevin T. Crampton, Wayne P. Hess, and Patrick Z. El-Khoury. 2018.

This was an attempt to understand the specifics of a TERS response in a material that has been thoroughly investigated using conventional Raman spectroscopy and microscopy. In enhanced Raman scattering, the selection rules for Raman bands are not the same as the selection rules for conventional Raman.

When we have graphene sandwiched between the tip and the plasmonic substrate, the electric field is perpendicular to the plane of the material, so it doesn't couple to the in-plane vibrations, but if we make a wrinkle, then we have a significant projection of this in-plane vibration to the optical electric field in the gap between the tip and the substrate. Thus energy can be absorbed and the signal goes up.

Understanding or beginning to understand the TERS response in materials that have been already thoroughly investigated using conventional Raman spectroscopy and microscopy, and building up the knowledge lays the foundation for interpretation of the new data that we are now obtaining on two-dimensional materials.

Scientific Papers

Preparing samples for the gap mode operation has always been tricky...

Transfer of van der Waals crystals to noble-metal surfaces to enable characterization of buried interfaces

Andrey Krayev, Connor S. Bailey, Kiyoung Jo, Shuo Wang, Akshay Singh, Thomas Darlington, Gang-Yu Liu, Silvija Gradecak, P. James Schuck, Eric Pop, and Deep Jariwala. 2019.

When a thin sample is sandwiched between a plasmonic substrate and the TERS tip, and you excite the tip, you create a significant dipole moment in the tip. There is an electrostatic reflection of this dipole in this plasmonic substrate. As a result, you have optical electric fields strongly concentrated in the gap between the tip and the substrate.

When both the scattered and incoming fields are enhanced equally, the Raman signal is proportional to the fourth power of the electric field. So, if you manage to increase the electric field 10 times, then your Raman signal will be enhanced 10,000 times. When measuring Raman photons from such small volumes of material, this “gap mode” enhancement is important.

Preparing samples for the gap mode operation has always been tricky because most of the time you cannot easily grow high-quality transition-metal dichalcogenides on gold. The standard procedure is to grow the TMDs on silicon dioxide substrates, overcoat it with a polymer, then dissolve the silicon dioxide layer (which often damages the TMD layer) and then transfer to a gold surface and finally remove the polymer layer. It’s an extremely dirty, tedious, and invasive procedure.

The idea for a better method of transfer, presented here, came from knowledge of the strong affinity of gold to chalcogen atoms, whether it's sulfur or selenium. You can just coat with gold, without any adhesive layers, then apply a transfer layer of epoxy. After the epoxy is cured, you simply strip the crystals from the growth substrate. The exposed surface is a replica of the extremely well-polished silicon substrate, yielding a nearly atomically-flat gold surface with the TMD crystals embedded, flush with the gold surface – ideal for Tip Enhanced Raman Scattering characterization in gap mode.

This technique is being heavily used for research purposes. Scientists credit HORIBA as the catalyst for bringing groups of researchers together to investigate this phenomenon. It attracted researchers from MIT, Columbia, Stanford, and the University of California at Davis to HORIBA for this technique.

Scientific Papers

When you apply exfoliated two-dimensional materials to a substrate under ambient conditions, quite often, a small volume of air is trapped...

Imaging strain-localized excitons in nanoscale bubbles of monolayer WSe2 at room temperature

Thomas P. Darlington, Christian Carmesin, Matthias Florian, Emanuil Yanev, Obafunso Ajayi, Jenny Ardelean, Daniel A. Rhodes, Augusto Ghiotto, Andrey Krayev, Kenji Watanabe,Takashi Taniguchi, Jeffrey W. Kysar, Abhay N. Pasupathy, James C. Hone, Frank Jahnke, Nicholas J. Borys and P. James Schuck. 2020.

The breakthrough in this research was to acquire measurements where nanobubbles were present. Although theoretical models existed from which to derive results, no direct measurements had been achieved.

When you apply exfoliated two-dimensional materials to a substrate under ambient conditions, quite often a small volume of air is trapped between the substrate and this two-dimensional material. Blisters or bubbles form and, because this small volume is compressed in the process, the internal pressure is huge, and the material becomes strongly mechanically strained. This leads to a formation of localized states with unique quantum properties.

There are strong indications that these bubbles can be the source of single-photon emission at cryogenic temperatures, but also there are indications that they may also act as single photon emitters at room temperature.

One of the prospective applications is quantum computing. For entangled photons, which are used in quantum computing, researchers can monitor whether two photons separated by distance are changing. A change applied to one of them will immediately change the other at distance, faster than the speed of light. This is an example of a defect that you would like to engineer, which you certainly cannot see with ordinary spectroscopy or microscopy. And you can only investigate it if you have a nanoscale resolution. To engineer these defects to be the same every time and perfect is impossible without the right instruments to see them. This is absolutely crucial for the development of the next generation of quantum computing instrumentation.

It took a large international team of researchers, catalyzed by HORIBA, to achieve these results. Although the paper was published in 2020, the data was mostly collected in 2016 and 2017.

The most important point in this paper is the application of HORIBA TERS and tip enhanced photoluminescence (PL), and nanoscale imaging for the characterization of modern quantum materials and quantum defects in two-dimensional materials.

Transmission electron microscopy is also destructive, damaging the sample in the process of analysis.

Nanoscale Raman characterization of a 2D semiconductor lateral heterostructure interface

Sourav Garg, J. Pierce Fix, Andrey V. Krayev, Connor Flanery, Michael Colgrove, Audrey R. Sulkanen, Minyuan Wang, Gang-Yu Liu, Nicholas J. Borys*, and Patrick Kung Dec. 22, 2021.

This was an important study that showed the application of HORIBA's unique nanoscale spectroscopic imaging capabilities to characterize the important class of lateral heterostructures.
In principle, you can strip such heterostructures from the growth substrate, place them on a grid, and investigate them with a transmission electron microscope with atomic resolution. It will show startling results. But this usually looks only at an extremely small area, maybe only a few tens of nanometers square, at best. You don't see what's happening to the left and right, 100 nanometers away.

Transmission electron microscopy is also destructive, damaging the sample in the process of analysis.

With Tip Enhanced Raman Scattering and tip enhanced photoluminescence, even though the spatial resolution is not as good as transmission electron microscopy, HORIBA'S technology occupies the sweet spot between the conventional confocal microscopy with a spatial resolution of about 500 nanometers, and the atomic resolution of transmission electron microscopy. HORIBA is occupying the range somewhere in between, with a few nanometers to a few tens of nanometers of spatial resolution. Researchers can also cross-correlate their spectroscopic data with other observables provided by a scanning probe microscope: surface potential, conductivity, mechanical properties, and so forth.

This is unique. These lateral heterostructures are an important class of materials; as the synthetic technology and synthetic protocols improve, we will be able to create atomically sharp junctions, and hopefully even extend them in three-dimensional structures, creating densely-packed transistors more easily than the complex technology of creating five-nanometer transistors with the current technology.

In this paper, the authors demonstrated that within the same crystal, the width of the transition area can vary by more than an order of magnitude.

This is an example of trying to engineer both defects and areas with a lack of defects. The engineers may want to have the individual grains of the different TMDs be uniform across its structure. And then, they may want to have a sharp transition from one material to the other, so that any variation in the transition region may be considered a defect. Conversely, a wider, controlled transition width between materials may be considered desirable in some circumstances. Unless you can see it, you can't easily engineer it.

Applications

A myriad of nanoelectronics applications are foreseen, ranging from transistors to photodetectors, as well as in the energy field.

Correlated TERS, TEPL and SPM measurements of 2D materials

Agnès Tempez[1], Ophélie Lancry[1], Andrey Krayev[2] and Marc Chaigneau[1]
[1]HORIBA France SAS, Palaiseau, France,
[2]HORIBA Instruments, Inc. Irvine, CA, USA

Abstract

This application note reports on nano-characterization of 2D transition metal dichalcogenides (TMDCs) materials which are considered to be very high potential semiconductors for future nanosized electronic and optoelectronic devices. Scanning probe microscopy (SPM) giving access to the critical topographic and electronic properties at the nanoscale is coupled to photoluminescence (PL) and Raman spectroscopies by means of plasmon enhancement to yield correlated electrical and chemical information down to the nanoscale.

Keywords

AFM-Raman – 2D materials – Transition metal dichalcogenides (TMDCs) – TERS – TEPL – Heterogeneities – Nanomaterials – Opto-electronics – Heterojunctions

Context and issues

2D materials are defined as crystalline materials consisting of a single unit cell layer of that material. Among the large number of potentially stable 2D materials (more than 700), graphene and the family of transition metal dichalcogenides (TMDCs) are under thorough study as candidates for tomorrow's nanoelectronics building blocks. Monolayer TMDCs are tunable band gap semiconductors and complement zero gap graphene. A myriad of nanoelectronics applications are foreseen, ranging from transistors to photodetectors, as well as in the energy field (nanogenerators, green electronics, electrocatalytic hydrogen generation and energy storage).

Many challenges remain before the promise of 2D materials is realized in the form of practical nano-devices, e.g.: (i) understanding growth mechanisms of these crystals, to be able to fabricate defect-free large area films, (ii) controlling transfer processes from growth substrates to other substrates, (iii) controlling their vertical or lateral integration. An information-rich, nanoscale characterization technique is required to qualify these materials and assist in the deployment of 2D material-based applications.

Raman and photoluminescence spectroscopies are the techniques of choice to characterize monolayer crystalline materials in terms of electronic behavior (band gap, carrier concentration) and structural quality (defect location and density). Because these conventional spectroscopies are far-field optical techniques (the spot size is diffraction-limited), their applications are restricted to the micro- and macro-worlds. Plasmon-enhanced optical spectroscopies (TEPL: Tip enhanced Photoluminescence, TERS: Tip Enhanced Raman Spectroscopy) bridge the gap to NanoPL and NanoRaman and offer optical nanometric spatial resolution. These new spectroscopic techniques can now be combined with other SPM modes for multi-parameter analysis of 2D materials [1,2]. The work presented in this article opens up new possibilities for the characterization of chemical, optoelectronic, topographic and electronic properties of 2D materials.

Correlated TEPL and SPM of MoS_2 flakes on Au/Si substrate

Molybdenum disulfide (MoS_2) is a promising semiconducting transition metal dichalcogenide 2D material for next generation photovoltaic solar cells, optoelectronic circuits and sensors due to its great excitonic recombination property, high carrier mobility and low leakage current.

NEXT »

Applications

Correlated TERS, TEPL and SPM measurements of 2D materials, cont.

One of the advantages of two dimensional TMDCs, e.g. with respect to graphene, comes from quantum confinement, enabling the indirect-to-direct band-gap transition as a function of number of individual layers. Nano-scale characterization is needed to provide the understanding necessary to engineer nanodevices integrating monolayer MoS_2.

Monolayer MoS_2 has a band gap about 1.8 eV, as revealed by photoluminescence (PL) spectroscopic analysis. The PL spectrum is decomposed in two peaks due to excitonic features: The A_0 mode derived from an exciton consisting of one electron and one hole bound by Coulomb interaction, and the A^- mode derived from a trion, a charged three-body exciton consisting of an exciton combined with another electron. It has been reported that the PL intensity decreases with increasing number of MoS_2 layers and that the PL intensity to Raman intensity ratio is related to the number of layers [3].

Tip enhanced optical spectroscopies based on the amplification of signal from the nano-region under the SPM tip will allow for actual nano-characterization. In the case of TMDCs, Tip enhanced Photoluminescence (TEPL) is capable of revealing variations in emission within a submicron size flake. Complementary morphological, chemical, and electronic structure information may be acquired simultaneously – and with nanometer spatial resolution – through AFM imaging.

TEPL measurements are performed on MoS_2 flakes transferred to a gold-on-silicon substrate using a NanoRaman™ system from HORIBA Scientific integrating an Atomic Force Microscope (AFM) (OmegaScope, based on SmartSPM) and a Raman microscope (XploRA) with a 100× WD objective tilted by 60° with respect to the sample plane. A 638 nm p-polarized laser is focused onto the cantilever-based silver coated TERS tip (OMNI TERS-FM probe). An AFM topography map is first recorded to locate MoS_2 flakes, as well as to provide electrical analysis with KPFM (Kelvin Probe Force Microscopy) giving the contact potential difference (CPD) and capacitance using a silver coated tip in frequency modulation mode (15 nm lift in dual pass setup) (Figure 1).

Here, as with other 2D materials, it is key to correlate electronic characteristics with nanoscale excitonic and chemical properties provided respectively by TEPL and TERS measurements [3-6].

A PL map of the same two flake apexes (6 × 9 µm (60 × 90 pixels)) is collected with a 100 ms integration time spectrum (640-840 nm) at each pixel (100 nm step). Two PL maps are actually recorded together with topography in a special mode called “Spec-Top™” mode with “dual spec” option: For each pixel (i) one spectrum (sum of the near-field and far-field signals) is acquired with the tip in direct contact with the surface with a typical interaction force of 2-10 nN and (ii) another spectrum is acquired with tip in tapping mode (a few nm away from the sample surface, considered to be the far-field contribution). In between two pixels of the map, the sample moves in semi-contact mode to preserve the sharpness and plasmonic enhancement of the tip.

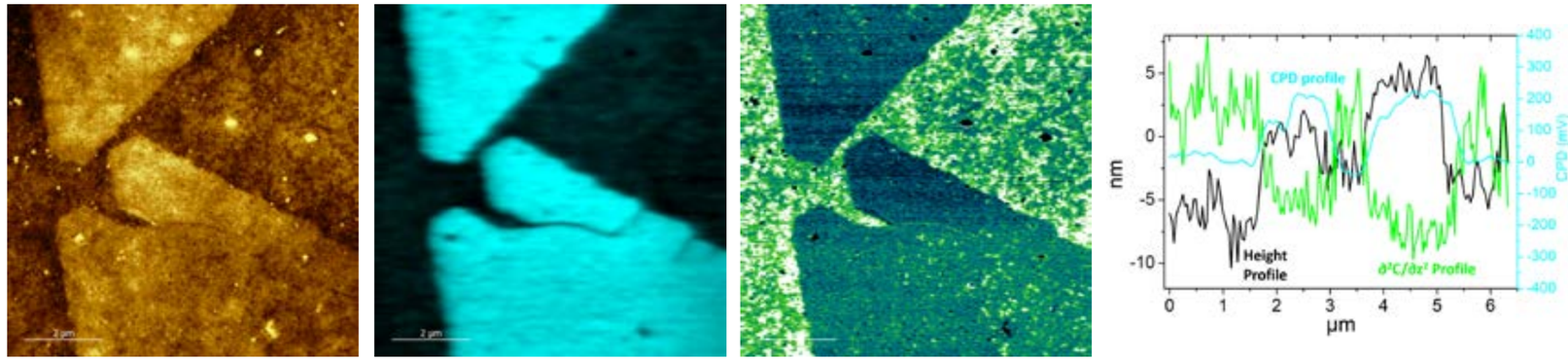

Figure 1: AFM topography, CPD and capacitance measurements on MoS_2 flakes on Au/Si substrate.
The lower right graph shows section analysis (topography, CPD and capacitance) along the white arrows displayed on the different AFM images.

« PREVIOUS

NEXT »

Home Introduction Stories Scientific Papers Applications Multimedia Contact

HORIBA Scientific

Applications

Correlated TERS, TEPL and SPM measurements of 2D materials, cont.

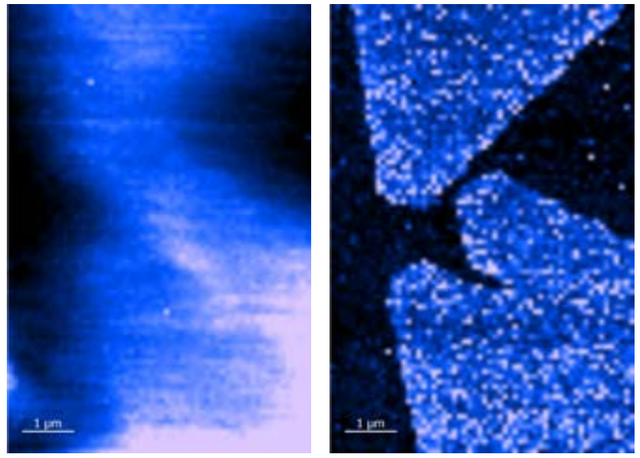

Figure 2: (left) Conventional far-field Photoluminescence map and (right) NanoPL (or TEPL) map of the same MoS_2 flakes.

Two PL maps are shown in Figure 2, the as-acquired far-field PL map (“tip up”) and the near-field or true NanoPL map (TEPL) generated upon subtracting the far-field spectrum (“tip up”) from the spectrum in contact (far-field + near-field or “tip down”) for each pixel. Both PL images are generated from the integration of PL band from 640 to 740 nm. The improved spatial resolution in the TEPL image (right) compared with the far-field PL image can be clearly seen: The edges of the flake, indistinguishable in the conventional far-field microPL image are perfectly defined in the TEPL image. In addition, as shown in the overlay with the topography (Figure 3), edges perfectly match those of the AFM height image. Two spectra are plotted in the graph of Figure 3 from averaging 4-pixels, one from interior of the flake (red) and from the substrate (blue).

A Gaussian fit gives a peak at 660 nm (1.88 eV) which corresponds to the band gap of monolayer MoS_2. The topography profile indicates an apparent thickness that is much higher (~4-6 nm) than the expected monolayer thickness (0.8 nm), which is likely due to the roughness of the gold surface (RMS = 3 nm) onto which the flake was transferred.

This first example of TEPL on MoS_2 shows that the TEPL method, not limited by diffraction, provides a drastic improvement of the optical resolution compared to far-field photoluminescence (microPL) and is also more accurate than AFM topographic imaging to confirm the presence of monolayer flakes. The next sections of this article will demonstrate how TEPL and TERS are capable of revealing nanoscale heterogeneities impossible to access with conventional optical techniques.

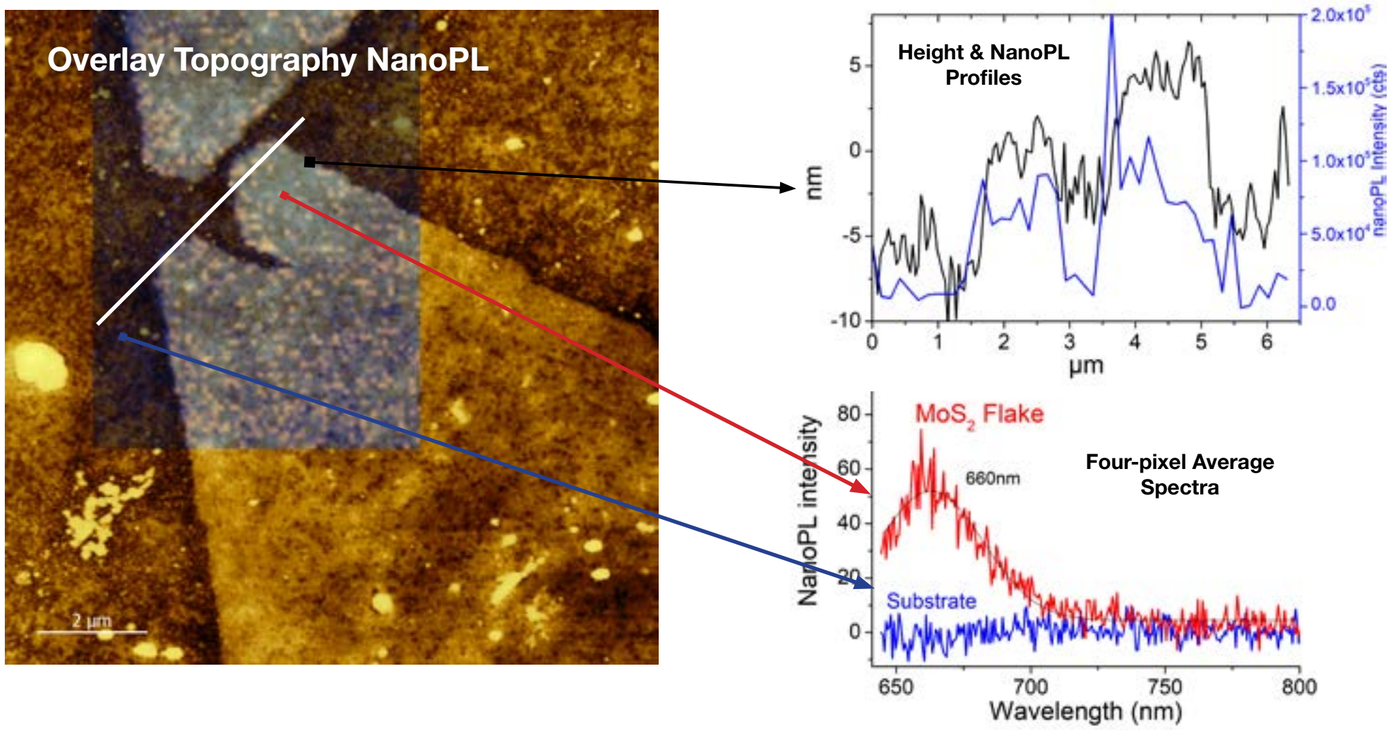

Figure 3: (left) Overlay of the AFM topography and TEPL images of MoS_2 flakes, (top right) AFM height and TEPL section analysis and (lower right) TEPL spectrum from interior of the flake and from the substrate.

« PREVIOUS
NEXT »

Correlated TERS, TEPL and SPM measurements of 2D materials, cont.

TTEPL measurements of WS_2 flakes on SiO_2/Si

Tungsten is the largest and heaviest transition metal in the family of common transition metals and, in contrast with molybdenum, is more abundant in the Earth's crust, cheaper, and less toxic. Monolayer tungsten disulfide (WS_2) is a direct-gap semiconductor with an energy gap close to 2 eV and high photoluminescence quantum yield (≈ 6%) (higher compared to other 2D semiconductors, e.g. ≈ 0.1% in monolayer MoS_2). It has also exceptional properties such as large spin–orbit coupling (≈ 420 meV), large exciton/trion binding energy, and nonblinking photon emission. The most common stacking structure of WS_2 is 2H, in which the W atoms of a given layer are sitting exactly on top of the S atoms of its neighboring layer.

In this section, correlated AFM and TEPL measurements are performed on WS_2 flakes grown pseudo-epitaxially on a silica on silicon (SiO_2/Si) substrate using a NanoRaman™ system integrating an Atomic Force Microscope (OmegaScope) with a confocal Raman LabRAM HR Evolution microscope. A 532 nm p-polarized laser is focused onto the cantilever-based silver coated TERS tip.

Figure 4 shows AFM topography of a 14 µm triangular flake with 512 lines resolution. Far-field (FF) and near-field + far-field (NF+FF) maps are acquired with 500 ms integration time spectra and steps of 93 nm. PL images are generated from the integration of PL tail from 640 nm to 690 nm. Figure 4 shows two PL images: the as-acquired far-field and the near-field or TEPL calculated from subtraction of FF map from NF+FF map. One can observe the higher resolution of the TEPL image with respect to the far-field image.

(i) The contour of the triangular single crystalline flake, as well as that of the thicker inner center triangle, are much more well defined in the TEPL map than in the far-field image.
(ii) Dark spots of size ranging from 100 nm to 200 nm can clearly be seen in the TEPL map. They are likely to be nanocrystallites visible as bright features of few tens of nm of height in the AFM topography image.
(iii) The PL response non-uniformity on the outer monolayer part of the flake is resolved at the nanoscale, which reveals a lot of inhomogeneities.

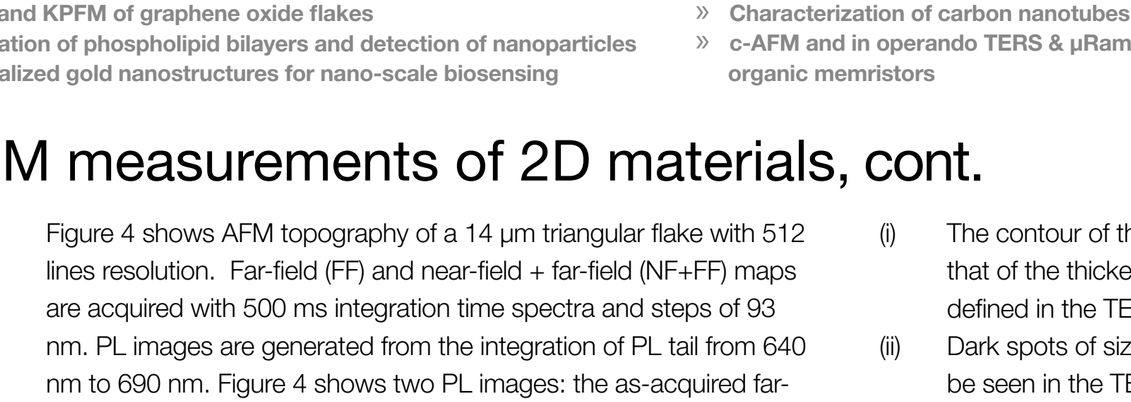

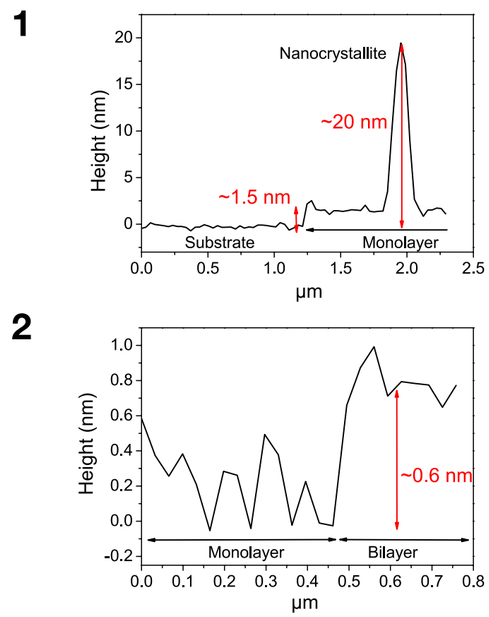

Figure 4: Topography, near-field and far-field PL images of WS_2 flake on SiO_2/Si. The graphs show two section analysis done along the arrows 1 and 2 shown on the AFM topographic image.

« PREVIOUS

NEXT »

Home Introduction Stories Scientific Papers Applications Multimedia Contact

HORIBA Scientific

Correlated TERS, TEPL and SPM measurements of 2D materials, cont.

This higher resolution is also demonstrated through the comparison of the PL intensity profiles crossing the flake through the inner center triangle showing (Figure 5):

(i) Abrupt rise going from substrate onto the monolayer WS_2 flake in the near-field profile compared to slow rise in the far-field.
(ii) More pronounced dip in the near-field profile when crossing the ~20 nm high nanocrystallite (height profile "1" in Figure 4) than in the far-field profile.
(iii) More abrupt decrease (higher than one order of magnitude) going from monolayer to bilayer (height profile "2" in Figure 4 shows a 0.6 nm difference) in the near-field than in the far-field profile.
(iv) A tremendous gain in signal to noise ratio: The dynamics go from 1.5 decades in far-field to more than 5 orders of magnitude in near-field PL.

TEPL reveals deep sub-diffraction limit details within the 2D WS_2 flake that are not resolved in conventional PL measurements [7,8]. Edge effects, nanocrystallites, grain boundaries, etc. are seen in the TEPL image with improved signal to noise ratio and vastly improved resolution.

Correlated TEPL and SPM of WSe_2 flakes on SiO_2/Si

As a 2D material, WSe_2 consists in a layer of tungsten atoms sandwiched between two layers of selenium atoms. When the thickness of a WSe_2 crystal is reduced from bulk to monolayer (1L), its energy band transitions from indirect (band gap ~ 1.2 eV) to direct (band gap ~ 1.7 eV). 1L WSe_2 possesses a high exciton

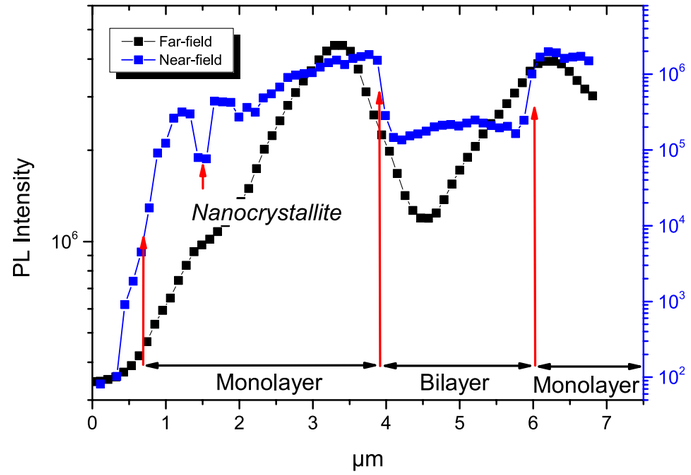

Figure 5: Section analysis of the PL signal in far-field (black) and in near-field (blue) along the arrows represented in Figure 4.

binding energy (~790 meV), high PL quantum yield (QY, 10%) and long photoluminescence (PL) lifetime (up to nanoseconds), which are superior to 1L MoS_2 and WS_2. Furthermore, 1L WSe_2 exhibits natural p-type doping, ultra-low thermal conductivity (0.05 W $m^{-1}K^{-1}$) and high carrier mobility (>100 cm^2 $V^{-1}S^{-1}$). This combination of properties makes 1L WSe_2 a promising candidate for novel opto-electronic devices such as high QY light emitting diodes and quantum light sources. The development and implementation of WSe_2 2D applications require an optical characterization technique on the order of tens of nanometers. Correlated TEPL and SPM provide substantial information related to the nanoscale optical properties of WSe_2 with a resolution down to a few nanometers [9].

These measurements were performed using the same NanoRaman™ system from HORIBA Scientific described in the previous sections of this article. An optical image (Figure 6a) of the entire sample (20×8 mm) is first obtained under the Raman microscope using the mosaic mode (10× objective images are rapidly acquired and stitched). With this full view of the entire sample and the top-view image of the OmegaScope top camera (10× objective), navigation on the sample positioned for correlative SPM measurements is facilitated. It becomes easy to identify and reach areas of interest (Figure 6b).

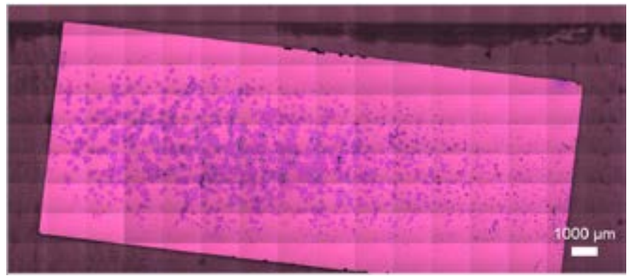

Figure 6a: Optical image of entire sample of WSe_2 on SiO_2/Si obtained with Raman microscope using Mosaic mode.

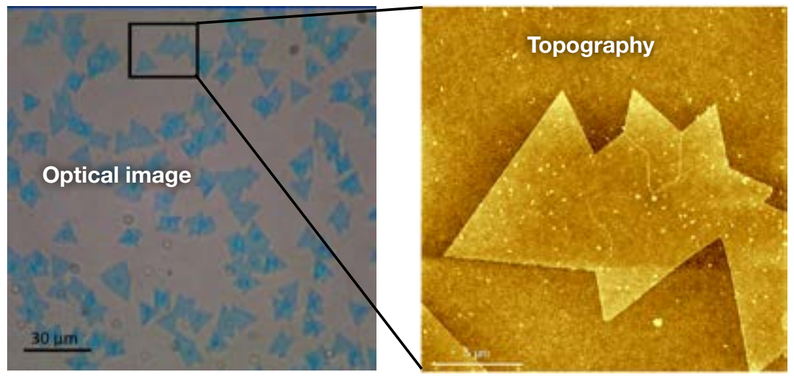

Figure 6b: Optical and AFM topographic images of WSe_2 flake on SiO_2/Si.

« PREVIOUS
NEXT »

HORIBA Scientific

Correlated TERS, TEPL and SPM measurements of 2D materials, cont.

The OmegaScope top-view image shows a region of interest which is then selected for detailed analysis: Several monolayer triangular flakes (clearly observed in a light blue color) that have merged. The corresponding AFM topography image (20×20 µm, 512 lines) shows a fraction of a large polygon flake consisting of several merged triangular flakes with different orientations. The bright spots on the flake are overlying nanocrystallites. On this high-resolution topography AFM image, some grain boundaries (GB) are also discerned.

Two PL maps are acquired corresponding to “near-field + far-field” (NF+FF) and “far-field” (FF) using “Spec-Top™” mode with “dual spec” option. The acquisition time of each spectrum was 50 ms and pixel size was 116 nm. The "dual spec" option gives access to the true TEPL map upon subtraction of FF map from the NF+FF map.

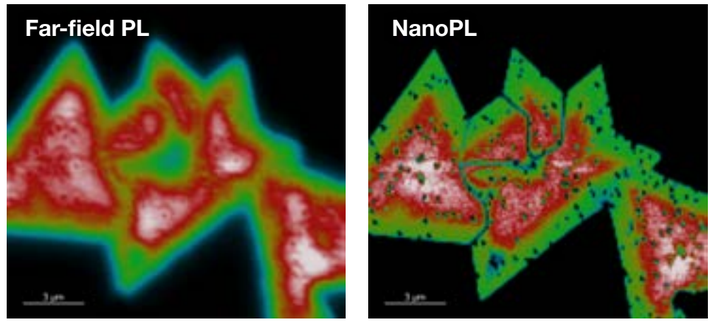

Figure 6c: Conventional far-field PL and TEPL images of WSe_2 flake on SiO_2/Si.

Figure 6c shows the far-field and near-field PL images generated from integration of the PL band from 700 to 800 nm.

The far-field image with an optical resolution of 550 nm shows some variation of PL intensity over the large 20 µm size polygonal flake with lower PL along the edges and GB than in the center of the flakes. However, this far-field image cannot render nanoscale excitonic variations due to the optical diffraction limit; the higher resolution pure near-field TEPL image reveals much more details (Figure 6c):

(i) Much sharper edges.
(ii) A distinct 800 nm wide lower PL (30% quenching) edge all around the flakes.
(iii) Clearly defined grain boundaries but appearing with different contrast (PL is quenched with different ratio depending on tilting angle between two merging flakes).
(iv) Dark spots (10% of center flake PL intensity) of size less than 200 nm corresponding to overlying nanocrystallites also observed in the topography image.

Average spectra taken from center and edge areas show TEPL quenching and slight red shift of edge with respect to center (Δ = 17 meV) (see graph in Figure 7). TEPL spectra taken from several nanocrystallites and along a GB exhibit much lower intensity and broader peaks. This TEPL measurement, showing different spectral signatures, reveals a nanoscale excitonic heterogeneity.

These optoelectronic properties of WSe_2 can be further studied using the combination of TEPL and Kelvin Probe Force Microscopy (KPFM).

In the present example of several WSe_2 flakes merging at different angles, the dependence of the phonon and excitonic processes at the grain boundaries can be observed as a function of tilting angle at the nanoscale as well as their sensitivity to light.

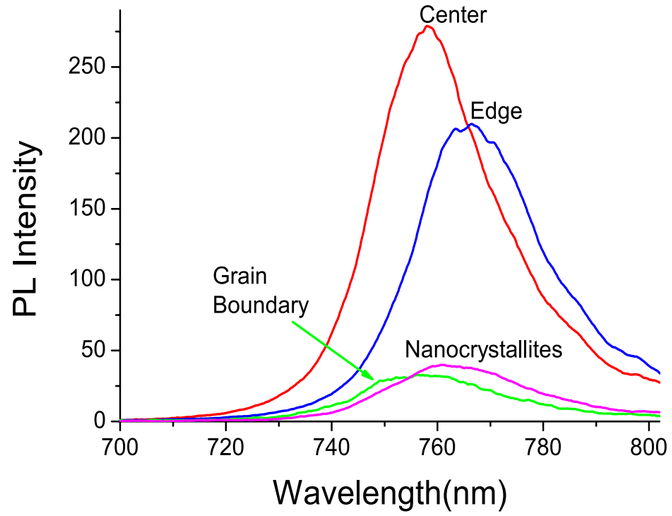

Figure 7: Tip enhanced Photoluminescence (TEPL) spectra taken from different locations of the WSe_2 flakes.

« PREVIOUS

NEXT »

Home Introduction Stories Scientific Papers Applications Multimedia Contact

HORIBA Scientific

Applications

Correlated TERS, TEPL and SPM measurements of 2D materials, cont.

Frequency modulated Kelvin probe measurements (FM-KPFM) are therefore conducted with the same silver-coated tip as the TEPL measurements with the 633 nm laser illumination OFF and ON (Figure 8). The contact potential difference (CPD) and the second derivative of capacitance ($\partial^2C/\partial z^2$) with respect to the tip-sample distance (relative change of capacitance) signals are collected both with and without illumination. In the images, the GB show different CPD and $\partial^2C/\partial z^2$ contrast depending on the angle of intersection. With no laser illumination some GB show higher CPD signal than basal plane while the GB between two flakes rotated by 180° (indicated as twin GB in Figure 8) show lower CPD than basal plane. Under laser illumination the higher CPD-GB feature even higher CPD while twin GB show slightly higher CPD signal than basal plane. As for the $\partial^2C/\partial z^2$ maps there is also clear contrast in GB signals depending on the tilting angles. The capacitance of twin GB is found to be more sensitive to light than other orientations, as they appear clearly under illumination but are not visible in the laser OFF map. These two distinct types of contrast observed in CPD and $\partial^2C/\partial z^2$ maps corresponding to “families” of tilting angles are consistent with the TEPL map also exhibiting GB with different contrast (Figure 6c). This could be linked to different defects density and type, as well as stoichiometry variation. In addition, it is important to note that the absence of GB between the flake in the bottom right of the map and the upper one corresponds to perfect lattice match and coincides with no contrast in CPD, $\partial^2C/\partial z^2$, and PL maps.

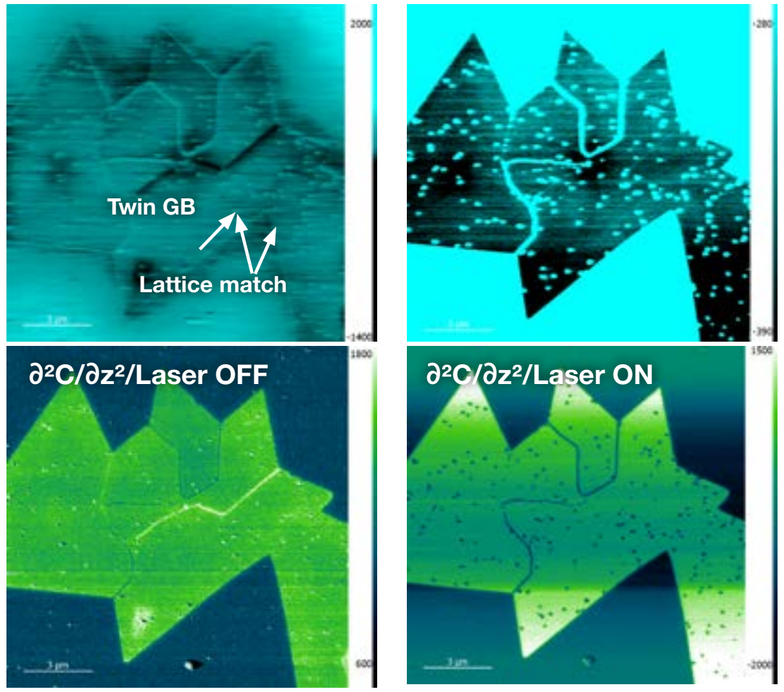

Figure 8: FM-KPFM measurements on the same WSe_2 flake showing contact potential difference (CPD) and the second derivative of capacitance ($\partial^2C/\partial z^2$) under 633 nm laser illumination and without illumination.

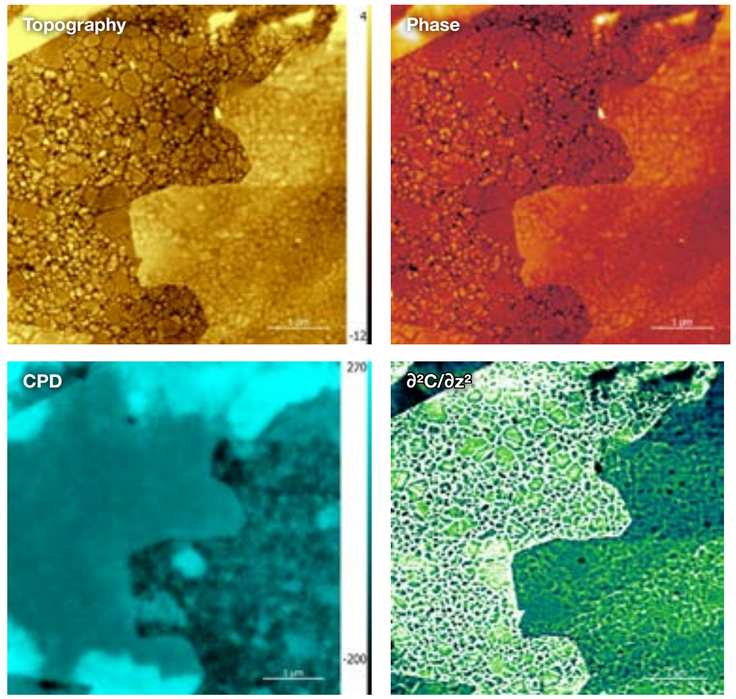

Figure 9: Topography, phase shift, CPD and $\partial^2C/\partial z^2$ measurements of WS_2 flake exfoliated on template stripped silver.

Correlated TERS and SPM of WS_2 flakes on template stripped silverure

WS_2 flakes are exfoliated on template stripped silver. Topography, phase shift, contact potential difference (CPD), and $\partial^2C/\partial z^2$ are measured with a NanoRaman™ system (HORIBA Scientific) in the dark for 5.5 x 5.5 µm images with 400 lines resolution (Figure 9). Surface potential (CPD) image presented in Figure 9 shows significant inhomogeneities of both the silver substrate and the WS_2 flake. TERS measurements are performed using a 638 nm p-polarized laser focused onto the vicinity of cantilever-based silver coated TERS tip.

« PREVIOUS

NEXT »

Applications

Correlated TERS, TEPL and SPM measurements of 2D materials, cont.

Two Raman maps are acquired corresponding to “near-field + far-field” (NF+FF) and “far-field” (FF) using “Spec-Top™” mode with “dual spec” option. The acquisition time of each spectrum is 150 ms and pixel size is 44 nm. Figure 10 shows the far-field (conventional µRaman) and near-field (TERS) images generated from the integration of 418 cm^{-1} peak (in blue), and the 347 cm^{-1} peak (in green) corresponding to the A_{1g} and 2LA(M) bands, respectively. The µRaman image with a diffraction-limited optical resolution features the flake but with blurred contours and a homogeneous distribution of both Raman signal intensities.

Correlated TERS and SPM of WSe_2 flakes on Au thin film

The understanding of charge transport and optimization of transistor mobility and current density in the fabrication of TMDCs-based semiconductor devices requires study of semiconductor-insulator interfaces such as with SiO_2/Si. Equally important is the interface between the semiconducting TMDC and the contact metal, as it is the locus of charge carrier injection and collection. In this case the interface between WSe_2 and gold is probed using scanning probe microscopy (SPM) and TERS. The sample is prepared by mechanical exfoliation of WSe_2 on 120 nm thick gold.

A combination of topography, contact potential difference (CPD), TERS, and photocurrents maps is collected for nanoscale cross-correlations with a NanoRaman™ system (HORIBA Scientific) in a previously described configuration. In the AFM topography image (Figure 11a), flakes with thicknesses in the range of 0.8-3 nm range can be seen, corresponding to 1-4 layers of WSe_2.

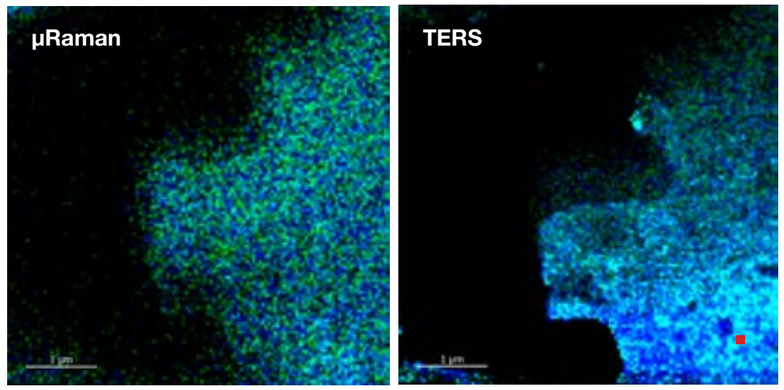

Figure 10: (Top) Conventional µRaman and TERS images of the same of WS_2 flake. (Bottom) Typical TER spectra taken from the square areas in the TERS image.

Kelvin probe measurements in frequency modulation (FM-KPFM) mode are conducted in the same area. The contact potential difference (CPD) map (Figure 11b) which gives the distribution of the surface potential across the sample tells us about the change in electronic properties of the material and about the presence of contamination layers. As shown in CPD image, variations in surface can be as high as 150 meV within a flake between adjacent domains.

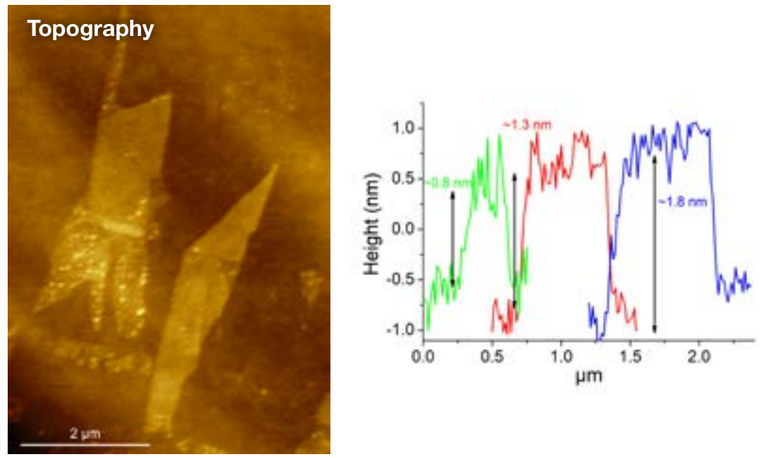

Figure 11a: AFM topography and height profiles of WSe_2 flakes on Au. The different colored profiles correspond to the arrows in the image.

The TERS map is also acquired on the same area of the sample in "Spec-Top™" mode. The blue-color map shown here is the intensity response of the large [217-262 cm^{-1}] band centered at 240 cm^{-1}. A striking observation occurs immediately when looking at the CPD and TERS map side by side (Figure 11b, top).

« PREVIOUS
NEXT »

Correlated TERS, TEPL and SPM measurements of 2D materials, cont.

The TERS intensity map correlates extremely well with the CPD with high Raman intensity coinciding with higher surface potential, and domains exhibiting low Raman intensity are also areas with lower surface potential. This is nicely illustrated by the graph plotting CPD and Raman intensity profiles on a line with variation of CPD as high as 150 meV and of Raman intensity of a factor 100 (Figure 11b, bottom). Plotting two average TERS spectra from both high (blue) and low (red) CPD value areas evidences, in the high intensity area (blue) the presence of additional Raman peaks (LA(M) at 135 cm^{-1}, A(M) at 240 cm^{-1}, 2LA(M) at 260 cm^{-1} as well as complex peaks at around 375 cm^{-1} and 390 cm^{-1}) as a result of Raman resonant conditions met with the 638 nm excitation laser which overlaps with a broad shoulder on the high energy side of A exciton (1.74 eV; 712 nm). The lower CPD value areas exhibit non-resonant Raman with the single A_{1g}+E_{2g} peak. This correlation featuring nanoscale heterogeneities of the surface potential with matching Raman response is not feasible using conventional confocal Raman microscopy, for which the spatial resolution is limited by diffraction to approximately 400-500 nm at the 638 nm pump wavelength used in our experiments; clearly insufficient to resolve domains 10 nm-100 nm in lateral size.

Complementary measurements of WSe_2 exfoliated on another metal, namely template stripped silver has shown nanoscale inhomogeneities with similar correlation between Raman and surface potential [9]. In addition, photocurrent measurements at the same nano-resolution confirm the semi-conducting nature of WSe_2 and that surface potential variation most likely results from intrinsic non-uniformity of the WSe_2 crystalline structure. Nanodomains with higher CPD have negative photocurrent and low CPD regions exhibit photocurrent of opposite sign, which can be interpreted as due to nanodomains having complementary doping types.

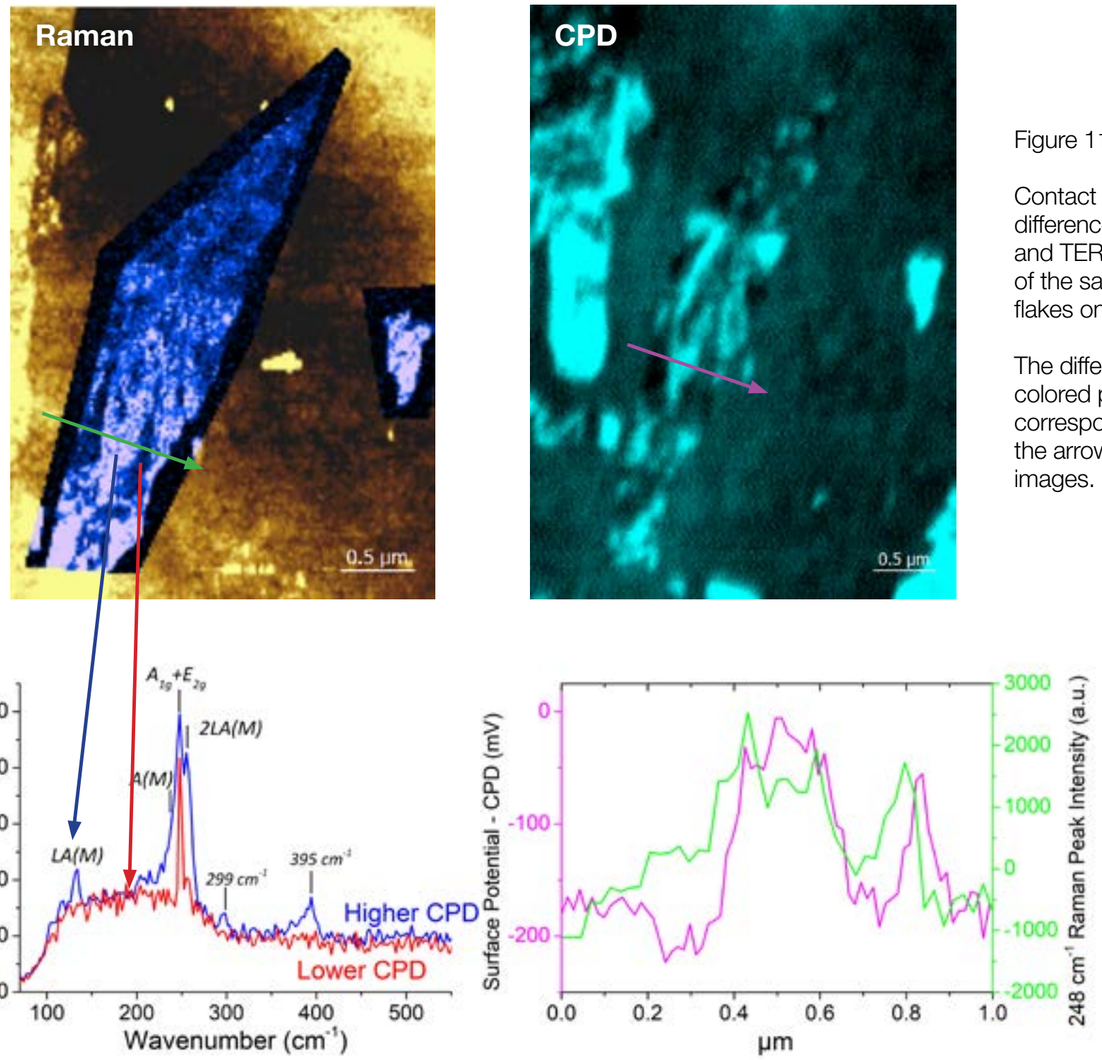

Figure 11b:

Contact potential difference (CPD) and TERS images of the same WSe_2 flakes on Au.

The different colored profiles correspond to the arrows in the images.

« *PREVIOUS*

NEXT »

Correlated TERS, TEPL and SPM measurements of 2D materials, cont.

TEPL of WS_2 /WS_xSe_{1-x} /WSe_2 heterostructure on SiO_2 /Si

Building up nanodevices from 2D layered materials requires heterostructures. The electrical and optical properties of such heterojunctions will depend on the alignment of the energy bands at the interface. Using alloys of transition metal dichalcogenides allows for band gap engineering which is likely to lead to sharp and well controlled interfaces.

TEPL has already been applied to the $MoSe_2$-WSe_2 heterojunction for the study of quantum plasmonic injection and aging effect [10, 11]. Here we present TEPL data obtained on a lateral single layer WS_2 / WS_xSe_{1-x} / WSe_2 heterostructure grown on SiO_2 /Si.

The 10×10 µm AFM topography and phase shift images (512 lines) show the apex of 60 µm triangular flake with a contrast allowing to distinguish the presence of both binary and ternary alloys (Figure 12).The nicely defined interfaces seen on both images allow the width of the ternary WS_xSe_{1-x} layer to be measured: 700 nm on one side of the flake apex and 350 nm on the other side. The height profile (not shown) across the three materials shows a rise of 0.6 nm from WS_2 to the ternary alloy, no measurable height change from the ternary alloy to the peripheral WSe_2, and a WSe_2 thickness of about 2.5 nm.

Tip enhanced Photoluminescence (TEPL) is performed using a NanoRaman™ system, 532 nm excitation laser and cantilever-based silver coated TERS tips. Two PL maps are acquired on the same run using “Spec-Top™” mode with “dual spec” option. The acquisition time of each spectrum is 50 ms and pixel size is 100 nm. A three color map (Figure 13) including the TEPL response from WS_2 (peak centered at 625 nm), WS_xSe_{1-x} (peak centered at 665 nm), WSe_2 (peak centered at 765 nm) confirms the presence of the three single layer compounds as well as a difference in the WS_xSe_{1-x} PL signal quenched on the left side of the apex (appearing narrower on the height and phase shift images). The graph showing average spectra from the three regions indicates the integration PL response intervals (Figure 13, right).

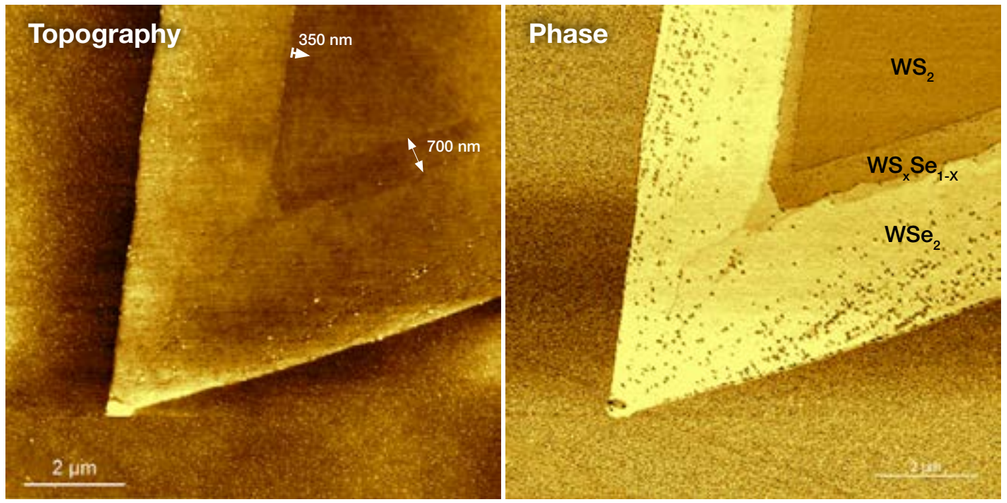

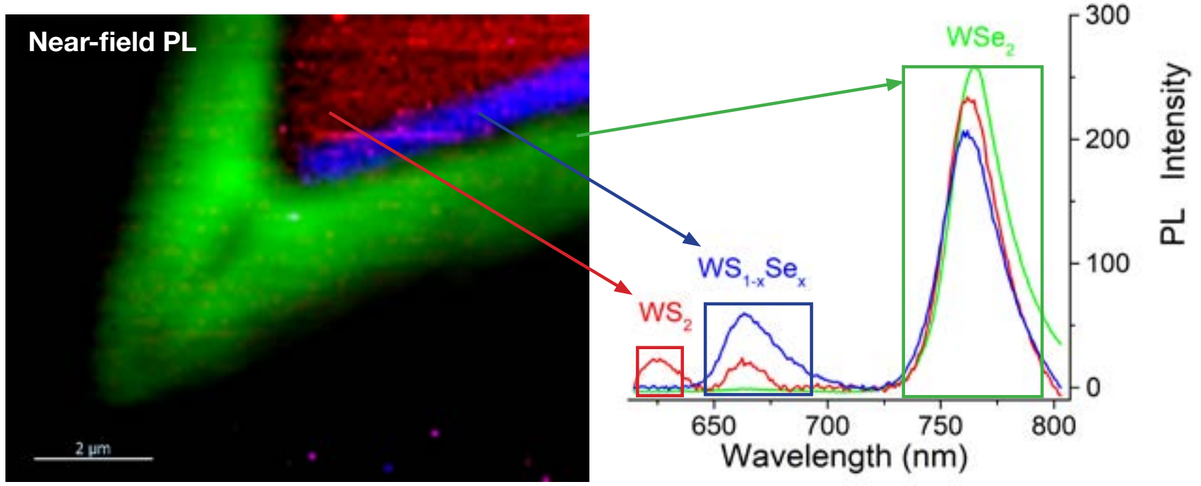

Figure 12 (top):

AFM topography and phase images of the 2D heterostructure.

Figure 13 (below):

(left) TEPL (aka near-field PL) of the WS_2 / WS_xSe_{1-x} / WSe_2 heterostructure on SiO_2 /Si,

(right) TEPL spectra from different regions of the heterojunction.

« *PREVIOUS*

NEXT »

Home Introduction Stories Scientific Papers Applications Multimedia Contact

HORIBA Scientific

Applications

Correlated TERS, TEPL and SPM measurements of 2D materials, cont.

Two true TEPL maps (far-field subtracted) are generated for the WS_xSe_{1-x} PL and the WSe_2 PL responses and are overlaid with an AFM topography map (Figure 14). The WSe_2 TEPL map shows some inhomogeneities due to excitonic heterogeneities at the nanoscale, as illustrated by the signal profile (insert in Fig. 14). These nanoscale variations could not be seen in the topography and phase shift images. The WS_xSe_{1-x} TEPL map shows an intense ~600 nm wide stripe for the right-side alloy and a much less intense and narrower stripe on the left side of the flake apex.

This correlates well with the first observations from the AFM images. The graph comparing average spectra extracted from both regions gives some further insight with PL response for the left side being shifted to lower energy (1.84 eV versus 1.87 eV for the right side). The observed PL peak shift is associated with the alloying across the interfaces, and the observed peak shift can be directly linked to the change in alloy composition.

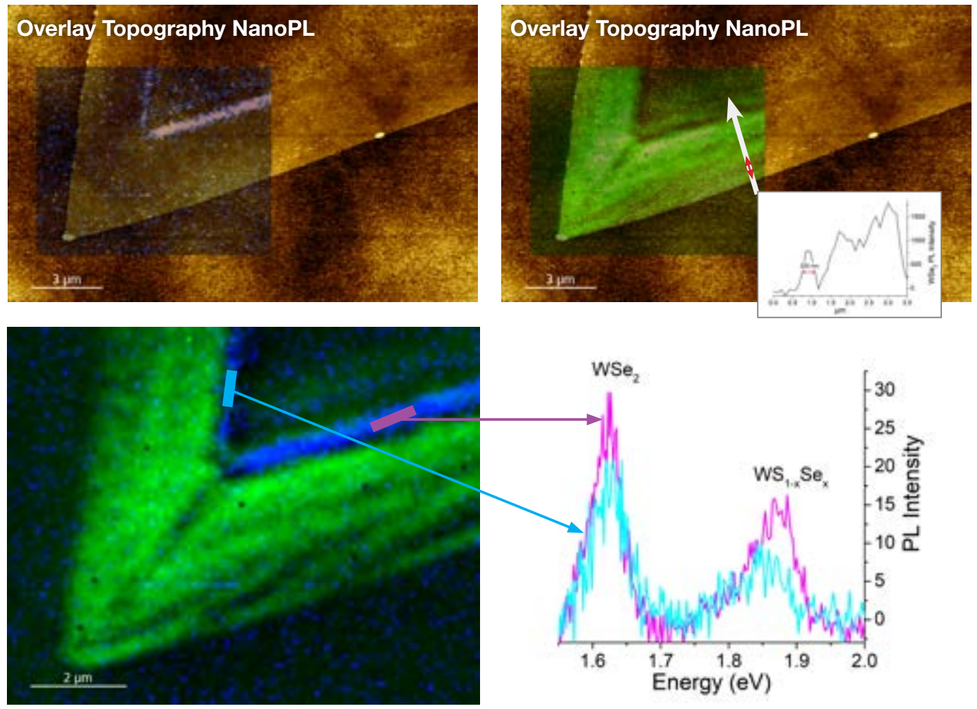

Figure 14: (Top) Overlay of AFM topography with (left) WS_xSe_{1-x} TEPL and (right) WSe_2 TEPL images. (Bottom left) Overlay of WSSe and WSe_2 PL. (Bottom right) Typical spectra from the WSSe regions.

Conclusions

In this application note, we have presented new nano-imaging capabilities with correlated TERS, TEPL and SPM measurements of different 2D materials and heterojunction. We have demonstrated that TEPL, not limited by diffraction, provides a drastic improvement of the optical resolution compared to conventional far-field photoluminescence (microPL) and is also more accurate than AFM topographic imaging to confirm the presence of transferred MoS_2 monolayer flakes. Single crystal WS_2 and WSe_2 flakes directly grown on SiO_2/Si have been also analyzed with TEPL: NanoPL response maps nicely overlay on topography images (monolayer, bilayer, nanocrystallites). Moreover, we have shown the sensitivity of electronic properties (contact potential and capacitance related to Fermi level and charge accumulation) upon light illumination. Beside these semiconductor/dielectric (SiO_2) interfaces, results from probing TMCD/metal interfaces, namely WS_2 on silver and WSe_2 on gold have been also shown. TERS and Kelvin probe measurements revealed nanoscale inhomogeneities both observed in CPD and Raman maps. Finally, NanoPL together with AFM topography data on a lateral single layer WS_2/WSxSe$_{1-x}$/WSe_2 heterostructure grown on SiO_2/Si have been presented and revealed nanoscale PL response variations beyond the smooth nano-resolution topography.

« *PREVIOUS*

References

[1] Nature Communications 9, 2891 (2018).
[2] ACS Appl. Nano Mater. 1 (2), 572 (2018).
[3] Nanoscale 10, 14055 (2018).
[4] Nanoscale 10, 2755 (2018).
[5] Nano Lett.17 (10), 6027 (2017).
[6] Phys. Rev. B 97, 085305 (2018).
[7] 2D Mater. 4, 021024 (2017).
[8] Sci. Adv. 5:eaau8763 (2019).
[9] 2D Mater. 5 035003 (2018).
[10] Phys. Rev. B 98, 041402(R) (2018).
[11] Opt. Mater. Express 9, 1620 (2019).

Acknowledgments

We thank Eddy Robinson for the manuscript correction. We thank Thomas Carlier for help in data processing. We thank all the R&D team (Alexey Belyayev, Dmitry Evplov, Vasily Gavrilyuk, Sergey Katsur, Alexander Yagovkin, Yury Turlapov, Maxim Eremin, Sergey Kostromin, Patrick Hsia, Philippe de Bettignies) for the development and the support.

MXenes are a large 2D materialsfamily gaining interest for their high electronic conductivity and hydrophilic surface.

TERS characterization of single- to few-layer $Ti_3C_2T_x$

A. Sarycheva[1], M. Shanmugasundaram[2], A. Krayev[2], Y. Gogotsi[1], A. Tempez3, M. Chaigneau[3]

[1]A. J. Drexel Nanomaterials Institute and Department of Materials Science and Engineering, Drexel University, Philadelphia, Pennsylvania 19104, United States
[2]HORIBA Scientific, Piscataway, New Jersey 08854, United States
[3]HORIBA FRANCE SAS, Palaiseau, France

Abstract

This application note reports on TERS characterization of $Ti_3C_2T_x$ MXene flakes. MXenes are a large 2D materials family gaining interest for their high electronic conductivity and hydrophilic surface. Nano-resolved chemical imaging of single-layer and few-layer flakes of $Ti_3C_2T_x$ MXene deposited on a gold substrate has been realized at a laser power density on the sample about an order of magnitude lower as compared to confocal Raman measurements. Spectra feature an intense peak at around 201 cm^{-1} and two well-defined peaks at around 126 and 725 cm^{-1}. While the intensities of these peaks decrease with the increasing number of layers, the relative intensity of the 126 and 725 cm^{-1} bands, as compared to the 201 cm^{-1} band, increases. The peak positions of the main MXene bands do not significantly change in flakes of different number of layers, suggesting weak coupling between the MXene layers. This note also shows that TERS signal can be used to monitor the onset of degradation of single- and few-layer flakes of $Ti_3C_2T_x$ well before significant morphological changes appear, and thereby assess their environmental stability.

Keywords

TERS, Raman spectroscopy, MXenes, two-dimensional materials, plasmonics, interface, vibrational properties.

Context and Issues

MXenes are a growing 2D materials family with a M_nX_n-$1T_x$ general formula, where M is a transition metal, X is C and/or N, and T_x stands for the functionalization group (O, OH, F, Cl, etc.) resulting from their wet-chemical synthesis. They have unique properties such as high electronic conductivity and a hydrophilic redox-active surface [1-3]. Some Mxene compounds exhibiting semiconducting properties have been theoretically predicted [4].

MXenes' properties may be tuned by varying the transition metal [5], the number of layers (n) [6], and the surface terminations [7]. The influence of the stoichiometric ratio on the properties is known for some systems but the effects of local heterogeneities still need to be investigated. The control of nanoscale composition would ultimately allow for engineering properties locally, gaining more control over the 2D material-based systems.

Potential / Input from technique

Raman spectroscopy provides valuable information about the structural properties of such materials [8-9] but Raman microscopy fails to image chemical nano-heterogeneities due to the optical diffraction limit. Furthermore, in the case of MXenes, the conventional Raman signal is very weak and the integration time required to collect a decent S/N spectrum is tens of seconds at the laser power level, still not damaging for the sample, which makes the imaging de-facto prohibitive. Tip Enhanced Raman Spectroscopy (TERS) overcomes the low Raman signal level by enhancing Raman scattering up to 6 orders of magnitude and enables nanoscale chemical mapping [10].

NEXT »

Home Introduction Stories Scientific Papers Applications Multimedia Contact

HORIBA Scientific

TERS characterization of single- to few-layer $Ti_3C_2T_x$, cont.

Starting point, what is known?

TERS achievements in establishing structure–property relationships in 2D materials on a nanometer scale are now well documented [11]: characterization of local defects, strain, and Moiré pattern in graphene [12], doping and nanoscale strain-related structural heterogeneities [13] which affect their optoelectronic properties in a large number of transition metal dichalcogenides (TMDCs).

In this application note, we report on TERS measurements carried out on monolayer to few-layer thick $Ti_3C_2T_x$ and Ti_3C_2 flakes. The reader may refer to the article by Sarycheva et.al in ACS Nano: Tip Enhanced Raman Scattering Imaging of Single- to Few-Layer Ti3C2Tx MXene [14].

Description of sample and measurements

MXene crystals were synthesized using the method described in [15] and then deposited on gold substrates. The gold substrate permits the so-called gap mode TERS conditions, in which an optical electric field is greatly amplified in the cavity created by the apex of the TERS tip and plasmonic gold surface.

AFM and TERS measurements were performed using a nanoRaman system (XploRA-nano, HORIBA Scientific) integrating an atomic force microscope (SmartSPM) and a Raman microscope (XploRA) with a 100× WD objective tilted by 65° with respect to the sample plane for excitation and collection. 785 or 830 nm excitation p-polarized lasers were focused onto the cantilever-based gold coated AFM-TERS tip (OMNI-TERS-SNC-Au, Applied Nanostructures Inc.). The power on the sample was about 350 µW for 785 nm excitation and about 450 µW for 830 nm. It should be also noted that the far-field (confocal µRaman) signal from the $Ti_3C_2T_x$ crystals was negligible at the laser power level and integration times used in TERS experiments, especially for the mono-, bi- and tri-layer thick flakes. The maps were acquired in SpecTop or Dual Two Pass modes. While both modes imply direct contact with the sample for recording strong TERS signal, in the SpecTop mode, transition between the pixels of the TERS map is performed in alternating-contact mode. Figure 1 displays a schematic diagram of the TERS experiments and Raman-active vibrations of $Ti_3C_2T_x$ MXene.

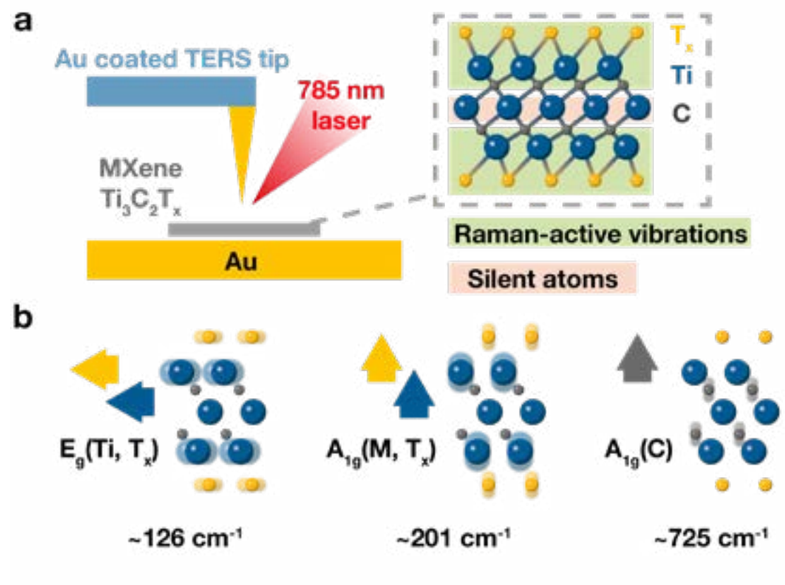

Figure 1: (a) TERS schematic diagram and $Ti_3C_2T_x$ atomic crystal arrangement; (b) Raman active vibrations of $Ti_3C_2T_x$ discussed in this work: in-plane Eg vibration at 126 cm-1 mainly appears when the excitation wavelength matches the surface plasmon resonance of $Ti_3C_2T_x$, and out-of-plane vibrations at 201 and 725 cm-1 correspond to vibrations of Ti, C, Tx, and C, respectively.

« PREVIOUS

NEXT »

Home Introduction Stories Scientific Papers Applications Multimedia Contact

HORIBA Scientific

TERS characterization of single- to few-layer $Ti_3C_2T_x$, cont.

Figure 2a shows a topographic image of several MXene flakes on gold substrate. The height profile inset in Figure 2a goes across a monolayer (1L), bilayer (2L), and a small overlap between the two. A TERS map collected over these flakes with 785 nm excitation is presented in Figure 2c. It shows the distribution of the intensity of three main $Ti_3C_2T_x$ Raman peaks: ~126 cm^{-1} band, a resonant Raman band, also described as Eg vibration of T_i, C, and T_x groups (green color), 201 cm^{-1} band, which corresponds to A1g (T_i, C and T_x) vibration (blue color) and another resonant Raman band at 725 cm^{-1} which corresponds to A1g (C) vibration (red color).

The change of absolute and relative intensities of major Raman bands as a function of layer thickness can be observed by looking at average spectra of typical flake areas plotted in Figure 2b. The absolute intensities of all three major bands at 126, 201, and 725 cm^{-1} are highest for the monolayer flake and decrease with the number of layers because of lower coupling between the tip and the substrate. The out-of-plane A1g (Ti, C, T_x) is the most enhanced peak in the monolayer flake which is expected as this vibration is aligned with the laser optical electric field of the band-gap mode tip-substrate cavity. The other out-of-plane A1g (C) mode is less enhanced.

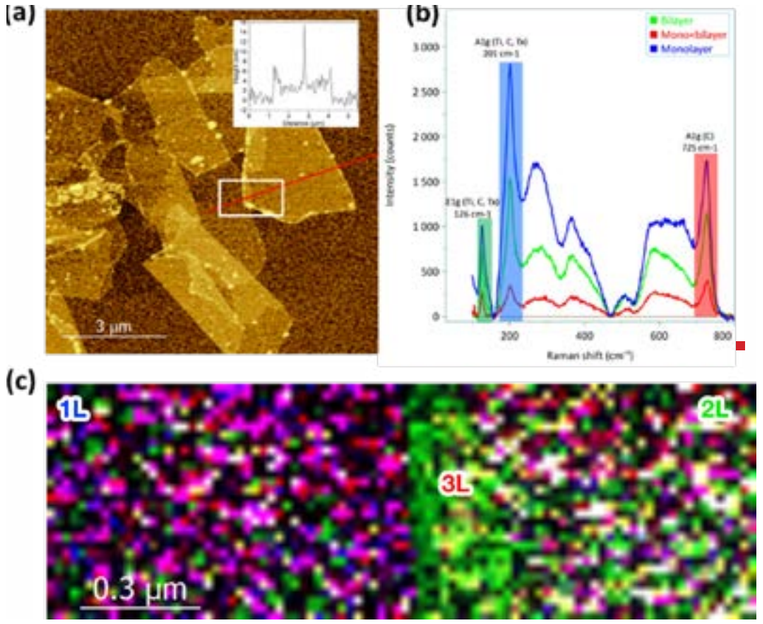

Figure 2: (a) Topographic AFM image of several $Ti_3C_2T_x$ flakes on Au substrate. The white dashed rectangle indicates the TERS scan area c); Inset: Height profile along the line showing that there are slightly overlapping single-layer and bilayer crystals; (b) TERS spectra averaged over the monolayer (blue spectrum), bilayer (green spectrum), and trilayer regions (bilayer overlapped with the monolayer, orange spectrum). The background was subtracted and spectra were offset vertically for clarity. (c) 1.8 µm × 0.6 µm,90 pixels/line TERS map showing the distribution of the intensity of correspondingly colored bands.

In the deposition process of single- to few-layer thick MXene flakes from aqueous solution, some folds and nanowrinkles form when the flakes get attached to the substrate. A topographic image of a 5 nm thick (trilayer) $Ti_3C_2T_x$ flake with such wrinkles crossing the flat flake surface is presented in Figure 3a.

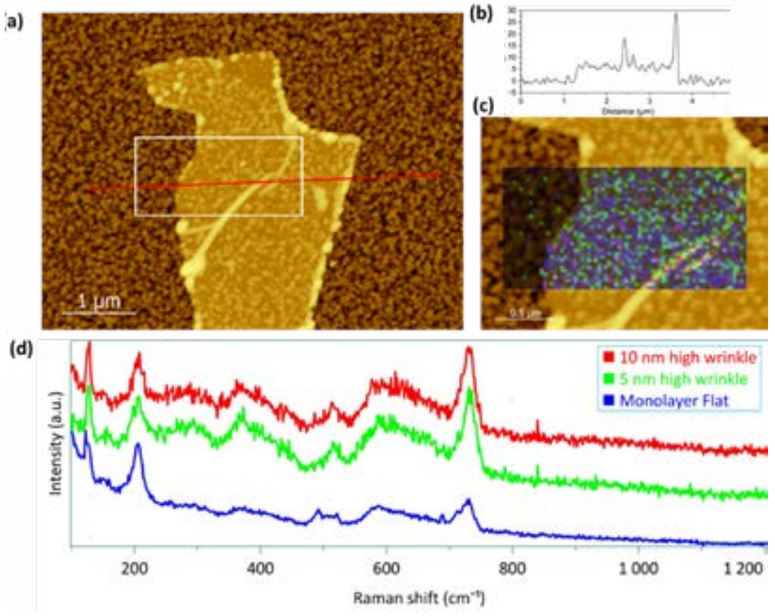

Figure 3: (a) Topographic AFM image of a tri-layer (5 nm-thick) $Ti_3C_2T_x$ crystal on gold substrate. Two wrinkles of 5 and 10 nm in height can be seen in this topography image. Increased height at the edges of the flake could come from the formation of titania nanoparticles as a result of MXene degradation; (b) AFM trace along the line shown in panel a; (c) combined 2 µm × 1 µm, 72 pixels per line TERS map showing the distribution of the intensity of 126 cm^{-1} (green color), 201 cm^{-1} (blue color), and 725 cm^{-1} (red color) peaks overlaid over the topography image. (d) TERS spectra averaged over the flat part of the crystal (blue spectrum), large 10 nm wrinkle (black spectrum), and small 5 nm wrinkle (gray spectrum). Spectra were offset vertically for better visualization.

« PREVIOUS

NEXT »

TERS characterization of single- to few-layer $Ti_3C_2T_x$, cont.

The height profile across the line shows that the wrinkles were about 5–10 nm high. A combined TERS map (Figure 3c) collected at 785 nm laser excitation shows the intensity distribution of the three same $Ti_3C_2T_x$ Raman peaks as in Figure 2c: ~126 cm^{-1} band (green color), 201 cm^{-1} band (blue color), and 725 cm^{-1} band (red color). TERS spectra plotted in Figure 3d shows the contrast between the dominant out-of-plane A1g ($Ti_3C_2T_x$) vibration in the flat area and the dominance of the two resonant A1g (C) and Eg vibrations over the wrinkles. In addition, it should be noted that the main A1g ($Ti_3C_2T_x$) peak shifts from 201 to 202–203 cm^{-1} over the wrinkles. From previous studies in graphene and graphene oxide deposited on gold, nanoscale wrinkles may feature increased TERS response due to improved coupling of the in-plane carbon modes (D, G, and 2D) to the optical field in the tip–sample gap in vertical walls of the wrinkles [16]. In our case, we observe simultaneous enhancement of both the in-plane Eg mode at 126 cm^{-1} and the out-of-plane A1g (C) mode at 725 cm^{-1}, which indicates that the TERS enhancement mechanism in the case of the wrinkles in MXenes is different from the one observed in graphene and graphene oxide. It has been reported earlier that MXenes with their metallic nature may support surface plasmon resonances in the visible and near-infrared range. The transversal surface plasmon resonance being around 780 nm, the resonant Raman conditions in $Ti_3C_2T_x$ are met when using the 785 nm excitation. The mechanical deformation at the wrinkles may induce sharper or more intense plasmonic resonance (versus the adjacent flat material) and results in enhanced intensities of the two resonant 126 and 725 cm^{-1} modes. Comparison with TERS map (data not shown here) collected at 830 nm displaying lower (three times in peak height) intensity of the 725 cm^{-1} band further confirms the resonance effect observed at 785 nm.

An improved synthetic method can produce flakes with highly stoichiometric Ti_3C_2 composition. Figure 4a shows an example of these flakes and one can notice the cleanliness of the edges compared to the T_iO_2 particles surrounding the edges of the above studied $Ti_3C_2T_x$ flakes. This is due to removal of salts through rinsing. In addition, such “cleaner” flakes feature a longer lasting TERS signal. The batches that did not undergo thorough rinsing lost TERS activity within about a week in ambient after deposition, way before significant morphological changes occurred in the deposited flakes, which makes TERS a useful tool for monitoring the early stages of Ti_3C_2 degradation. The stability of the cleaned MXene samples has thus been examined by collecting AFM topography images and TERS spectra from the same group of monolayer flakes every 10 days for 2 months.

The sample was stored in a glass Petri dish under ambient conditions (~21°C), without direct exposure to the sunlight. As we can see from Figure 4a–d, after two months in ambient conditions, a slightly elevated (about 1 nm or less) borderline of the crystals was found, indicating potential oxidation and/or hydrolysis along the edges due to the exposure to ambient oxygen and humidity. Nonetheless, the monolayer crystals are still clearly visible, their morphology did not change, and all main Raman features are observed in their TERS spectrum (Figure 4d).

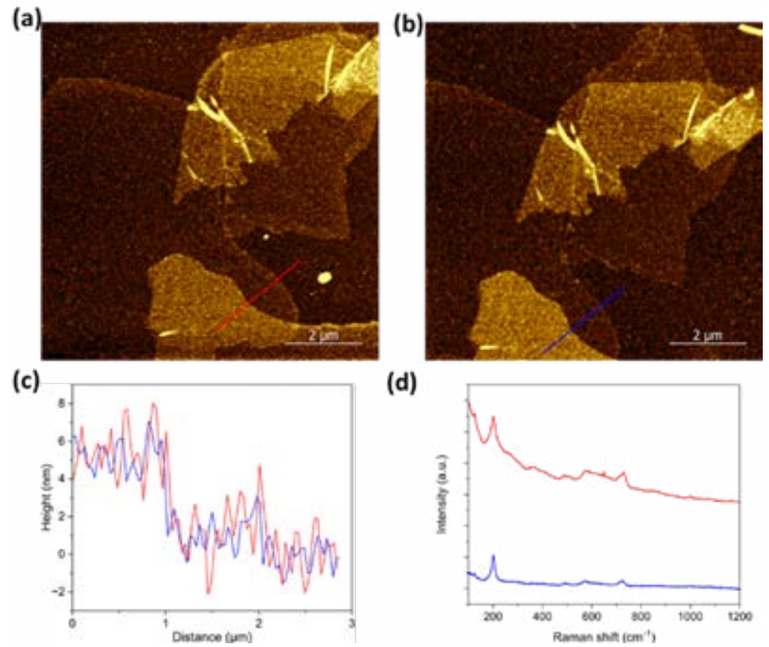

Figure 4: (a,b) Topographic images and corresponding AFM line scans of the same area taken immediately after deposition and (c) after 2 months of storage. (d) TERS spectra averaged over several locations on the monolayer flakes taken right after deposition (blue spectrum) and after 2 months of storage (red spectrum). The TERS activity of the monolayers was preserved after two months under ambient conditions and no significant morphological changes in the crystals were found. Difference in the background intensity of TERS spectra is due to varying plasmonic response of the TERS probes utilized for the corresponding measurements over an extended period of time.

« PREVIOUS

NEXT »

Home Introduction Stories Scientific Papers Applications Multimedia Contact

HORIBA Scientific

TERS characterization of single- to few-layer $Ti_3C_2T_x$, cont.

Conclusions and perspectives

This note shows that TERS can be used to image, with nanoresolution, single- to few-layer thick flakes of Ti3C2Tx MXene deposited on gold substrate.

It is observed that the relative intensity of the Eg peak at 126 cm-1 and A1g (C) peak at 725 cm-1, as compared to the intensity of the 201 cm-1 peak, increases with thickness. This observation can be used to differentiate monolayers from the few-layer thick flakes based on their TERS spectra. Special TERS response from nanowrinkles in $Ti_3C_2T_x$ was observed: both the absolute and relative intensities of 126 and 725 cm-1 bands were increased as compared to the adjacent flat area. Finally, we showed that the intensity of the TERS signal from the MXene crystals can be used for monitoring the early stages of degradation in ambient conditions.

References

1. M. Naguib, V.N. Mochalin, M. W. Barsoum, and Y. Gogotsi, Y. Adv. Mater. 26, 992–1005 (2014).
2. A. Bhat, S. Anwer, K.S. Bhat, et al., npj 2D Mater Appl 5, 61 (2021).
3. Anasori, B., Lukatskaya, M. R. & Gogotsi, Y. Nat Rev Mater 2, 16098 (2017).
4. XH. Zha, Q. Huang, J. He, et al. Sci Rep 6, 27971 (2016).
5. M. Han, K. Maleski, C. E. Shuck, et al., J. Am. Chem. Soc., 142, 19110–19118 (2020).
6. B. Anasori, C. Shi, E.J. Moon et al., Nanoscale Horiz., 1, 227–234 (2016).
7. J. L Hart, K. Hantanasirisakul, A. C. Lang, et al., Nat. Commun., 10, 522 (2019).
8. P.-H. Tan, Raman spectroscopy of Two-Dimensional Materials, Springer Series in Materials Science, vol 276, Singapore (2019).
9. A. Sarycheva, Y. Gogotsi, Chem. Mater., 32, 3480–3488 (2020).
10. N. Kumar, B.M., Weckhuysen, A.J.., Wain, et al., Nat Protoc 14, 1169–1193 (2019).
11. References in Correlated TERS, TEPL and SPM measurements of 2D materials HORIBA application note (2020)
12. Gadelha, A.C., Ohlberg, D.A.A., Rabelo, C. et al., Nature 590, 405–409 (2021).
13. T. P. Darlington, C. Carmesin, M. Florian, et al., Nat. Nanotechnol., 15, 854–860 (2020).
14. A. Sarycheva, M. Shanmugasundaram, A. Krayev, and Y. Gogotsi, ACS Nano, 16, 4, 6858–6865 (2022).
15. T. S. Mathis, K. Maleski, A. Goad et al., ACS Nano, 15, 6420–6429 (2021).
16. A. Bhattarai, A. Krayev, A. Termiyazev, et al., Nano Lett., 18, 4029–4033 (2018).

« PREVIOUS

NEXT »

Home Introduction Stories Scientific Papers Applications Multimedia Contact

HORIBA Scientific

Tip Enhanced Raman Spectroscopy (TERS) has emerged as a powerful analytical technique...

TERS characterization of graphene nanoribbons

Ophélie Lancry, Agnès Tempez, Marc Chaigneau
HORIBA FRANCE SAS, Palaiseau, France

Abstract

This application note reports on the TERS nanocharacterization of graphene nanoribbons (GNRs) fabricated by electron beam lithography. The chemical nanoresolution achievable by TERS reveals the presence of amorphous carbon at the edge of the GNRs and locates organic residues. TERS can be considered as a valuable tool for characterizing nanopatterned graphene, an essential step for the development of graphene-based nano-devices.

Keywords

Graphene, Nanoribbons, Nanopatterning, Tip Enhanced Raman Spectroscopy.

Context and issues

No need to recall the exceptional properties of graphene which has driven tremendous research since Novoselov's scotch tape experiment [1-2]. Graphene is thus now foreseen for a handful of electronic and optoelectronic nano-devices [3]. Making nano-devices out of graphene requires nanopatterning. With a sub-10 nm resolution, electron beam lithography (EBL) is an option but it can generate defects and contamination [4-6]. As a result, determining the quality of patterned graphene is essential and detection of defects demands a sensitive chemical nanocharacterization tool.

Potential/ Input from technique

Tip Enhanced Raman Spectroscopy (TERS) has emerged as a powerful analytical technique providing high chemical sensitivity for surface molecular imaging with a nanoscale spatial resolution [7-10]. TERS enables characterization of nanopatterned graphene and reveals the presence of defects and impurities left by the resist, which could result in an unwanted doping effect and lower carrier mobility.

Starting point, what is known?

TERS has been successfully used to characterize a variety of graphene properties, such as number of layers, local strain, edge, surface adsorbates [10], and artificial defects.

Description of sample and measurement

Using natural graphite crystals and mechanical exfoliation method, monolayer graphene flakes were isolated on SiO_2 (≈300 nm)/ Si substrate. Then flakes have undergone the following process steps (schematically illustrated in Figure 1) to produce graphene nanoribbons:

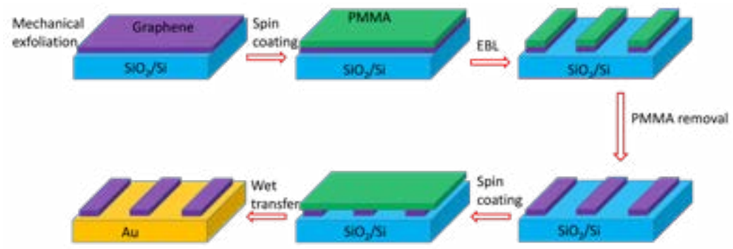

Figure 1: Schematic diagram of fabrication steps of GNRs and their transfer from SiO_2 / Si substrate to Au coated SiO_2/Si substrate.

- Electron resist (PMMA) deposition: spin coating and baking;
- EBL: beam exposition, development of exposed regions (in solvent), removal of non-protected graphene using oxygen plasma. The protecting PMMA mask is then removed in acetone and the sample is dried: GNR with a width of about 60±5 nm, a length of >100 µm and an interdistance of 140 nm are created on SiO_2 / Si substrate;
- Transfer of GNR on gold-coated substrate by wet method: Spin coating of 200 nm thick PMMA, baking, taping of frame (windowed on GNR region), KOH dipping to detach GNR from SiO_2 / Si, application on a 100 nm Au coated substrate, PMMA removal, and annealing to reduce PMMA residues.

NEXT »

Applications

TERS characterization of graphene nanoribbons, cont.

TERS measurements were performed in gap mode using a NanoRaman system from HORIBA Scientific integrating an atomic force microscope (OmegaScope, based on SmartSPM) and a Raman microscope (LabRAM Evo) with a 100× WD objective tilted by 60° with respect to the sample plane. A 638 nm p-polarized laser (130 µW) was focused onto the cantilever-based gold-coated AFM-TERS tip (OMNI TERS-SNC-Au, App Nano). Transition between the pixels of the TEPL map is performed in alternating contact mode, which preserves both the sharpness and plasmonic enhancement of the tip, eliminating lateral forces that might otherwise result in sweeping aside or picking up loosely attached contaminants from the sample surface.

First, AFM topography and phase images are measured to locate GNRs. As shown in Figures 2a and 2b, GNRs are not clearly seen in the topography image due to the high roughness of the gold surface (RMS ≈1.0 nm) but a nice contrast in the phase image enables measurement of GNR width to be 57.2 ± 8.4 nm, which agrees well with the designed width of 60 nm.

Next, a TERS spectrum is collected in the interior of the GNRs. As shown in Figure 2c, the spectrum features the G peak (~1585 cm^{-1}) corresponding to the E_{2g} phonon at the centre of the Brillouin zone and the 2D peak (~2637 cm-1, overtone of the D peak) originating from scattering of the electron by two phonons having momentums q and -q [11]. The 2D peak is fit with single Gaussian peak with a width of 42 cm-1 which indicates the monolayer nature of the GNRs [11].

TERS mapping was conducted in the marked area of Figures 2a and 2b, with scanning area of 600×300 nm^2 and a pixel size of 5 nm. The Raman intensity maps of the D, G and 2D modes are shown in Figures 2d, 2e, and 2f, respectively upon fitting with three Lorentzian curves at ~1340, ~1585, and ~2637 cm^{-1}.
TERS D peak intensity profile extracted from the line marked in Figure 2d is shown in Figure 2g to estimate the TERS spatial resolution. A fitted Gaussian peak exhibits a width of 5 ± 0.4 nm, which means, given the 5 nm pixel size, that resolution is limited by the sampling step and could be better than 5 nm (reported values as low as 1 nm for graphene 10,12-13] and graphene oxide [14]).

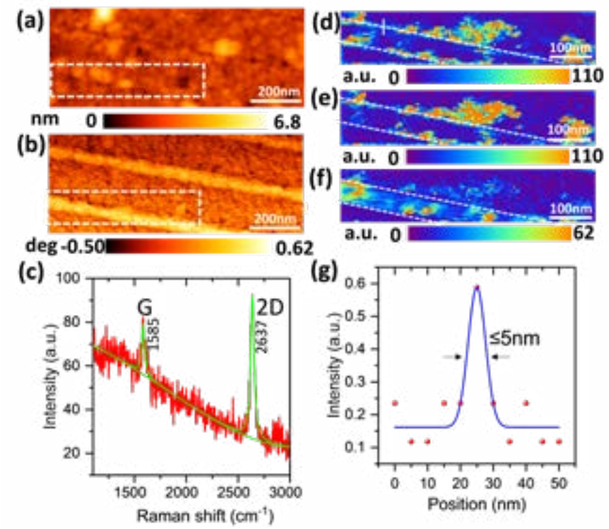

Figure 2: AFM topography (a) and phase (b) images of GNRs; (c) TERS spectrum measured in the GNR centre fitted by two Lorentizan functions; (d) D (e) G and (f) 2D TERS images of the GNR in marked regions of (a)-(b) 120×60 pixels, pixel size: 5 nm, exposure time: 0.7 s; (g) The typical spatial resolution obtained by fitting the line profile along the marked line in (c) using a Gaussian function.

Higher D and G signals are observed on the edge of the nanoribbon where 2D intensity is higher in the inner part. The D peak (~1340 cm^{-1}), which arises from the TO phonons around the K point of the Brillouin zone and requires scattering by a defect in order to maintain the conservation of momentum is an indication of the defect density. The EBL process splits the graphene flake into nanoribbons with large length/width ratio and induces the formation of high density of defects at the cutting interface, i.e. GNR edges [4]. A high D peak intensity is usually observed on the edges of mechanically exfoliated [11-12], or chemical vapor deposition grown graphene flakes. However, if one looks at spectra (1-5) taken on a line across the GNR edge from the substrate to the inner GNR (in the zoomed region in Figure 3a), further information can be extracted. Spectra 2 and 3 taken on the GNR edge not only feature enhanced D and G peak signals, but also no 2D peak.

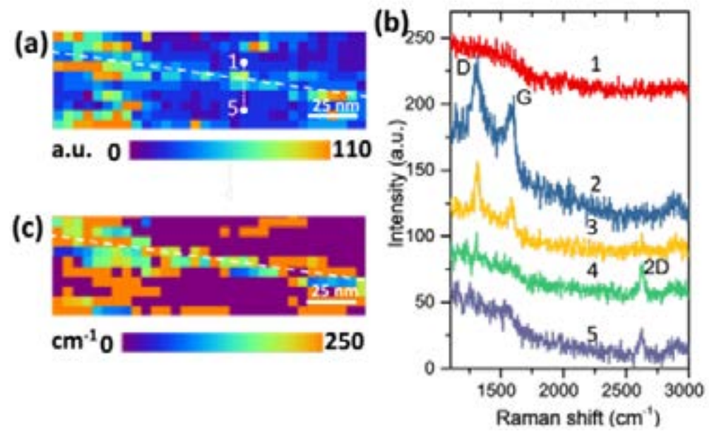

Figure 3: TERS D peak intensity (a) and width (b) images of an area at the GNR edge in Figure 2(c); (c) Five TERS spectra along the marked line in (a).

« PREVIOUS
NEXT »

TERS characterization of graphene nanoribbons, cont.

Furthermore, the width of both D (width going from 38 to 86 cm^{-1}) and G (width going from 28 to 66 cm^{-1}) bands increases going from spectrum 3 to spectrum 2 whilst approaching the GNR edge. This is in contrast with what is observed at the edge of mechanically exfoliated monolayer graphene [12] and indicates the presence of a disordered graphene phase [15]. This implies that upon EBL, a band of damaged graphene (amorphous/disordered graphene) of a width of 5-10 nm is induced due to high energy electron bombardment.

The presence and local distribution of organic contamination have also been analyzed by plotting the 2890 cm^{-1} Raman band (stretching vibration C-CH_3) and upon fitting it with a single Lorentzian function. The TERS intensity image (Figure 4a) indicates the presence of organic adsorbates on spots in both GNR and substrate areas. Four spectra are plotted in Figure 4b on four locations featuring high intensity of the 2890 cm-1 Raman band: two in GNR area (P1-P2), two on the substrate (P3-P4). The presence of C-CH3 signature indicates the presence of organic contaminants on the GNR samples, which most likely comes from the PMMA residues during the resist deposition process or/and the Si/SiO2 to Au transfer substrate step.

Conclusion and perspectives

This application note shows how TERS imaging can reveal the presence and the location of defects or contamination induced upon nanopatterning of graphene using EBL. The spatial resolution achieved by TERS imaging of the EBL-fabricated GNRs of a width of ~60 nm is better than 5 nm. Damage along the GNR edge as a result of electron bombardment is observed under the form of amorphous carbon with a thin width (5-10 nm). Organic contaminants originating from PMMA residues can be seen within the GNR or attached to the edge.

Such degradation (amorphous carbon or adsorbates) can not be solely visualized by the AFM topography or phase imaging, which makes TERS a powerful tool for characterizing patterned graphene to develop graphene based nano-devices.

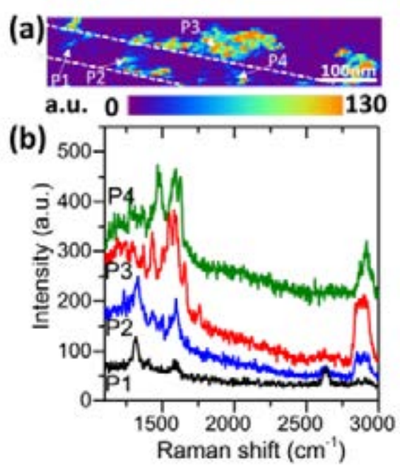

Figure 4: (a) TERS intensity image of the C-CH_3 band at ~2900 cm^{-1}. (b) Four TERS spectra collected at marked positions P1-P4 in (a).

Acknowlegdments

Weitao Su from Hangzhou Dianzi University and Naresh Kumar from ETH Zurich are thanked for insightful scientific discussions regarding data analysis and interpretation of results.

References

1. P. Avouris, Graphene: Electronic and Photonic Properties and Devices, Nano Lett., 10, 11, 4285–4294 (2010).

2. K. S. Novoselov, A.K. h Geim, S. K. Morozov, D. Jiang, Y. Zhang, S. V. Dubonos, I. V.; Grigorieva, A. A. Firsov, Electric Field Effect in Atomically Thin Carbon Films, Science, 306, 666-669 (2004).

3. Wang, R., Ren, XG., Yan, Z. et al. Graphene based functional devices: A short review. Front. Phys. 14, 13603 (2019).

4. Jiyu Fan, J.M. Michalik, L. Casado, S. Roddaro, M.R. Ibarra, J.M. De Teresa, Investigation of the influence on graphene by using electron-beam and photo-lithography, Solid State Communications, 151, 21, 1574-1578, (2011).

5. I.-S. Byun, D. Yoon, J. S. Choi, I. Hwang, D. H. Lee, M. J. Lee, T. Kawai, Y.-W. Son, Q. Jia, H. Cheong, B. H Park, Nanoscale Lithography on Monolayer Graphene Using Hydrogenation and Oxidation, ACS Nano, 5, 8, 6417–6424 (2011).

6. B . H. Son, H. S. Kim, H. Jeong, Ji-Yong Park, S. Lee, Y. H. Ahn, Electron beam induced removal of PMMA layer used for graphene transfer, Sci Rep 7, 18058 (2017).

7. A. Bhattarai, A. Krayev, A. Temiryazev, D. Evplov, K. T. Crampton, W. P. Hess, P. Z. El-Khoury, Nano Lett., 18, 6, 4029–4033 (2018).

8. R. Beams, Tip-enhanced Raman scattering of graphene, J. Raman Spectrosc., 49: 157– 167 (2018).

9. N. Kumar, B. Stephanidis, R. Zenobi, A. J. Wain, D. Roy, D., Nanoscale Mapping of Catalytic Activity Using Tip Enhanced Raman Spectroscopy, Nanoscale, 7, 7133-7137 (2015).

10. J. Stadler, T. Schmid, R. Zenobi, Nanoscale Chemical Imaging of Single-Layer Graphene, Acs Nano, 5, 8442-8448 (2011).

11. A.C. Ferrari, J. C. Meyer, V. Scardaci, C. Casiraghi, M. Lazzeri, F. Mauri, S. Piscanec, D. Jiang, K. S. Novoselov, S. Roth, and A. K. Geim, Raman Spectrum of Graphene and Graphene Layers, Phys. Rev. Lett., 97, 187401-187405 (2006).

12. W. Su, N. Kumar, N. Dai, D. Roy, Nanoscale Mapping of Intrinsic Defects in Single-Layer Graphene Using Tip Enhanced Raman Spectroscopy. Chem. Commun., 52, 8227-8230 (2016).

13. K.-D. Park, M. B. Raschke, J. M. Atkin, Y. H. Lee, M. S. Jeong, Probing Bilayer Grain Boundaries in Large-Area Graphene with Tip Enhanced Raman Spectroscopy, Advanced Materials, 29, 1603601 (2017).

14.W. Su, N. Kumar, A. Krayev, M. Chaigneau, In Situ Topographical Chemical and Electrical Imaging of Carboxyl Graphene Oxide at the Nanoscale. Nature Communications, 9, 2891 (2018).

15. A. Jorio, R. Saito, G. Dresselhaus, M.S. Dresselhaus, Raman Spectroscopy in Graphene Related Systems, Wiley-VCH. https://doi.org/10.1002/9783527632695 (2011).

« *PREVIOUS*

Home Introduction Stories Scientific Papers Applications Multimedia Contact

Tip Enhanced Raman Spectroscopy (TERS) has emerged as a powerful analytical technique providing high chemical sensitivity...

Correlated TERS and KPFM of graphene oxide flakes

Weitao Su[1], Naresh Kumar[2], Andrey Krayev[3] , Jana Kalbacova[4] & Marc Chaigneau[5]

[1]Hangzhou Dianzi University, Hangzhou, China. [2]National Physical Laboratory, Hampton Road, Teddington, UK [3]HORIBA Instruments Incorporated, Novato, USA. [4]HORIBA Jobin Yvon GmbH, Bensheim, Germany [5]HORIBA France, Palaiseau, France

Abstract

AFM-Raman and its TERS mode are used to show nanoscale surface mapping of structural defects and chemical groups on graphene oxide (GO) flakes with 10 nm spatial resolution. TERS mapping is combined with Kelvin probe force microscopy (KPFM) measurements for simultaneous topographical, electronic and chemical imaging of GO surface. The multi-parameter measurement methodology proposed in this note extends the capability of TERS allowing a direct correlation of local chemical composition and physical properties at the nanoscale not only for 2D materials but for almost any sample surface.

Keywords

Graphene oxide (GO), Tip Enhanced Raman Spectroscopy (TERS), Kelvin Probe Force Microscopy (KPFM), correlated measurements

Context and issues

Visualizing the distribution of structural defects and functional groups present on the surface of two-dimensional (2D) materials, such as graphene oxide challenges the sensitivity and spatial resolution of most advanced analytical techniques. Here we demonstrate mapping of functional groups on a carboxyl-modified graphene oxide (GO–COOH) surface with a spatial resolution of ≈10 nm using Tip Enhanced Raman Spectroscopy (TERS).

Potential/ Input from technique

Tip Enhanced Raman Spectroscopy (TERS) has emerged as a powerful analytical technique providing high chemical sensitivity for surface molecular mapping with nanoscale spatial resolution under ambient conditions. In TERS, a metallic scanning probe microscopy (SPM) probe placed at the focal point of a laser undergoes localized surface plasmon resonance (LSPR), which together with the lightening rod effect leads to the enhancement and confinement of the electric field at the TERS probe apex. This effect simultaneously improves the sensitivity, as well as the spatial resolution of Raman microscopy by enhancing the Raman signal from analyte molecules directly underneath the TERS probe. Furthermore, we take the surface characterization a step further by combining TERS with Kelvin probe force microscopy (KPFM) and thus demonstrate in situ topographical, chemical and electrical nanoscopy of a GO–COOH surface.

Starting point, what is known?

Carboxyl graphene oxide samples consist mostly of carbon and oxygen as well as different functional groups: C–O–C, C–O, C–CH3, C=O, COOH and C–H. With Raman spectroscopy the typical signature bands of graphitic material can be observed at ~ 1350 cm^{-1} (D band) and at ~ 1590 cm^{-1} (G band). Whereas the G band, representing the tangential stretch of the carbon atoms, is present in all graphitic substances, the D band appears only in the presence of defects. Thus, with D/G band intensity ratio (ID/IG) a relative defect concentration can be established. The differentiation of functional groups can be accomplished via specific band positions corresponding to different bonds (see Table 1 for detailed description).

Raman band position (cm^{-1})	Tentative assignment
1097	C–O (νs, C–O)
1179	C–O–C (νs, C–O–C)
1330	C–CH3 (δs, C–CH3)
1420	C–H (β, C–H)
1654	C=O (νs, C=O)
1747	COOH (νs, COOH)

νs: symmetric stretching mode, β: bending mode, δs: symmetric deformation mode

Table 1. Tentative assigment of Raman bands from carbon-containing bonds.

NEXT »

Applications

Correlated TERS and KPFM of graphene oxide flakes, cont.

Description of sample and measurement

The GO–COOH samples measured in this work by TERS were prepared by spin-coating GO–COOH (ACS Material, USA) on a Au coated glass substrate. A NanoRaman™ system combining an Atomic Force Microscope (SmartSPM, HORIBA Scientific) with a Raman spectrometer (XploRA, HORIBA Scientific) is used in side illumination/collection (objective lens ×100, NA=0.7). The p-polarized 638 nm laser light is focused onto the apex of the gold TERS tip, allowing simultaneous SPM and spectroscopic Raman measurements at the same location of the sample.

To perform a detailed chemical analysis of the sample, a 1 × 1 µm² area was mapped. TERS spectra were collected 10 nm apart with acquisition time of 400 ms. Mapping of several flakes of carboxyl graphene oxide is presented in Figure 1. The areas with few layer flakes that cannot be easy identified in the topographic image, become clearly visible in the TERS maps of D band and G band. Furthermore, analyzing all 10,000 TERS spectra helps to identify the functional carboxyl groups, and thus to spatially locate them at the nanometer scale with the TERS maps.

For further investigation, TERS mapping followed by Kelvin probe microscopy mapping was performed on an area of 2.5 x 1.7 µm² including a carboxyl graphene oxide flake. For TERS mapping the step size was 16.7 nm and acquisition time 75 ms. Figure 2 displays the ID/IG ratio as well as the contact potential difference (CPD). The graph in Figure 2 which plots CPD versus ID/IG ratio for a number of points in the mapped area highlights the inverse correlation between surface potential and ID/IG ratio. In other words high ID/IG relates with highly negative CPD.

Conclusion and perspectives

In summary, we have demonstrated nanoscale TERS mapping of structural defects and functional groups present on a GO–COOH surface with an unprecedented spatial resolution of ≈10 nm. Furthermore, we have pushed nanoscale surface characterisation a step forward by demonstrating in situ electrical and chemical nanoscopy of a GO–COOH sample by combining TERS with KPFM. This in situ multi-parameter measurement methodology greatly extends the capability of TERS allowing a direct correlation of local topography, chemical composition and electronic properties at the nanoscale not only in 2D materials but on almost any sample surface. In particular, we expect this work to open up the possibility of optimising optoelectronic devices based on novel 2D materials such as graphene, GO, single-layer MoS_2 via non-destructive, simultaneous and nanoscale multi-parameter characterisation of their surface properties even under operational conditions.

« *PREVIOUS*

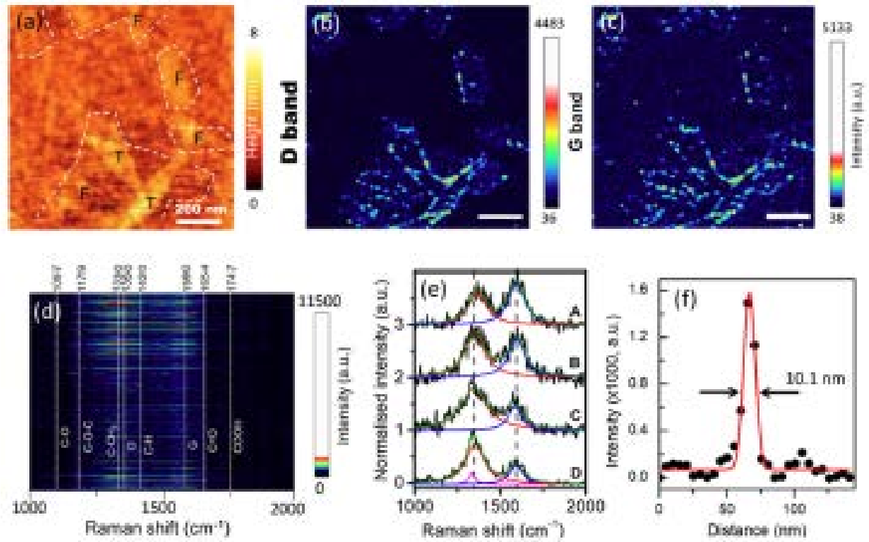

Figure 1: TERS mapping of GO-COOH flakes: topographic image with outlines of few layer (F) and thick layer (T) flakes (a), TERS maps of the D band (b) and G band (c), all measured TERS spectra are stacked with designated signature positions of the COOH functional groups (d), example of GO spectra with different ID/IG ratios (e), and example of spatial resolution D band profile across the edge of a flake (f).

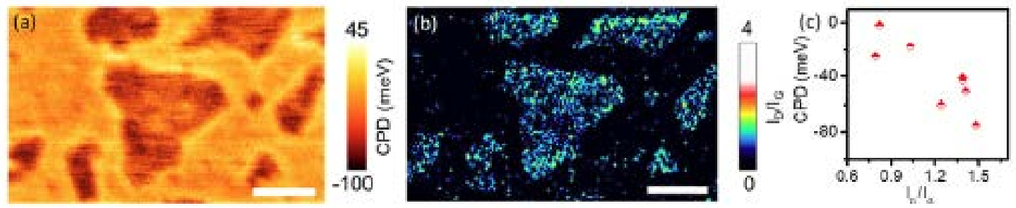

Figure 2: In-situ electrical and chemical TERS mapping of GO-COOH flakes: contact potential difference value (CPD) (a), TERS map of ID/IG ratio (b), and graph plotting CPD value as a function of corresponding ID/IG ratio for a selection of points in the mapped area (c).

Bibliography

Su, W., Kumar, N., Krayev, A., & Chaigneau, M. “In situ topographical chemical and electrical imaging of carboxyl graphene oxide at the nanoscale”, Nature communications, 9(1), 2891 (2018).

...nanomaterials have been introduced to mimic the interactions between nanoparticles (NPs) and cellular membranes and better understand their toxicity on human health.

TERS characterization of phospholipid bilayers and detection of nanoparticles

A. Tempez[1], P. Burgos[2], A. Holland[2], M. Chaigneau[1]
[1]HORIBA FRANCE SAS, Palaiseau, France, 2HORIBA UK Ltd, Northampton, UK.

Abstract

This application note reports on TERS characterization of binary phospholipid bilayer systems deposited onto a gold coated coverslip. Such samples are used as model samples for directly and chemo-selectively visualizing the distribution of a lipid constituent at the nanometer scale. In addition, nanomaterials have been introduced to mimic the interactions between nanoparticles (NPs) and cellular membranes and better understand their toxicity on human health. The sensitivity of TERS for the detection and identification of NPs in phospholipid bilayers is demonstrated down to femtomolar concentration with a spatial resolution down to 7 nm. A specific liquid cell has also been developed to permit TERS measurements in solution and results of graphene oxide containing samples are presented.

Keywords

TERS, Raman spectroscopy, phospholipid bilayers, nanoparticles, nanomaterials risk assessment, nanomaterials toxicity, cells, membranes, graphene.

Context and issues

Nanomaterials (NMs) have gained prominence in technological advancements due to their tunable physicochemical properties, electrical and thermal conductivity, catalytic activity, light absorption, etc., with enhanced performance over their bulk counterparts. Despite their unique advantages and applications in both domestic and industrial sectors, the unpredictability of how nanoparticles behave at the nanoscale presents a double-edged sword and has raised the issue, as with any new material, of possible human health impacts. Due to the growth in the production of NMs and their increasing use in industrial applications, issues relating to their potential toxicity are inevitable. When nanoparticles are released into the environment, the cell membrane represents an initial interaction site for eukaryotic cells. Phospholipid bilayers which are the major constituents of membranes act as a barrier of selective permeability and carry out other specific roles in the cell. Studying the interactions between nanoparticles and cellular membranes requires a molecular chemical probe with nanometer resolution capability.

Potential/Input from technique

Raman spectroscopy is a non-destructive and non-labelling technique which provides detailed information about chemical structure as it detects characteristic molecular vibration frequencies. But Raman microscopy fails to image nano-objects such as nanoparticles or lipid domains at the nanometer scale due to the optical diffraction limit. Tip Enhanced Raman Spectroscopy (TERS) which provides nanoscale chemical mapping represents a promising tool for directly and chemo-selectively visualizing the distribution of a lipid constituent at the nanometer scale in bilayers and hence the presence and arrangement of nanoparticles inside the bilayers.

Starting point, what is known?

While TERS has become a tool of choice to characterize 2D materials [1-2] (e.g. graphene and transition metal dichalcogenides) and nanoparticles [3], it has been also successfully used to study biological samples including cells [4], viruses [5], proteins [6] and biomembranes [7]. A recent publication [8] from the group of Zenobi demonstrates TERS capability to probe the molecular organization of supported dipalmitoylphosphatidylcholine (DPPC) monolayers on Au (111) and highlights the correlation of topography and nanoresolved Raman response.

NEXT »

Applications

TERS characterization of phospholipid bilayers and detection of nanoparticles, cont.

In this application note, we report on TERS measurements carried out on binary (DPPC/Cholesterol and 1,2-Dimyristoyl-sn-glycero-3-phosphoethanolamine (DMPE)) phospholipid bilayer systems (Figure1). Such systems are closer models to biomembranes compared to monolayers of one lipid molecule. As a first step such samples were characterized by TERS. Then they are injected with nanoparticles to test their potential interaction and impact on molecular arrangement of membranes lipids. Measurements were carried out in air first and then in water, the ultimate goal being to be able to characterize nanoparticles within a lipid bilayer in water to closely mimic behavior of the transport nanomaterials across the membranes of eukaryotic cells.

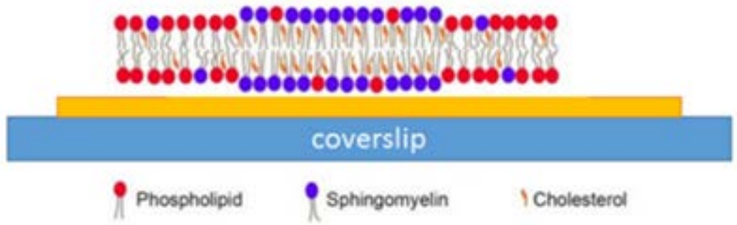

Figure 1: Schematic diagram of supported bilayers on gold coated glass coverslip.

Description of sample and measurement

The bilayer models were prepared using the Langmuir trough technique, with lipids deposited onto a gold coated coverslip at pressures between 25 and 30 mN/m.

TERS measurements were performed with either an XploRA Nano system or a LabRAM HR Nano system (both HORIBA Scientific, France) both combining a state-of-the art scanning probe microscope (OmegaScope) with a true confocal Raman micro-spectrometer. The laser excitation (red: 638 nm (XploRA) or 633 nm (LabRAM), 90 µW, p-polarized) is incident on the sample at an angle of 60° with respect to the sample plane. The laser light was focused using a 100× objective (NA=0.7) mounted on a piezo scanner for precise positioning and focusing of the Raman laser spot at the apex of the probe tip. The TERS probes were cantilever-based gold or silver coated AFM-TERS tips (OMNI TERS-SNC-Au/Ag, App Nano for HORIBA Scientific). Silver tips were used for air measurements whereas gold tips were used for liquid measurements as silver suffers from greater oxidation in water.

TERS maps were recorded together with topography scans using the patented Spec-Top™ mode: for each pixel a Raman spectrum is acquired with tip in direct contact with the surface with a typical interaction force of 2-10 nN. In between two pixels of the map, the sample moves in semi-contact mode to preserve the sharpness and plasmonic enhancement of the tip.

Cholesterols play key roles in controlling molecular fluidity in a biological membrane. A bilayer made of a mixture of DPPC and cholesterol is a more realistic membrane model than a homogeneous phospholipid bilayer. Cholesterol contains a short, thermally flexible, hydrocarbon tail with a rigid hydrophobic ring structure that is attached to a small, hydroxyl group that acts as a hydrophilic head. Due to this smaller hydrophilic head and smaller hydrophobic tail cholesterol always fits in between the lipids in a bilayer.

Since cholesterol and DPPC have close Raman signatures, a sample was prepared with deuterated DPPC ($DPPC_{d62}$ with a deuterated chain) and non deuterated cholesterol (ratio of 3DPPC for 1 chol). It then becomes simple to distinguish C-D bonds vibrations from DPPC from C-H stretching modes from cholesterol (C-D vibrations occur at lower wavenumbers than C-H).

Figure 2 shows several recorded TERS images (750 ms/pixel; 33 nm/pixel) overlaid on the AFM image. The blue and green bands between 2000-2500 cm^{-1} are associated with the CD_2-CD_3 stretching of DPPC while the 3000 cm^{-1} bands correspond mainly to cholesterol (red on map).

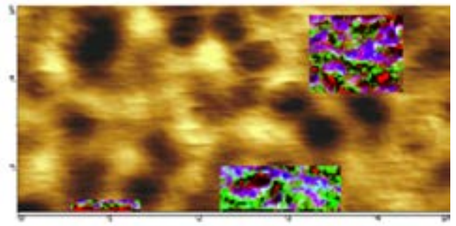

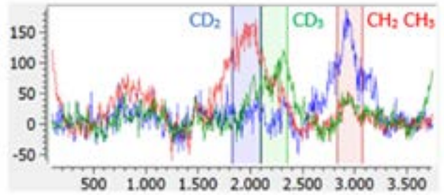

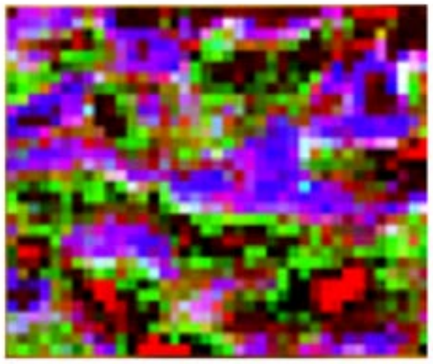

Figure 2:

(a) TERS maps of deuterated DPPC/Chol bilayers overlaid on AFM topographic image.

(b) Raman spectra defining cholesterol CH_2CH_3 band (red), and deuterated DPPC CD_2 band (blue), and CD_3 band (green).

(c) Zoom of top right TERS map.

« PREVIOUS
NEXT »

Applications

TERS characterization of phospholipid bilayers and detection of nanoparticles, cont.

It should be noted that the blue regions reveal areas where CD_2 bonds are preferentially excited while in green domains CD_3 bonds are more active. This is consistent with different orientation of the bonds, possibly related to the fluidity of the bilayers, since Raman signal intensity depends on the alignment of the laser polarization with the bonds, i.e. when they are parallel the signal is highest. Additionally, the formation of small (≈20-100 nm) nano-domains, enriched in cholesterol and localized preferentially in areas where the CD_2 bonds are excited is observed. These images clearly demonstrate the sensitivity of TERS to detect lipid bilayers.

Next lipid bilayers have been exposed to graphene oxide (GO) nanoparticles to explore interactions between them. As biosensor and drug delivery system candidates, the behavior of graphene materials in contact with cell membranes needs to be understood.

A 50 µl droplet of a picomolar suspension of GO in water was deposited onto a 3:1 ratio DPPC Cholesterol bilayer. This volume and concentration were selected to ensure a monolayer coverage of about 8.5%. The sample was left in air for 2 hours and then analyzed: Figure 3a shows three TERS maps on top of the topographic AFM image acquired with a laser power of 90 µW and acquisition time of 800 µs. Three spectra from single pixels of the TERS maps at locations shown in Figure 3b are depicted in Figure 3c. While the topography is similar to the non-GO exposed sample and does not evidence the presence of GO, the occurrence in pixel spectra of the D and G bands from GO and CH stretching bands from Chol and DPPC indicates that GO is able to cross the phospholipid membrane in 2 hours and is no longer lying on top of the lipid bilayers.

As shown in Figure 3c, signature bands are associated with a color for GO, Chol, DPPC/Chol which are G band (green), 1800 cm^{-1} shoulder (red) and 2900 cm^{-1} CH_3CH_2 (blue), respectively. Brown (mix of red and green) nano-areas indicate the presence of GO in cholesterol enriched phases while cyan (mixture of blue and green) nano-areas indicate the presence of GO in DPPC enriched phases. In a higher resolution map (not shown here) spectra from points distant by less than 7 nm exhibit D and G bands intensity variation of more than a factor of 5. Such a local GO concentration gradient clearly supports the fact that TERS, a non-labelled technique, can achieve a spatial resolution of only 7 nm.

After recording each TERS map, a scan of the tip is also acquired. The absence of any Raman peak in G-band spectral region confirms that there was no carbonaceous contamination on the tip and the laser power used is low enough to avoid burning the sample.

TERS is a suitable technique to detect the presence of femtomolar GO inside bilayers.

Finally, some preliminary data were obtained on bilayers in pure water. Pure water approaches the physiological environment of membrane cells since the assembly and stability of synthetic phospholipids bilayers is primarily driven by the hydrophobicity of the amphiphilic molecules. TERS in liquid is quite challenging in terms of laser-tip alignment and signal collection. Several hardware and procedure adjustments have been developed and details can be found in the **"AFM-TERS measurements in a liquid environment with side illumination/collection"** technical note in which CNT TERS mapping is reported.

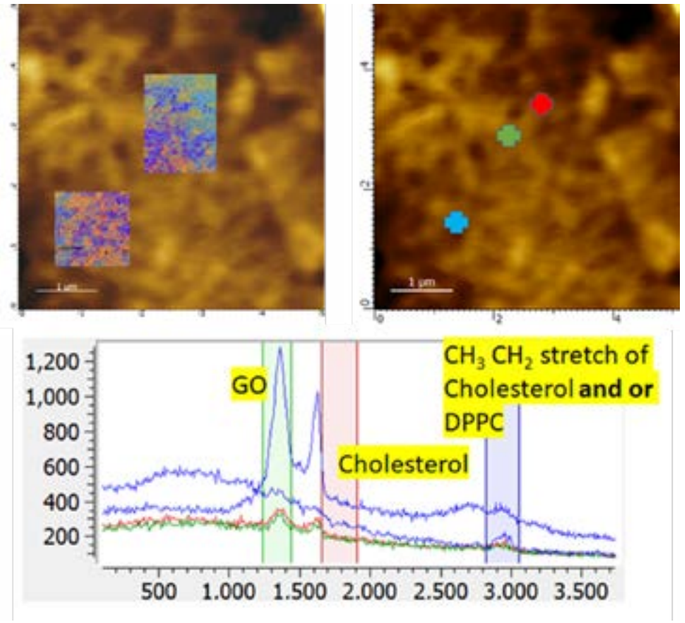

Figure 3: (a) TERS maps of DPPC/Chol bilayers and graphene oxide overlaid on an AFM topographic image. (b) topographic AFM scan of same area locating three cursors from which Raman spectra are extracted and displayed in (c).

« PREVIOUS

NEXT »

TERS characterization of phospholipid bilayers and detection of nanoparticles, cont.

A sample of a DMPE bilayer injected with a 50 µl droplet of a picomolar suspension of GO was prepared. 15 min after GO injection, the phase AFM scan in Figure 4a shows the presence of phospholipids micro-domains, but no GO sheets can be observed. A TERS map of the same area was obtained with an acquisition time of 2 s, a laser power of 180 µW and a pixel size of 31 nm. The TERS map overlaying the intensities of D band (red) and G band (blue) of GO as well as the CH stretching band (green) of DMPE exhibits some small islands –yellow colored – of 100 nm size enriched in GO.

The D and G bands are clearly observed as well as the CH_2-CH_3 stretch band in some areas. Near-field Raman average spectra (16 pixels) defining the range of three cursors of the TERS map are given in Figure 4a and Figure 4d.

Conclusion and perspectives

This application note shows how TERS chemically images the molecular arrangement of phospholipids bilayers with a spatial resolution never previously obtained of 7 nm in air without using any labelling technique.

The TERS microscope can visualize the phase separation in model membranes produced using the Langmuir trough method. This study also shows that injected graphene oxide particles can penetrate the bilayers within 3 hours of being deposited onto the artificial membranes in air.

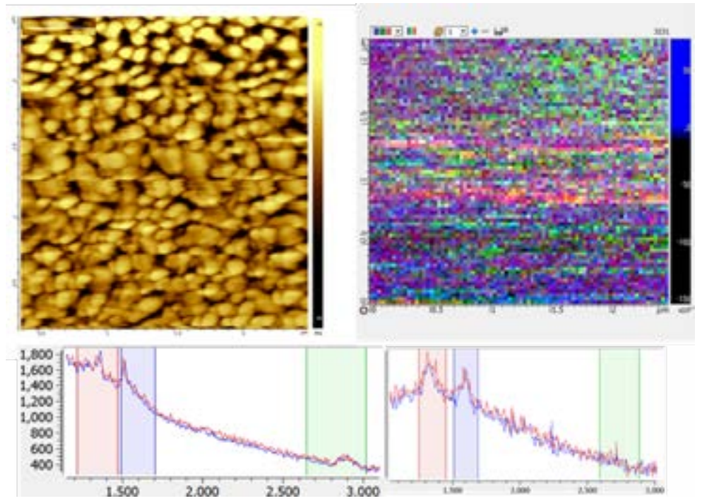

Figure 4: (a) Phase AFM map of a DMPE bilayer injected with a 50 µl droplet of a picomolar suspension of GO. The image was obtained in water in semi-contact mode at 1 Hz using a TERS tip. (b) TERS map acquired on the (a) area with an acquisition time of 2 s, a laser power of 180 µW and a pixel size of 31 nm. The TERS map overlays the intensity of D band (red) and G band (blue) of GO as well as the CH stretching band (green) of DMPE. (c) and (d) Near-field Raman average spectra (16 pixels) indicating the range of the three cursors of the TERS map.

A liquid cell has been specifically developed to carry out TERS measurements in water and a TERS map of DMPE bilayer exposed to GO evidences its penetration. These results demonstrate that TERS is an ideal tool for direct observation of molecular interaction mechanisms of cell membranes with nanomaterials.

Acknowledgments

The authors acknowledge financial support from the European Union Horizon 2020 Programme under grant agreement No 720952 (ACEnano).

References

1. References in Correlated TERS, TEPL and SPM measurements of 2D materials HORIBA application note
2. S. Garg, J. P. Fix, A. V. Krayev, C. Flanery, M. Colgrove, A. R. Sulkanen, M. Wang, G.-Y. Liu, N. J. Borys, and P. Kung, ACS Nano, Article ASAP (2022).
3. J. Hübner, T. Deckert-Gaudig, J. Glorian, V. Deckert, D. Spizter, Nanoscale, 12, 10306-10319, (2020).
4. N. Kumar, M. M. Drozdz, H. Jiang, D. M. Santos, D. J. Vaux, Chem. Commun., 53, 2451 – 2454 (2017).
5. T. Dou, Z. Li, J. Zhang, A. Evilevitch, D. Kurouski, Anal. Chem., 92, 16, 11297–11304 (2020).
6. N. Kumar, in Amino Acids, Peptides and Proteins, Vol. 43 (Eds.:. M. Ryadnov, F. Hudecz), The Royal Society of Chemistry, Croydon, 2019, pp. 127 – 153.
7. A. Nakata, T. Nomoto, T. Toyota, M. Fujinami, Anal. Sci., 29, 865 – 869 (2013).
8. Y. Pandey, N. Kumar, G. Goubert, R Zenobi, Angew. Chem. 133, 19189 (2021).

« *PREVIOUS*

Home Introduction Stories Scientific Papers Applications Multimedia Contact

HORIBA Scientific

TERS on functionalized gold nanostructures for nano-scale biosensing

A. Tempez[1], J-F. Bryche[2,3],M. Vega[2,3,4] , J. Moreau[4], P.G. Charette[2,3] M. Canva[2,3,4], T. Brulé[1], T. Carlier[1], M. Chaigneau[1]

[1]HORIBA FRANCE SAS, Palaiseau, France, [2]Laboratoire Nanotechnologies et Nanosystèmes, IRL 3463 – CNRS, Université de Sherbrooke, Sherbrooke, Canada, 3Institut Interdisciplinaire d'Innovations Technologiques [3]IT – Université de Sherbrooke - Sherbrooke, Canada. [4]Laboratoire Charles Fabry, UMR 8501 - CNRS, Université Paris-Saclay, IOGS, Palaiseau, France.

Abstract

This application note reports on TERS characterization of functionalized gold nanodisk arrays on a gold-coated glass substrate that have recently shown impressive results in SERS upon coupled plasmonic modes: the gold layer sustains propagative surface plasmons while the nanostructures sustain localized surface plasmon resonances. Nano-resolved TERS response distribution from grafted thiophenol molecules on nanodisks of 110 and 220 nm diameter feature strong signal localization on the periphery of the nanostructures, in agreement with numerical modeling. We demonstrate how TERS applied on plasmonic nanostructures is an excellent tool to characterize SERS effect distribution at the nanoscale. This work is directly related to the article by JF Bryche et al. [1].

Keywords

SERS, plasmonics, biosensors, TERS, Raman spectroscopy, functionalization, gold nanostructures, thiophenol.

Context and issues

Plasmonics is an emerging field making use of the resonant interaction obtained under certain conditions between electromagnetic radiation (light in particular) and free electrons at the interface between a metal and a dielectric material (e.g. air or glass). Surface-enhanced Raman scattering (SERS) is a powerful plasmonics-based analytical technique giving chemical information of molecules or molecular assemblies adsorbed on nanostructured metallic surfaces [2]. For bioanalytical sensor applications, these surfaces are engineered to maximize enhancement factors and molecular specificity.

Potential/ Input from technique

Tip Enhanced Raman Spectroscopy (TERS) which provides nanoscale chemical mapping has been used to map the electromagnetic near-field surrounding metal nanostructures [3] and multipolar plasmonic mode inside nanoparticles [4]. As TERS relies on the signal of an ultra confined volume, nano-scale geometry features such as edges or surface heterogeneities and their effect on sensing performance may be probed [5]. Hence TERS mapping of grafted nanostructures aims at confirming model predictions and quantifying SERS sensitivity enhancement. In addition, TERS could help to determine the optimal positioning of target molecules on the sensor surface through spatially selective surface functionalization.

Starting point, what is known?

Gold nanodisk arrays fabricated on continuous gold films deposited glass substrates have recently shown good response in SERS as well in SPR [6] as a result of the presence of coupled plasmonic modes. Indeed, the continuous metal layer sustains propagative surface plasmons while the nanostructures sustain localized surface plasmon resonances. Coupling between them can occur in specific conditions and give rise to hybrid modes with improved characteristics for sensing [7].

Next, an experimental study was conducted to study the effect of thiophenol localization on the SERS response of such gold nanodisks on a continuous gold layer: full coverage (or complete) functionalization was compared with selective_ nanodisks only_ functionalization.

NEXT »

TERS on functionalized gold nanostructures for nano-scale biosensing, cont.

As illustrated in Figure 1a, the “selective” sample was prepared upon lifting off a functionalized resist protected substrate (classic nanofabrication). The “complete” sample was prepared upon a second functionalization of the “selective” sample. A reference complete coverage sample was prepared in a one-step functionalization. The $\frac{I_{SERS-Selective}}{I_{SERS-complete\ coverage}}$ ratios of the SERS response (peak intensity of thiophenol 1075 cm^{-1} peak) were measured for three types of nanostructures and at three laser wavelengths (633, 660, and 785 nm) and are shown in Figure 1b. For all periods and all wavelengths (close and far from plasmonic resonance wavelength) ratios are very close to 1, which means that Raman response comes essentially from the nanostructures.

In parallel, numerical modeling of the electrical field distribution of nanostructured SERS substrates predicts high electrical field at the edges of the nanostructures. This is illustrated by results shown in Figure 2 for 220 nm diameter disks azranged in a square way of 400 nm period.

Here, we present TERS characterization of the same nanostructures that have undergone the selective functionalization. Sub-10 nm resolution TERS mapping will give further insight into localized effects of molecules contributing to the Raman signal. The reader may refer to the article by Bryche et al in Nanomaterials [1].

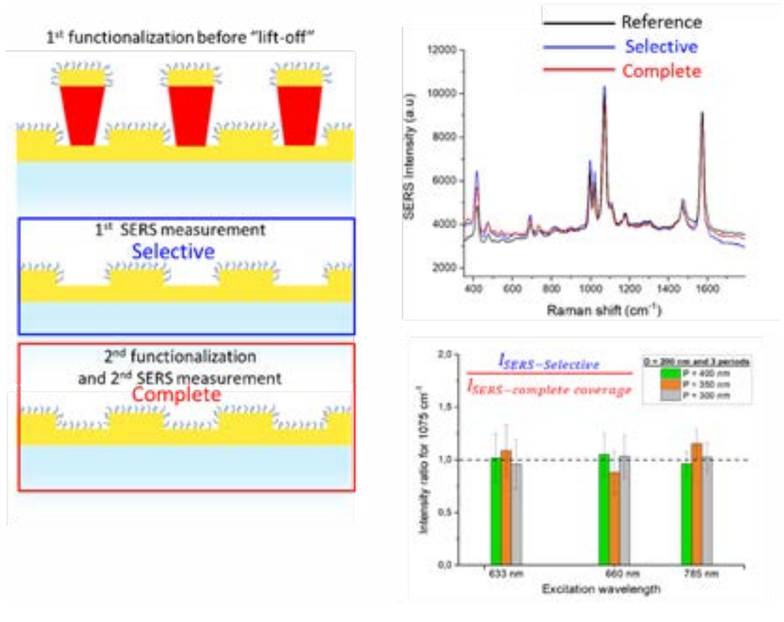

Figure 1: a) Schematic diagram showing the two-step functionalization of the gold nanostructures based on a lift-off process. b) Superposition of reference, selective and complete surface coverage functionalization SERS spectra (an offset on the y-axis has been applied to show the superposition). c) Ratio of SERS intensity between the selective and complete coverage functionalization at three excitation wavelengths (633, 660, and 785 nm) for the 1075 cm^{-1} peak.

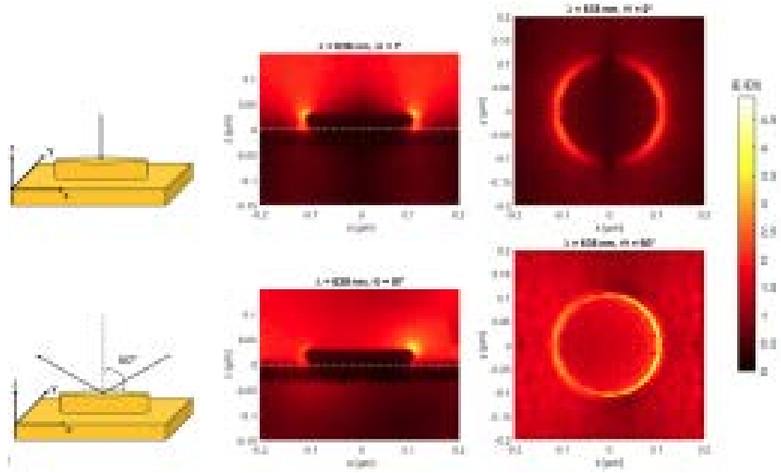

Figure 2: Side (x, z) and top (x, y) views of the normalized electric field distribution for 220 nm diameter gold nanodisks arranged in a square array of 400 nm period. The disks are excited with TM light at 638 nm with a) 0° incidence and b) 60° incidence angle. The white line outlines the top surface of the 30 nm gold nanofilm.

« *PREVIOUS*

NEXT »

Home Introduction Stories Scientific Papers Applications Multimedia Contact

HORIBA Scientific

TERS on functionalized gold nanostructures for nano-scale biosensing, cont.

Description of sample and measurement

Measurements were realized on gold nanodisk arrays fabricated on gold films. The nanostructures were prepared by e-beam lithography [3]. The 5×5 µm² scan topography and phase AFM images (Figure 3.a & Figure 3.b) confirm a well-defined gold nanodisk array with diameters (D) of 100 nm and a period (P) of 400 nm. 800×800 nm² AFM images (Figure 3.c & Figure 3.d) give a height of 32 nm±5 nm for the 220 nm diameter nanostructures.

The samples are functionalized with a 0.1 mM solution of thiophenol (C_6H_6S) over a 2.5 hr incubation time, as required to saturate the gold surface. The samples were then rinsed with ethanol for 5 min and dried with nitrogen. Raman response will be observed for the characteristic Raman peaks of thiophenol at 419/1000 cm^{-1} (out of plane C-C-C stretching), 1025 cm^{-1} (out of plane C-H stretching), 1075 cm–1 (C-C-C stretching in-plane and C-S stretching), and 1575 cm–1 (C-C stretching).

TERS measurements were performed with an XploRA Nano system (HORIBA Scientific, France) combining a state-of-the-art scanning probe microscope (OmegaScope) with a Raman micro-spectrometer. The laser excitation (638 nm, 80 µW, p-polarized) is incident on the sample at an angle of 60° to the normal of the sample plane. The laser light is focused using a 100× objective (NA=0.7) mounted on a piezo scanner for precise positioning and focusing of the spot at the apex of the probe tip. The TERS probes were cantilever-based gold or silver coated AFM-TERS tips (OMNI TERS-SNC-Au/Ag, App Nano for HORIBA Scientific).

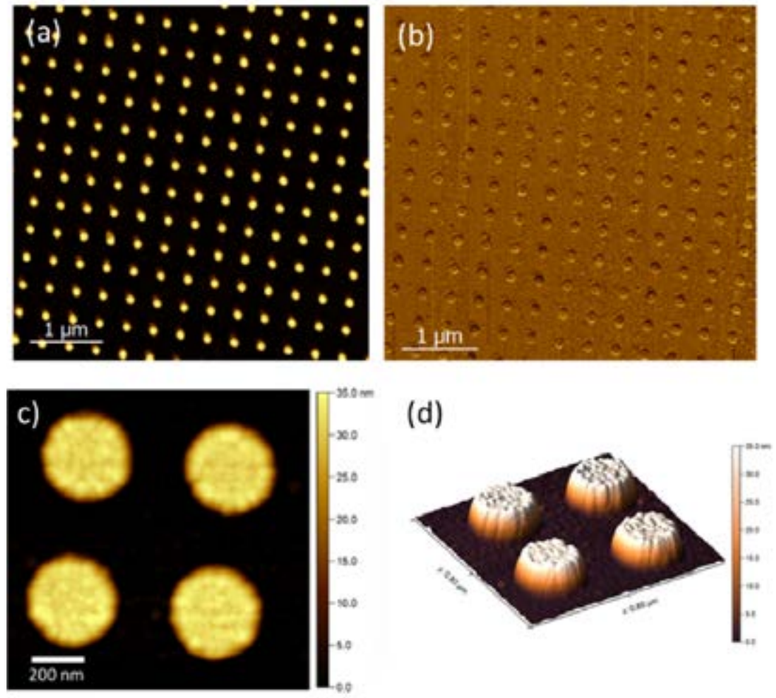

Figure 3: a) & b) 5×5 µm² height and phase AFM images of an array of uniform gold nanodisks (diameter=100 nm, period=400 nm); c) & d) 800×800 nm² AFM images in 2D and 3D views of the gold nanodisks (diameter=220 nm, period=400 nm) on gold film.

TERS enhancement was first measured by acquiring Raman spectra with the tip in contact with the sample surface with a typical interaction force of 2–10 nN (labeled “In Contact” in Figure 4) and with the tip a few nm away from the surface (labeled “No Contact” in Figure 4), both with acquisition times of 5 s.

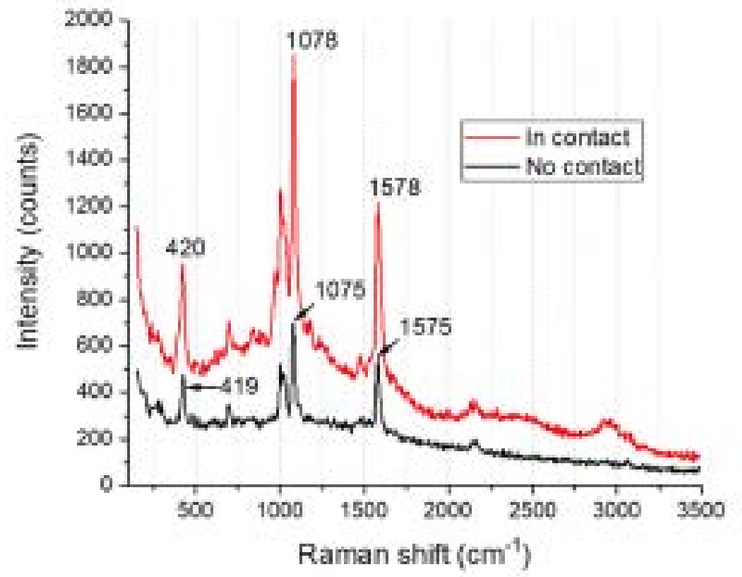

Figure 4: TERS signal confirmation with contact (red curve) and no contact (black curve) measurements at 638 nm with 80 µW and 5 s of acquisition. The tip is localized on the center of a nanodisk.

« PREVIOUS

NEXT »

Applications

TERS on functionalized gold nanostructures for nano-scale biosensing, cont.

Figure 5 shows AFM images (1650×1560 nm²) of the 220 nm gold nanodisks overlaid with corresponding TERS signal amplitude maps from the same area. At each point of the map, we performed TERS spectrum acquisitions with the tip in contact. The samples were displaced laterally in alternating-contact mode between pixels to preserve tip sharpness. High intensities of TERS signals in the zoomed picture correspond to the brightest point and are localized on the edges of the nanodisks, confirming our modeling predictions.

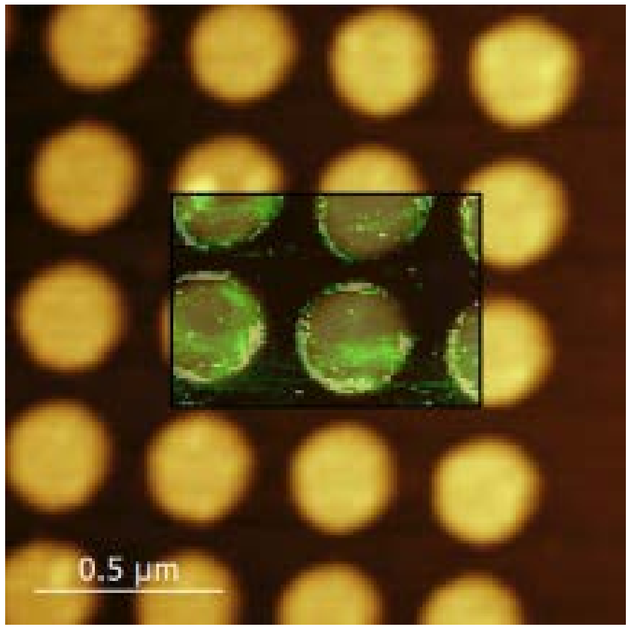

Figure 5: Overlay of TERS intensity (1578 cm^{-1} peak) map over the topographic AFM image, revealing that a higher Raman signal is seen on the edge of the nanostructures. The pixel size in the TERS image is 10×10 nm².

These results agree with a recent lower spatial resolution study [8] realised on gold nanodisks on a Si substrate functionalized with a MoS_2 monolayer.

Figure 6a results from the same TERS map as Figure 5 but is shown as an overlay of three characteristic peaks of thiophenol: (Blue) 1078 cm^{-1} peak, (Green) 1578 cm^{-1} peak, and (Red) 2900 cm^{-1}. All three signals are enhanced at the edge of the disks. Fig. 6b displays three Raman spectra averaging 36 spectra from 36 pixels for three regions: inter-disk, disk center, and disk edge.

In addition to higher signal and background, the spectrum of the disk edge region features spectral differences like additional bands at the lower wavenumbers of the 1578 cm^{-1} peak and much higher intensity in the 2900 cm^{-1} band. Surface-enhancement and tip-enhancement effects interleave in the observed spectra. Nevertheless, the spectral differences are linked to the Raman modes surface-enhanced under the 60° illumination as a result of the higher electric field in this direction. Further investigation on the Raman bands will be realized to compare with theoretical orientation of the molecule on the surface and check if the enhanced modes correspond to the molecular orientation. The TERS configuration with a 60° angle illumination in flat sample enhances modes perpendicular to the surface. Thus, this TERS geometry acts as a nanoprobe for SERS and allows to nanolocalize SERS hot spots based on spectral modes.

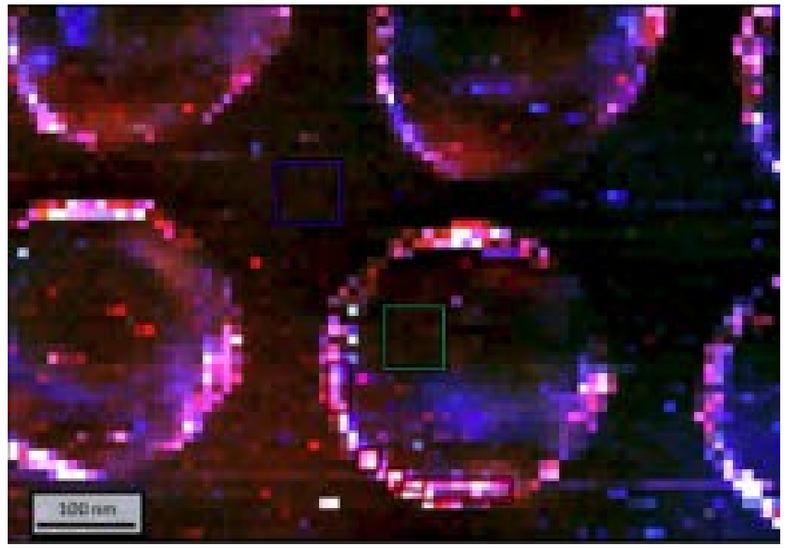

Figure 6: a) Overlay of three TERS intensity maps of 220 nm gold nanodisks with a 638 nm laser: (Blue) 1078 cm^{-1} peak, (Green) 1578 cm^{-1} peak, and (Red) 2900 cm^{-1} peak. b) TERS average spectra (36 pixels area) from three identified regions of the sample: disk center, disk edge and inter-disks.

« PREVIOUS

NEXT »

Home Introduction Stories Scientific Papers Applications Multimedia Contact

HORIBA Scientific

TERS on functionalized gold nanostructures for nano-scale biosensing, cont.

Picture of the XploRA Nano system combining the OmegaScope scanning probe microscope with the XploRA Raman micro-spectrometer

Conclusion and perspectives

This application note shows how TERS mapping is capable of characterizing SERS nanostructures. Through high-resolution TERS measurements (sub-10 nm), we have shown that molecules grafted onto the edge of the nanostructures edges exhibit higher TERS intensity, which is in line with modeled electric field distribution and preliminary SERS response measurements on complete and selective molecular coverage samples.

In addition, the spectral differences observed between the in and out areas of the SERS hot spots confirm that despite interleaved surface-enhanced and tip enhanced effects, TERS with a side illumination/collections configuration applied on plasmonic nanostructures is an excellent tool to characterize SERS effect distribution at the nanoscale.

These measurements suggest that deliberate and accurate positioning of target molecules at locations of high field concentrations on the nanostructures is advantageous for optimizing detection sensitivity and speed, especially at low molecular concentrations.

Acknowledgments

M. Vega is supported by an international doctoral scholarship from IDEX Paris-Saclay (ANR-11-IDEX-0003-02).

References

1. J-F. Bryche, M. Vega, A. Tempez, T. Brulé, T. Carlier, J. Moreau, M. Chaigneau, P.G. Charette, M. Canva, Nanomaterials, vol 12, no. 20, pp. 3586-3697, Oct. 2022. https://www.mdpi.com/2079-4991/12/20/3586
2. E. Le Ru, Principles of Surface-Enhanced Raman Spectroscopy. Elsevier, 2009.
3. A. Bhattarai, K. T. Crampton, A. G. Joly, L. Kovarik, W. P. Hess, and P. Z. El-Khoury, J. Phys. Chem. Lett., vol. 9, no. 24, pp. 7105–7109, Dec. 2018.
4. A. Bhattarai, B. T. O'Callahan, C.-F. Wang, S. Wang, and P. Z. El-Khoury, J. Phys. Chem. Lett., vol. 11, no. 8, pp. 2870–2874, Mar. 2020.
5. P. Z. El-Khoury and Z. D. Schultz, "From SERS to TERS and Beyond: Molecules as Probes of Nanoscopic Optical Fields," J. Phys. Chem. C, vol. 124, no. 50, pp. 27267–27275, Oct. 2020.
6. J.-F. Bryche, F. Hamouda, M. Besbes, P. Gogol, J. Moreau, M. Lamy de la Chapelle, M. Canva, and B. Bartenlian, Micro and Nano Engineering, vol. 2, pp. 122–130, Mar. 2019.
7. M. Sarkar, M. Besbes, J. Moreau, J.-F. Bryche, A. Olivéro, G. Barbillon, A.-L. Coutrot, B. Bartenlian, and M. Canva, ACS Photonics, vol. 2, no. 2, pp. 237–245, Jan. 2015.
8. M. Rahaman, A. G. Milekhin, A. Mukherjee, E. E. Rodyakina, A. V. Latyshev, V. M. Dzhagan, and D. R. T. Zahn, Faraday Discuss., vol.214, pp. 309–323, 2019.

« *PREVIOUS*

The AFM tip acts as a nanoantenna that enhances the incident electromagnetic field in a very confined way.

AFM-TERS measurements in a liquid environment with side illumination/collection

Patrick Hsia[1], Pierre Burgos[2], Alexander Yagovkin[1], Alexey Belyaev[1] and Marc Chaigneau[1]
[1]HORIBA FRANCE SAS, Palaiseau, France.
[2]HORIBA UK Ltd., Northampton, UK.

Abstract

The new breakthrough in Raman nanoscale chemical imaging is the measurement in a liquid environment. TERS measurements in liquids have significantly broadened their potential applications across scientific disciplines such as heterogeneous catalysis, electrochemistry, cellular biology and biomaterials. Implementation of TERS in liquids brings out some instrumental difficulties. AFM-TERS in liquids have been published very recently but only in bottom and top optical accesses. In this technical note, the special instrumental features of the TERS setup and experimental conditions of the measurements enabling TERS in liquids using side illumination/collection in order to keep optimal polarization conditions are presented: (i) the design of a side access liquid cell that allows high-throughput optics, (ii) the option to perform AFM imaging in true non-contact mode in liquids, and (iii) the alignment procedure of the Raman laser on the AFM-TERS tip in liquids using an objective mounted on a piezoelectric scanner. These latest instrumental developments are applied to nanoscale imaging of graphene oxide flakes and carbon nanotubes immersed in water. TERS resolution in liquids down to 20 nm is demonstrated along with true non-contact AFM images.

Keywords

AFM-Raman, Tip Enhanced Raman Spectroscopy (TERS), TERS in liquids, AFM non-contact in liquids.

Introduction

Atomic Force Microscopy (AFM) associated to Raman spectroscopy has proven to be a powerful technique for probing chemical properties at the nanoscale. The AFM tip acts as a nanoantenna that enhances the incident electromagnetic field in a very confined way. As a result, a localized enhanced optical signal can be obtained at the apex of the tip thanks to a complex mix of resonant and non-resonant effects. Techniques like Tip Enhanced Raman Spectroscopy (TERS) or Tip enhanced Photoluminescence (TEPL) can then be associated to the different physical information accessible with the AFM [1]. Nevertheless, some applications require a liquid environment such as in-situ investigation of biological samples, catalysis and electrochemical reactions. The development of AFM-Raman in liquids, with side illumination/collection in order to keep optimal polarization conditions, would open the path to these new perspectives and therefore broaden the applications of TERS.

The first experimental demonstration of TERS in a liquid was performed on a self-assembled monolayer (SAM) with a bottom illumination and collection configuration in 2009 [2]. Bottom backscattered configuration was also used in other works, e.g. for lipid bilayers [3], for catalytic reactions [4], SWCNTs [5], or probing molecules grafted on gold nanoplatelets [6, 7]. While excitation/collection can be performed with a high numerical aperture objective in a bottom configuration, it is limited to transparent samples, and incident polarization may have to be shaped. Top configuration has been used in electrochemistry unraveling mechanisms at the molecular scale [8, 9] and a resolution down to 8 nm has been demonstrated in STM-TERS [10] (Scanning Tunneling Microscopy combined with TERS). Side illumination through a glass window is also well spread in groups like Van Duyne's [11], Ren's [12, 13] or Domke's [14], but all these examples are STM-based and limited to conductive samples.

In this work, a dedicated cell suitable for side optical illumination and collection has been designed to perform AFM-based Tip enhanced spectroscopy in a water environment.

NEXT »

AFM-TERS measurements in a liquid environment with side illumination/collection, cont.

Experimental setup

1) Description of the AFM-Raman system, the cell and the optical adaptations:

Correlated AFM-TERS has been performed on graphene oxide (GO) and carbon nanotubes (CNTs) deposited on a gold-coated substrate. The sample has then been submerged in water inside a cell adapted on the sample stage of the OmegaScope AFM (HORIBA France). The 633 nm p-polarised laser and Raman signal are brought from and to a long focal spectrometer (LabRAM HR Evolution, 800 mm focal length, HORIBA France) via an optical coupling (Figure 1). To collect all Raman peaks of interest in one spectral window, a 300 grooves/mm grating is used.

Figure 1: HORIBA AFM-Raman LabRAM Nano

The cell is equipped with a glass window for side illumination/collection. Due to the difference of refractive index between air/glass and glass/water, the optical path is corrected using an additional lens placed in front of the side objective. As the cantilever is also in contact with water, the path of the AFM feedback laser diode (1310 nm) is deviated by the change of refractive index between air and water. An additional lens mounted on the cantilever holder itself is also added to correct the diode refraction in water (Figure 2).

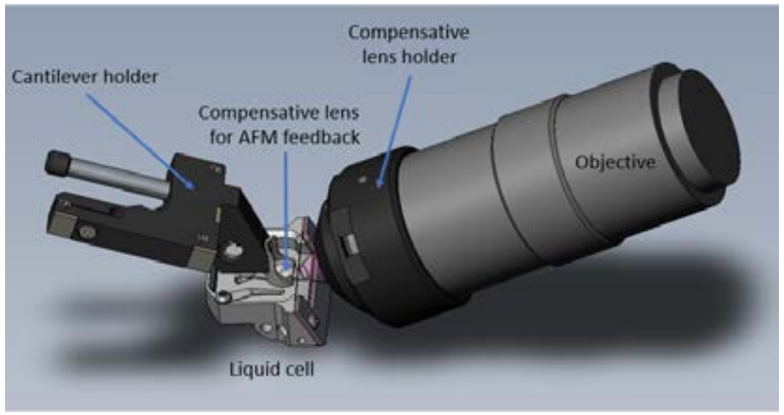

Figure 2: Representation of the liquid cell, the AFM tip holder, the objective, and the optical path (in pink) through the glass window of the liquid cell.

An objective tilted by 30° with respect to the sample plane with a super long working distance is used (Mitutoyo 50×, NA = 0.42, WD = 20.5mm). Although the issue of tip degradation can be addressed [2, 4], the TERS experiments in liquids are performed with gold coated AFM-TERS tips (OMNI-TERS-SNC-Au, AppNano, USA) which are known to have a better stability than silver tips.

2) AFM feedback in water

As described in the first section, the AFM tip holder dedicated to measurements in liquids is equipped with a non-removable lens for the feedback diode of the AFM. A droplet of water is first deposited between the lens and the cantilever in order to make the first AFM adjustments (i.e. the automated tip feedback laser adjustment on the cantilever and centering of the reflection on the four-quadrant photodiode). These adjustments are done before dipping the tip holder into the cell itself.

It is important to stress that the images shown in the results section are acquired in non-contact mode. The oscillation of the cantilever inside water generates several peaks and is highly dampened; for that reason, AFM imaging in contact mode is traditionally used in a liquid environment. The use of non-contact mode imaging in liquids in our experimental setup is made possible by increasing the driving amplitude of the oscillation which helps preserve the tip and the sample from degradation and contamination that can easily happen in contact mode.

3) Tip visualization: Towards a course alignment of the excitation laser

The OmegaScope AFM optical platform is equipped with two video units enabling the simultaneous visualization of the tip from both top and side optical paths. The optics and AFM tip are fixed while the sample and the cell approach the tip.

« *PREVIOUS*

NEXT »

Home Introduction Stories Scientific Papers Applications Multimedia Contact

HORIBA Scientific

AFM-TERS measurements in a liquid environment with side illumination/collection, cont.

In this configuration of TERS in liquids, the optical path goes through different diopters, then the focus of the tip observed by the side camera can change when the cell is moved away from or towards the objective during sample retraction/approach. To always keep the tip in focus, and thus simplify the Raman laser-to-tip alignment, the motorized and automated approach of the cell is inclined by 25° (Figure 3).

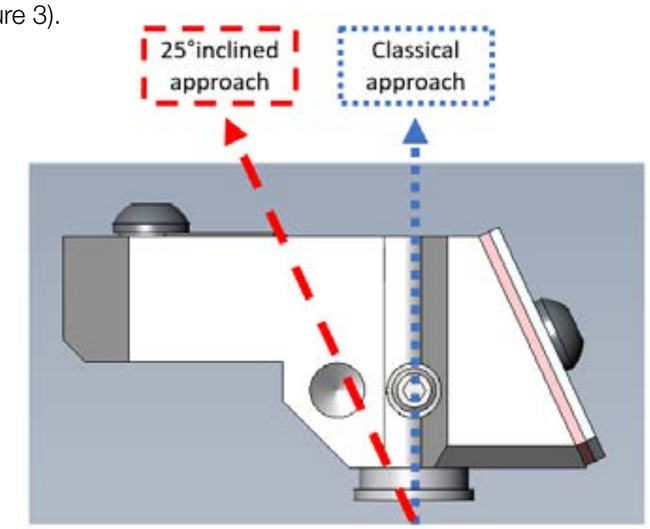

Figure 3 : Side view or the cell. The cantilever (not shown) is positioned above.

As a result, when the approach is completed, the excitation laser can be visible on the tip's apex and its position is already close to the optimal position for TERS measurements in a liquid (Figure 4). The shape of the laser spot in water is distorted compared to the one in air, and optical aberrations and parasitic reflections can be observed.

Thus, a fine and precise optical alignment is needed to achieve TERS conditions.

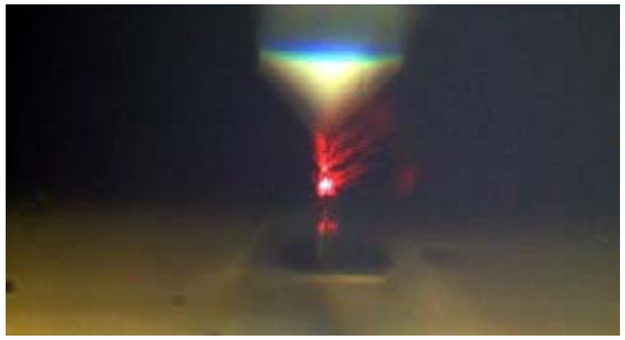

Figure 4: Laser focused in water near the tip apex, viewed by the side camera.

4) Fine optical alignment with the objective scanner

For TERS measurements, the alignment of the excitation laser and the tip is crucial to get the localized enhancement effect at the tip apex. The instrumentation should provide tools to finely focus the laser at the end of the AFM-TERS tip. In our AFM-Raman setup, the tip remains fixed and the excitation laser is brought to the tip's apex thanks to a so-called objective scanner that moves the laser position in a plane but also in depth for focalization. Different mappings with the objective scanner can be done: A scan in a plane at fixed focus (called "XY objective") or in a plan orthogonal to the first one that sweeps the focus (called "XZ objective" or "YZ objective").

XY objective scans are needed to precisely bring the spectroscopic laser spot to the tip apex with an accuracy below 500 nm.

Figure 5a shows objective scanner maps (with an inverted contrast as compared to TERS in an air environment) from the area under the background curve over the whole spectral range (peak area filtering) on a color scale (Figure 5c). The observed contrast can be attributed to the fact that water diffuses light more significantly than the cantilever/tip. In this case, the tip is in the water of the cell but far from the sample. The shape of the tip can be reconstructed. Each pixel contains a background spectrum.

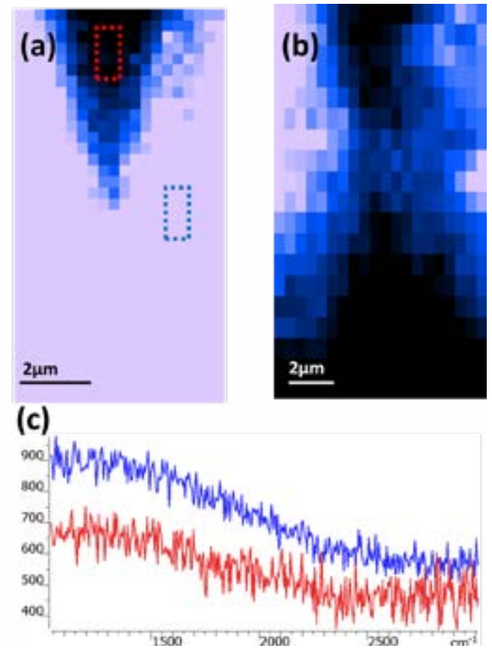

Figure 5: (a) XY objective scan obtained when the tip is a few millimeters from the sample's surface, (b) XY objective scan after the approach when the tip is interacting with the sample's surface, (c) background spectra from the selected colored rectangles in Figure 5a.

« PREVIOUS
NEXT »

AFM-TERS measurements in a liquid environment with side illumination/collection, cont.

Results

1) Non-contact AFM images in liquid environments

AFM images of graphene oxide (GO) flakes and CNTs were recorded in true non-contact mode with Au coated AFM TERS tips (Figure 6).

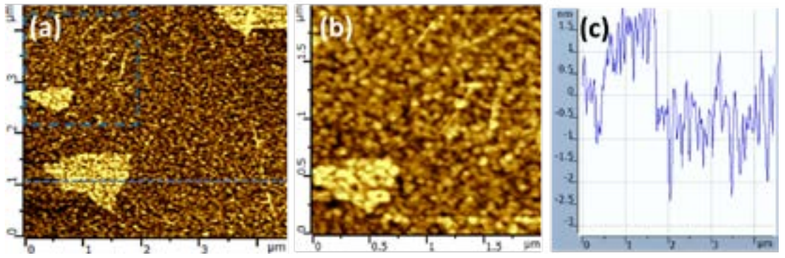

Figure 6: (a), (b) AFM topographic images of the sample in water obtained in true non-contact mode (256 × 256 pixels), (c) section analysis of the topographic signal along the dotted blue line on the AFM map.

Graphene oxide flakes, along with carbon nanotubes, are clearly discernable despite the roughness of the gold substrate. Mean roughness and RMS roughness are both inferior to 1 nm (averaging on the substrate shows RMS roughness of 700 pm, and 750 pm RMS roughness on the graphene flake) which clearly indicates high sensitivity in terms of AFM measurements. The section analysis of the topographic signal presented in Figure 6c shows a 840 pm step of graphene oxide. The image quality in non-contact mode is well preserved in water environment.

2) TERS mapping on GO and CNTs and calculation of the enhancement factor EF.

A TERS map in water of GO flakes and CNTs (2.2 × 1 µm (75 × 22 pixels)) is collected with a 2 s integration time spectrum at each pixel (30 nm step). The full TERS map is recorded in 1h and 50 minutes and illustrates the great stability of both the AFM system and the optical coupling (Figure 7).

Both topographic images and TERS maps are collected at the same time using a special mode called “Spec-Top™” [15] mode with “dual spec” option: For each pixel (i) one spectrum (sum of the near-field and far-field signals) is acquired with tip in direct contact with the surface with a typical interaction force of 2-10 nN and (ii) another spectrum is acquired with tip in tapping mode (a few nm away from the sample surface, considered to be the farfield contribution (FF)). In between two pixels of the map, the sample moves in semi-contact mode to preserve the sharpness and plasmonic enhancement of the tip.

GO and CNTs are both graphitic materials sharing similarities in their Raman spectra. Around 1600 cm^{-1} a G band is located that represents in-plane tangential movement of the carbon atoms and occurs in any graphite related material. Another around 1350 cm^{-1}, the D band (“D” stands for defects) is seen in both GO and CNTs. This vibration is visible only if defects are present in the carbon lattice. As a result, this band is used as an indication of the sample defect density. In otherwise structurally pristine carbon materials, a band around 2650 cm^{-1} is present: 2D band (sometimes called G’).

This band is not to be found with GO as its sp^2 structure is very disturbed by the adjacent functional groups. Additionally, GO can be distinguished from CNTs by the broader D and G [16, 17] bands.

In the TERS map plotting the D band intensity (Figure 7c) both GO and CNTs are visible. Higher concentration of defects is observed in the CNTs themselves and in GO oxide wrinkles and edge [18]. The TERS map plotting the 2D band intensity (Figure 7b) shows only the contribution of the carbon nanotubes. Thus, the two species can be clearly distinguished from each other. Their different Raman signatures are shown in the TERS spectra plotted in Figure 7d.

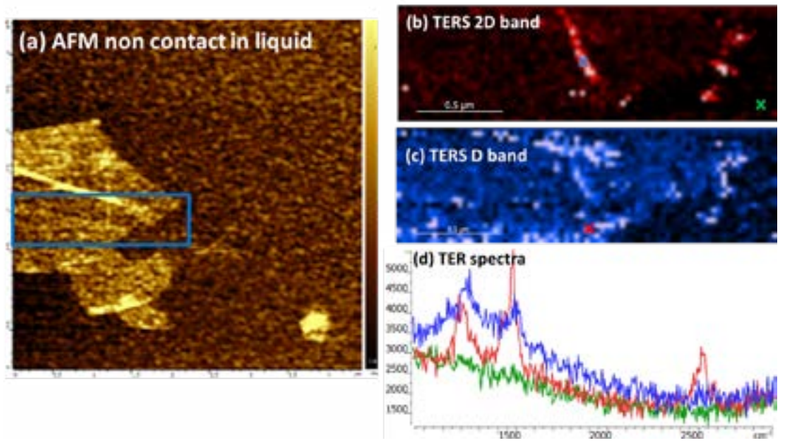

Figure 7: (a) AFM imaging (true non-contact mode) of a graphene oxide flake in water, (b) TERS map of the 2D band and (c) TERS map of the D band, (d) typical TERS spectra taken from the cross points on the TERS images.

« PREVIOUS

NEXT »

AFM-TERS measurements in a liquid environment with side illumination/collection, cont.

In order to push the limit of the optical resolution through TERS in liquids, Figure 8 presents a high resolution TERS image in a liquid of an individual CNT, 500 × 350 nm scanning area (300 × 200 pixels)), 2 s integration time spectrum at each pixel (1.7 nm step). The pure far-field map shows a homogeneous background with no Raman signature (not shown), whereas the near-field + far-field map shows peaks related to a single CNT (Figure 8 b). The TERS map (Figure 8 b in which D band is shown in yellow and 2D band in red) also demonstrates a chemical sensitivity down to the pixel size (1.7 nm): e.g. the intensity of the D peak at ~1350 cm^{-1} in the blue circle marked area close to the local lattice defects rises drastically from one pixel to the adjacent one (Figure 8 c).

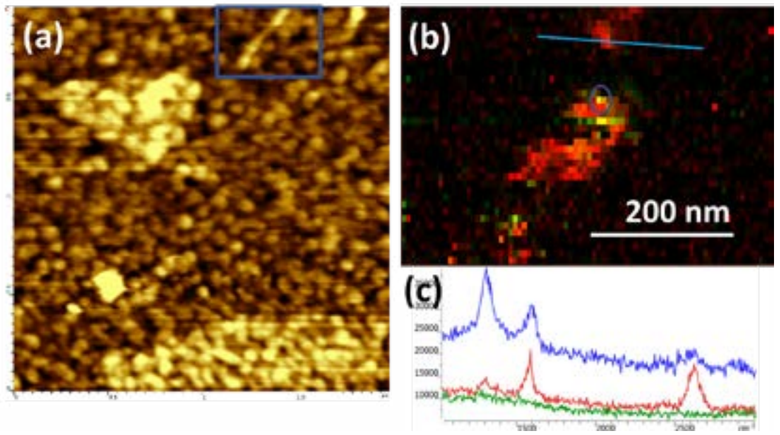

Figure 8: Correlated AFM-TERS measurements on a CNT in water; (a) 2 × 2 µm non-contact AFM image, (b) hyperspectral TERS image in water (overlay of the D and 2D bands intensities), (c) TER spectra in the area indicated by the blue circle. The three Raman spectra are separated by 1.7 nm (adjacent pixels in both X and Y directions).

In addition, the Full Width at Half Maximum (FWHM) of the TER intensity profile along the line across the CNT clearly demonstrates 20 nm spatial resolution (Figure 9).

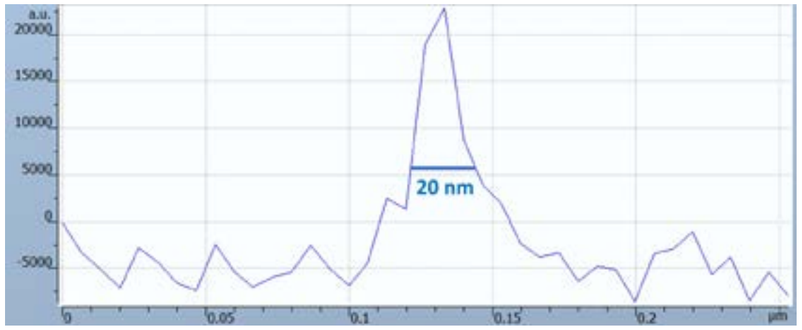

Figure 9: Section analysis of the TERS signal in water (2D band of the CNT) showing a 20 nm TERS resolution.

In our experiment, using a side backscattering configuration, this enhancement factor EF factor is given by [19]:

$$EF = \left(\frac{I_{nf}+I_{ff}}{I_{ff}}\right)\left(\frac{R_{focus}}{\frac{1}{2}R_{tip}}\right)^2 \cos\alpha$$

With R_{focus} = 1,200 nm (focal radius), R_{tip} = 20 nm (radius of curvature of the tip) and α = 60° (angle of incidence). I_{nf} and I_{ff} respectively stand for the component of the signal coming from the near-field (NF) and for the component of the signal coming from the far-field (FF).
Using this equation, the EF factor on the CNT calculated for the D band is:

$$EF_{CNT} = 2.1 \times 10^5$$

Where I_{nf+Iff} = 14500 and I_{ff} = 1000.

Conclusion

AFM-TERS in liquids using side backscattering illumination has been demonstrated on GO and CNTs immersed in water. Specifics of the AFM-Raman setup that enable TERS in liquids have been presented: new side access liquid cell, integrated compensative optics, 25° inclined motorized approach, durable and accurate Raman laser-to-tip alignment with objective scanner. Thanks to those latest instrumental developments, we presented the nanoscale hyperspectral imaging of isolated carbon nanotubes in a liquid with a spatial optical resolution routinely obtained in TERS maps of 20 nm and stability for long term mapping. This work is expected to significantly broaden the potential applications of AFM-TERS wherein non-destructive and label-free chemical mapping in liquid environments presents a key measurement challenge.

« PREVIOUS

NEXT »

Home Introduction Stories Scientific Papers Applications Multimedia Contact

AFM-TERS measurements in a liquid environment with side illumination/collection, cont.

References:

1. Tempez, A., Lancry, O., Krayev, A. & Chaigneau, M. Correlated TERS, TEPL and SPM Measurements of 2D Materials. https://www.horiba.com/en_en/tersfor2d/
2. Schmid, T., Yeo, B.-S., Leong, G., Stadler, J. & Zenobi, R. Performing Tip Enhanced Raman Spectroscopy in liquids. J. Raman Spectrosc. 40, 1392–1399 (2009).
3. Nakata, A., Nomoto, T., Toyota, T. & Fujinami, M. Tip Enhanced Raman Spectroscopy of Lipid Bilayers in Water with an Alumina- and Silver-coated Tungsten Tip. Anal. Sci. 29, 865–869 (2013).
4. Kumar, N., Wondergem, C. S., Wain, A. J. & Weckhuysen, B. M. In Situ Nanoscale Investigation of Catalytic Reactions in the Liquid Phase Using Zirconia-Protected Tip Enhanced Raman Spectroscopy Probes. J. Phys. Chem. Lett. 10, 1669–1675 (2019).
5. Kumar, N. et al. Nanoscale chemical imaging of solid–liquid interfaces using Tip Enhanced Raman Spectroscopy. Nanoscale 10, 1815–1824 (2018).
6. Bhattarai, A. & El-Khoury, P. Z. Nanoscale Chemical Reaction Imaging at the Solid–Liquid Interface via TERS. J. Phys. Chem. Lett. 10, 2817–2822 (2019).
7. Bhattarai, A.; Joly, A. G.; Krayev, A.; El-Khoury, P. Z. Taking the Plunge: Nanoscale Chemical Imaging of Functionalized Gold Triangles in H2O via TERS. J. Phys. Chem. C 123 (12), 7376–7380 (2019).
8. Touzalin, T., Joiret, S., Maisonhaute, E. & Lucas, I. T. Complex Electron Transfer Pathway at a Microelectrode Captured by in Situ Nanospectroscopy. Anal. Chem. 89, 8974–8980 (2017).
9. Touzalin, T., Joiret, S., Maisonhaute, E. & Lucas, I. T. Capturing electrochemical transformations by Tip Enhanced Raman Spectroscopy. Curr. Opin. Electrochem. 6, 46–52 (2017).
10. Touzalin, T., Joiret, S., Lucas, I. T. & Maisonhaute, E. Electrochemical Tip Enhanced Raman Spectroscopy imaging with 8 nm lateral resolution. Electrochem. Commun. 108, 106557 (2019).
11. Chen, X., Goubert, G., Jiang, S. & Van Duyne, R. P. Electrochemical STM Tip Enhanced Raman Spectroscopy Study of Electron Transfer Reactions of Covalently Tethered Chromophores on Au(111). J. Phys. Chem. C 122, 11586–11590 (2018).
12. Zeng, Z.-C.; Huang, S.-C.; Wu, D.-Y.; Meng, L.-Y.; Li, M.-H.; Huang, T.-X.; Zhong, J.-H.; Wang, X.; Yang, Z.-L.; Ren, B. Electrochemical Tip Enhanced Raman Spectroscopy. J. Am. Chem. Soc. 137 (37), 11928–11931 (2015).
13. Huang, S.-C. et al. Electrochemical Tip Enhanced Raman Spectroscopy with Improved Sensitivity Enabled by a Water Immersion Objective. Anal. Chem. 91, 11092–11097 (2019).
14. Martín Sabanés, N., Driessen, L. M. A. & Domke, K. F. Versatile Side-Illumination Geometry for Tip Enhanced Raman Spectroscopy at Solid/Liquid Interfaces. Anal. Chem. 88, 7108–7114 (2016).
15. Sergey A. Saunin, Andrey V. Krayev, Vladimir V. Zhishimontov, Vasily V. Gavrilyuk, Leonid N. Grigorov, Alexey V. Belyaev, Dmitry A. Evplov, U.S. Patent US9910066, 2018
16. Su, W.; Kumar, N.; Krayev, A.; Chaigneau, M. In Situ Topographical Chemical and Electrical Imaging of Carboxyl Graphene Oxide at the Nanoscale. Nat. Commun. 9 (1), 2891 (2018).
17. Dresselhaus, M. S.; Jorio, A.; Hofmann, M.; Dresselhaus, G.; Saito, R. Perspectives on Carbon Nanotubes and Graphene Raman Spectroscopy. Nano Lett. 10 (3), 751–758 (2010).
18. Bhattarai, A.; Krayev, A.; Temiryazev, A.; Evplov, D.; Crampton, K. T.; Hess, W. P.; El-Khoury, P. Z. Tip Enhanced Raman Scattering from Nanopatterned Graphene and Graphene Oxide. Nano Lett. 18 (6), 4029–4033 (2018).
19. HORIBA AFM-Raman FAQ: https://www.horiba.com/en_en/technology/measurement-and-control-techniques/microscopy-and-imaging/nanoraman/what-is-the-definition-of-ters-enhancement-factor/

« *PREVIOUS*

Home Introduction Stories Scientific Papers Applications Multimedia Contact

HORIBA Scientific

TERS is capable of distinguishing between combustion engine emitted nanoparticles of different structure.

Characterization of nanoparticles from combustion engine emission using AFM-TERS

Ophélie Lancry[1], Jennifer Noble[1], Agnès Tempez[1], Sébastien Legendre[1], Marc Chaigneau[1], Philipp Kreutziger[2], Marcus Rieker[2], Cristian Focsa[3]

[1] HORIBA Scientific - HORIBA France SAS, Palaiseau, France.
[2] HORIBA Automotive Test Systems - HORIBA Europe GmbH, Oberursel, Germany.
[3] PhLAM Laboratory, Lille 1 University, Villeneuve d'Ascq, France.

Abstract

In the frame of the European PEMs4Nano project, nanoparticles from combustion engine emission have been deposited on gold substrates and imaged by AFM and its combined nano-resolution chemical TERS mode. Focus has been on sub-23 nm particles which are investigated for their health impact and are to be soon under regulation rules. Particles imaged by AFM are characterized by their size with a resolution of +/- 1 nm. Correlated TERS maps with a pixel size of 7 nm and below reveal the chemical complexity through the deconvoluted D and G band signatures. Using the D1 over (G+D2) band intensity ratio which is an indicator of the degree of order in soot structure, TERS is capable of distinguishing between combustion engine emitted nanoparticles of different structure.

Keywords

Nanoparticles, AFM-Raman, Tip Enhanced Raman Spectroscopy (TERS), engine emission, combustion, carbon.

Context and issues

Particulate emissions from on-road motor vehicles are currently the focus of intensive research due to the impact of ambient particulate matter levels on climate and human health. Estimates of the health impact attributable to air pollution indicate that PM2.5 (particles with diameter below 2.5 µm) concentrations in 2012 were responsible for 432,000 premature deaths originating from long-term exposure in Europe (over 40 countries), of which 403,000 were in the EU-28. Although improvement in engine technology has led to a significant decrease in the number and mass of emitted particles, a new concern is raised nowadays by even smaller particles.

Specifically, sub-23 nm particles can be produced, sometimes in high concentrations, in both diesel and gasoline direct-injection (GDI) engines [1]. Harmfulness of the particles has been shown to correlate better with surface area than with mass [2][3], which becomes important for ultrafine particles even though their residence time in the atmosphere is shorter. In addition, it has been estimated that the percentage of sub-23 nm solid particles fraction could reach 30-40% for gasoline vehicles utilizing direct injection and be potentially higher when alternative fuels are being used [4]. These nanoparticles are currently not measured by regulations in force (certification procedures have a cut-off size of 23 nm).

It becomes urgent to develop robust, reliable and reproducible measurement technology, supporting the engine development process, as well as future certification procedures on the chassis dyno and during real driving emissions (RDE) measurements.

[1] Giechaskiel, B., et al., 2014. SAE International Journal of Fuels and Lubricants 7, 950–964.
[2] Donaldson, K., et al., 1998. SIAM Journal of Scientific Computing 29, 553–560.
[3] Oberdörster, G., 1996. Inhalation Toxicology 8, 73–90.
[4] Giechaskiel, B., et al., 2017. Aerosol Science and Technology 51, 626–641.

NEXT »

Home Introduction Stories Scientific Papers Applications Multimedia Contact

HORIBA Scientific

Characterization of nanoparticles from combustion engine emission using AFM-TERS, cont.

Existing regulation focuses on particle number and mass which are key to control the environmental impact. However, it is also critical to determine the chemical composition and especially the surface chemical composition of the nanoparticles to understand the potential reactivity with the environment, including impact on human health.

Potential/Input from technique

AFM can image combustion generated nanoparticles provided they are deposited on flat substrates and suitable scanning conditions are used. AFM images will allow characterization of their size and mechanical properties, both of which are critical to determining how they are transported and how they can affect human health. However, no chemical information will be given by AFM. On the other hand, Raman spectroscopy is widely used for chemical characterization, but imaging is limited by a spatial resolution around 200 nm because of the diffraction limit. Tip enhanced optical spectroscopies (Tip Enhanced Raman Spectroscopy (TERS), and Tip enhanced Photoluminescence (TEPL) based on signal amplification from the nano-region under the tip will allow for actual chemical nano-characterization.

Starting point, what is known?

Raman spectroscopy has been demonstrated as an excellent chemical characterization tool for soot particles, as it is sensitive not only to crystal structure but also to molecular structure (short range order). An example of a Raman spectrum of a soot particle is shown in Figure 1 for the first order Raman region 800-2000 cm^{-1}).

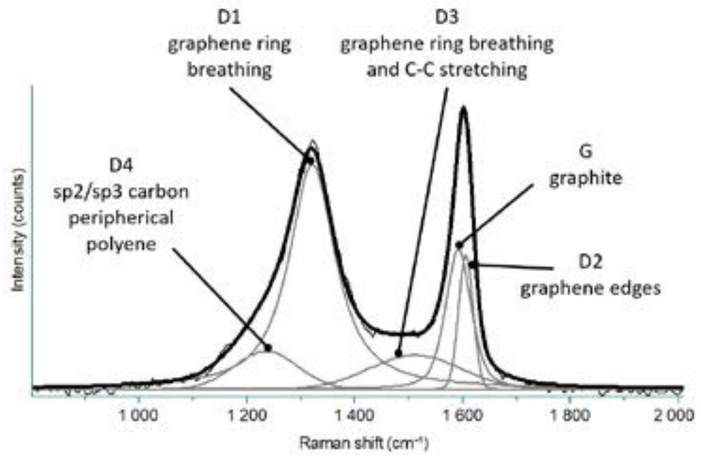

Figure 1: Typical Raman spectrum of carbon material, five-band fitting method, routinely applied to combustion soot.

The five-peak deconvolution shown in Figure 1 results from the curve fitting method of the Sadezky procedure [5]. It contains two main features: The G band, derived from in-plane motion of carbon atoms and appearing at around 1580 cm^{-1}; and the D band, attributed to lattice motion away from the center of the Brillouin zone and appearing around 1270-1450 cm^{-1}, depending on the structural nature of the material. More details about the band characteristics and assignments are given in Table 1. This method allows for distinguishing different types of soot according to their degree of graphitization.

Description of sample and measurement

Combustion-generated nanoparticles were produced using a generic single cylinder test engine in standard engine operating conditions and with gasoline fuel. The collection of size-selected particles of a wide size range from 10 µm to 10 nm was performed using a NanoMoudi II (model 125R, MSP, TSI company, PEMs4Nano consortium partner).

[5] Sadezky, A, et al., 2005. Carbon 43, 1731-1742.

	Raman shift	Intensity	Vibrations	
D4	~1350 cm^{-1}	low	sp^3 carbon or polyene C=C or sp^2sp^3 CC	Disordered graphitic lattice
D3	~1500 cm^{-1}	medium	Defects (in place) or amorphous sp^3 C affecting C=C stretching	Amorphous carbon
D2	~1620 cm^{-1}	high	Aromatic C=C stretching from isolated graphene units	Disordered graphitic lattice
D1	~1350 cm^{-1}	very high	In-plane defects	Disordered graphitic lattice
G	~1580 cm^{-1}	high	sp^2 C=C stretching	Ideal graphite

Table 1:. First order Raman bands and vibrations reported for soot

« PREVIOUS

NEXT »

Home Introduction Stories Scientific Papers Applications Multimedia Contact

HORIBA Scientific

Applications

Characterization of nanoparticles from combustion engine emission using AFM-TERS, cont.

The NanoMoudi is a cascade impactor Micro-Orifice Uniform-Deposit Impactor (MOUDI II™), which combines aerodynamic design and micro-orifice nozzles to reduce jet velocity, pressure drop, particle bounce and entrainment during particle sampling (Figure 2). Particles were collected on gold-coated silicon wafers for 30-60 minutes, ensuring a smooth surface for AFM measurements and a low surface density. The smallest size bin, nominally containing particles with aerodynamic diameter 18-10 nm, was chosen for AFM-TERS studies

Figure 2: NanoMoudi particle size-selected collector.

A NanoRaman system from HORIBA Scientific combining an Atomic Force Microscope (SmartSPM) with a Raman spectrometer (LabRAM HR Evolution) is used in a reflection configuration for Tip enhanced Raman measurements (TERS). The incident laser (633 nm, p-polarised) is focused through the 100×, 0.7 NA, 7 mm long working distance objective lens (Mitutoyo) in side-illumination geometry with an angle of 60° with respect to the vertical axis. The collection of back-scattered signal is performed through the same objective. The probes used for AFM-TERS are cantilever-based silver TERS tips (Ag-coated OMNI TERS probe, AppNano, manufactured only for HORIBA Scientific).

The size of single particles and their distribution were determined by AFM measurements. A 1.2×1.2 µm image (300×300 pixels) is displayed in Figure 3 and exhibits two particles of 10 nm (particle 1) and 6 nm (particle 2) height. The diameter as measured by the FWHM (Full Width at Half Maximum) of particle 1 and particle 2 is respectively 48 nm and 43 nm. However, the lateral resolution is highly dependent on the tip used, especially when the radius dimension of the scanned object is close to the one of the tip (tip-sample convolution phenomenon). With a tip radius of 1 nm according to the manufacturer, the error on the particle diameter is +/- 1 nm.

Within this image, two smaller areas containing particles with diameters below 10 nm were defined and characterized by TERS to determine their chemical structure (Figure 4): the pixel size of zone 1 and zone 2 is respectively 7 nm and 5 nm, the acquisition time is 100 ms per pixel. The TERS maps (Figure 4) correspond to the distribution of carbon material on the surface by monitoring the G band intensity (1500-1700 cm^{-1}, Figure 4, Zone 1) and an overlay of the G band and D1 band (in green) intensities (1200-1700 cm^{-1}, Figure 4, Zone 2). Three carbon particles identified by their TER spectra match perfectly with the particles highlighted on the topography image. The fourth one (particle 1) presents a feature related to the presence of amorphous carbon-based species. This signal originates from a crevice formed by the grain boundary between micro-crystals of the Au film (seen in the AFM image, Figure 3).

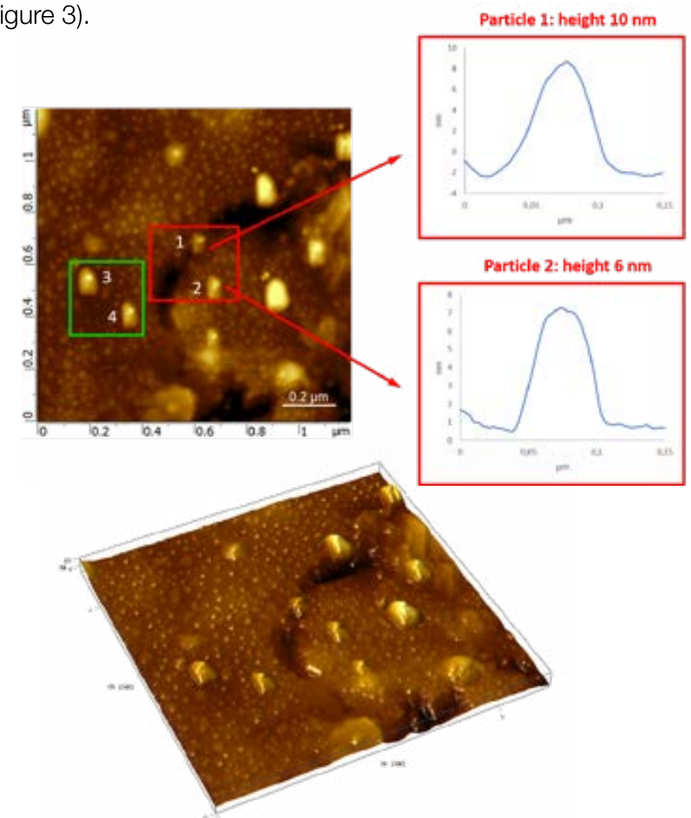

Figure 3: (top) AFM images of particles collected from the single cylinder test engine and their cross-section, (bottom) 3D AFM topographic image of the same area.

« PREVIOUS
NEXT »

HORIBA Scientific

Applications

Characterization of nanoparticles from combustion engine emission using AFM-TERS, cont.

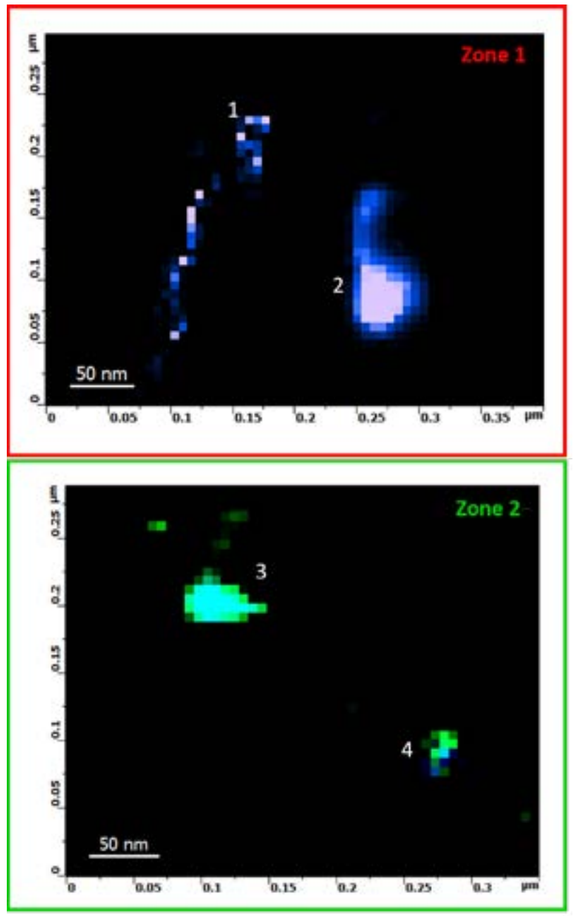

Figure 4: TERS images of particles collected from the single cylinder test engine: (top) G band intensity map (Zone 1) and (bottom) overlay of the G band and D1 band intensities (Zone 2).

Average spectra of the three measured particles were extracted. They exhibit very different profiles indicating major structural differences between particles produced by the same engine regime and the same size bin. Five-band deconvolution analysis already applied to Raman spectra of soot particles[5] was used within LabSpec 6 software. The fit results are presented in Figure 5 and Table 2. The G, D1, D2 and D3 bands are fitted with a Lorentzian profile, whereas the D4 band is fitted with a Gaussian profile. The ratio of areas of the D1 on the (G+D2) bands is a strong indicator of the degree of order in soot structure[6]. This value increases from 1.5 (particle 4, Figure 5c) to 2.5 (particle 3, Figure 5b) and to 3 (particle 2, Figure 5a), suggesting that particle 2 has much more disordered structure than the others. However, the presence of organic materials on the surface of the particles is indicated by higher D4 band intensity in the spectra of particles 3 and 4.

Particle	Band	Position, cm^{-1}	Width, cm^{-1}	D1/(G+D2)
Particle 2	G D1 D2 D3 D4	1589.7 1315.5 1611.5 1530.7 1208.0	43.4 111.4 24.7 117.8 80.4	**3**
Particle 3	G D1 D2 D3 D4	1589.7 1315.5 1611.5 1530.7 1208.0	38.5 137.1 19.0 304.1 140.0	**2.5**
Particle 4	G D1 D2 D3 D4	1589.7 1315.5 1611.5 1530.7 1208.0	44.6 92.8 20.1 213.9 175.1	**1.5**

Table 2: Deconvolution results.

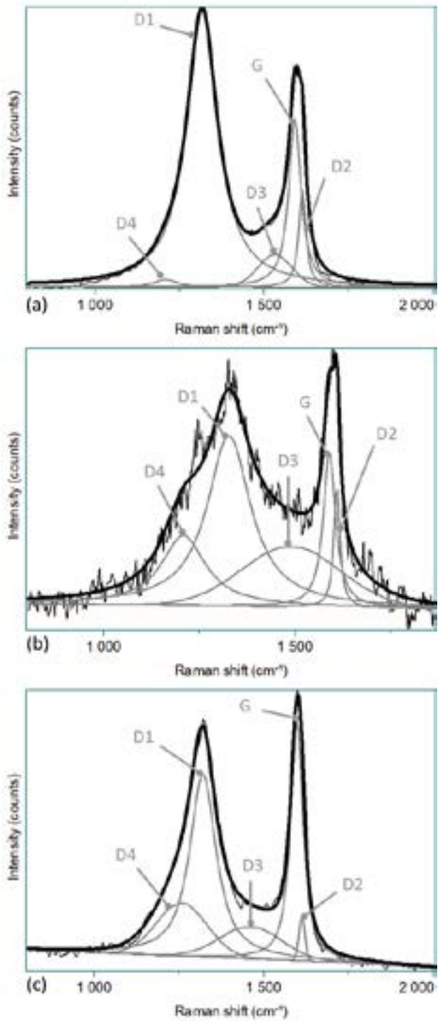

Figure 5: Five-band deconvolution applied to TERS spectra of particle 2 (a), particle 3 (b) and particle 4 (c).

Conclusion and perspectives

This application note presents AFM-TERS results on combustion-generated nanoparticles for the first time. The combination of AFM and Raman through the NanoRaman platform enables morphological characterization (size distribution) and discrimination between the different particles on the surface (chemical information) at the nanoscale, revealing the diversity of carbon structures generated during gasoline combustion.

Acknowledgments

This project has received funding from the European Union's Horizon 2020 research and innovation program under Grant Agreement no. 724145.

[6] Carpentier, Y, et al. 2012. Astronomy & Astrophysics, 548, A40.

« *PREVIOUS*

Home Introduction Stories Scientific Papers Applications Multimedia Contact

HORIBA Scientific

Applications

The use of the remarkable surface driven properties of nanomaterials is now widespread with applicationsin medical, aerospace, microelectronics industries, and many other application areas.

TERS characterization of explosive nanoparticles

Jakob Hübner[1], Tanja Deckert-Gaudig[2], Julien Glorian[1], Volker Deckert[2], Denis Spitzer[1], Agnès Tempez[3], Marc Chaigneau[3]

[1]French-German Research Institute of Saint-Louis, St Louis, France,
[2]Leibniz Institute of Photonic Technology (IPHT), Jena, Germany,
[3]HORIBA FRANCE SAS, Palaiseau, France.

Abstract

This application note reports on TERS characterization of crystalline nanoparticles that are prepared by spray flash evaporation of two explosive organic compounds: CL-20 and HMX. The TERS surface sensitivity reveals that TER intensities of CL-20 and HMX band markers are inverted in comparison with their intensities in the bulk, which leads to the conclusion that the surface of the CL-20/HMX co-crystals nano-plates is HMX-terminated. This surface structure gives insights for an impact ignition mechanism and explains the close impact sensitivity values of HMX and CL-20/HMX co-crystals.

Keywords

Nanoparticles, nanocrystals, energetic materials, explosives, surface, Tip Enhanced Raman Spectroscopy.

Context and issues

The use of the remarkable surface driven properties of nanomaterials is now widespread, with applications in medical, aerospace, microelectronics industries, and many other application areas.

Co-crystals which consist of mixing two or more compounds in a crystalline manner are also applied to engineer materials with superior properties to single compound crystals. Co-crystals nanoparticles are used in the pharmaceutical industry to fabricate medicine with improved effects and in the explosives industry to make highly energetic and safe materials.

For example, co-crystals made from a high energy/high friction sensitivity compound, 2,4,6,8,10,12-hexanitro-2,4,6,8,10,12-hexaazatetracyclo[5.5.0.0.0]dodecane (CL-20) and a lower energy/low friction sensitivity compound, 1,3,5,7-tetranitro-1,3,5,7-tetrazocane (HMX) feature the “best of both worlds”: Higher detonation velocity than pure HMX and lower impact sensitivity than CL-20 (close to that of HMX) [1, 2]. In addition, the nanosize of the co-crystals further improves the sensitivity characteristics, making it better than pure HMX [3].

TRIOS platform with its CombiScope AFM

So far, it is not understood how co-crystallinity, combined with nanostructuring, leads to the enhanced behavior of these nanoparticles. Only a technique capable of probing single nanocrystals can bring an answer about their observed pyrotechnical properties.

Potential/Input from technique

Tip Enhanced Raman Spectroscopy (TERS) has emerged as a powerful analytical technique providing high chemical sensitivity for surface molecular mapping with nanoscale spatial resolution. The higher electromagnetic field locally created at the apex of the irradiated tip enhances the Raman signal from the sample made in contact with, or really close to, the tip. The signal originates from the nanoregion underneath the tip, thus probing minute sample amounts and ensuring nanometer lateral resolution. The strong field enhancement rapidly decays within a few nanometers which makes TERS ideal for nanoobjects observation but also makes it a highly surface sensitive technique.

NEXT »

TERS characterization of explosive nanoparticles, cont.

In the case of energetic nanoparticles, TERS offers the additional advantage of being a low input energy compared to electron microscopies in which the electron beam tends to induce the dissociation of energetic organic molecules. TERS analysis also becomes crucial as the structural information given by single crystal XRD is bound to the ability to grow sufficient size crystals.
Starting point, what is known?

The AFM-TERS investigation of differently prepared energetic hexolite (i.e. a mixture of TNT [2,4,6-trinitrotoluene] and RDX [1,3,5-trinitro-1,3,5-triazine]) nanocomposites has led to the structure determination of RDX/TNT core/shell and patchy 15–20 nm sized nanoparticles[4].

Description of sample and measurement

The CL-20/HMX nanocrystals are prepared by spray flash evaporation: A pressurized solution of one or more compounds is sprayed through a heated cone nozzle into a reactor under vacuum. The strong pressure drop results in instantaneous evaporation of the solvent and subsequent formation of nanoparticles which are collected through a filter system. When the precursor solution contains more than one molecular compound, the formed nanosized products can be a mixture of single crystalline compounds, core shells particles and nano co-crystals. Here, as in Ref [1] (first synthesis of CL-20/HMX co-crystals) the precursor solution was prepared in a 2:1 CL-20:HMX molar ratio.

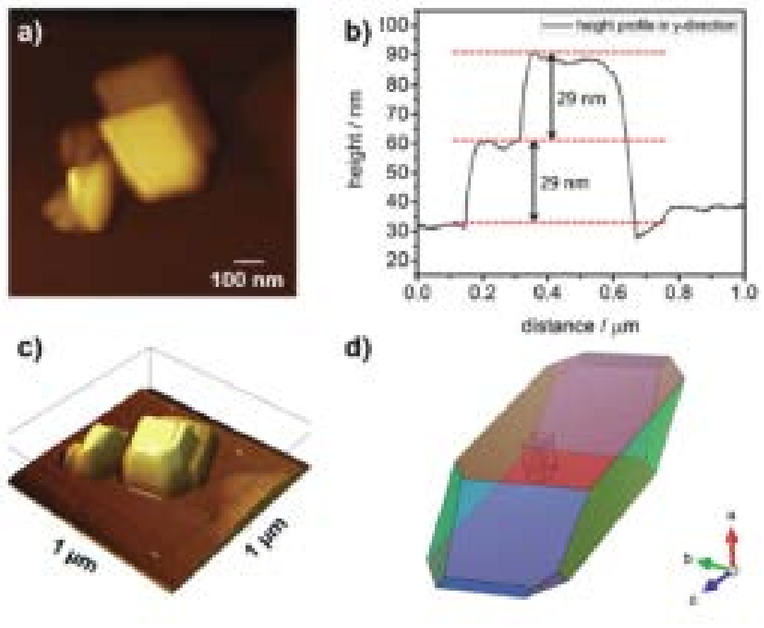

Figure 1: (a) Topographic map of n-CL-20/HMX co-crystals; (b) height profile of particles shown in (a) along the y-direction. (c) 3D image of (a); (d) crystal morphology simulated by using crystal faces.

In this work, for AFM and TERS analysis, nanoparticles are applied onto glass cover slides by depositiong a spatula tip between two cover glasses. The sample is spread on the glass surface through pressureless rubbing of the two slides against each other.

TERS tips are AppNano Access-NC AFM probes coated with a 25 nm thick silver layer on top of a 3 nm titanium adhesion layer in an argon plasma sputtering system. SEM observation indicates the formation of a single silver nanoparticle at the apex of the tip.

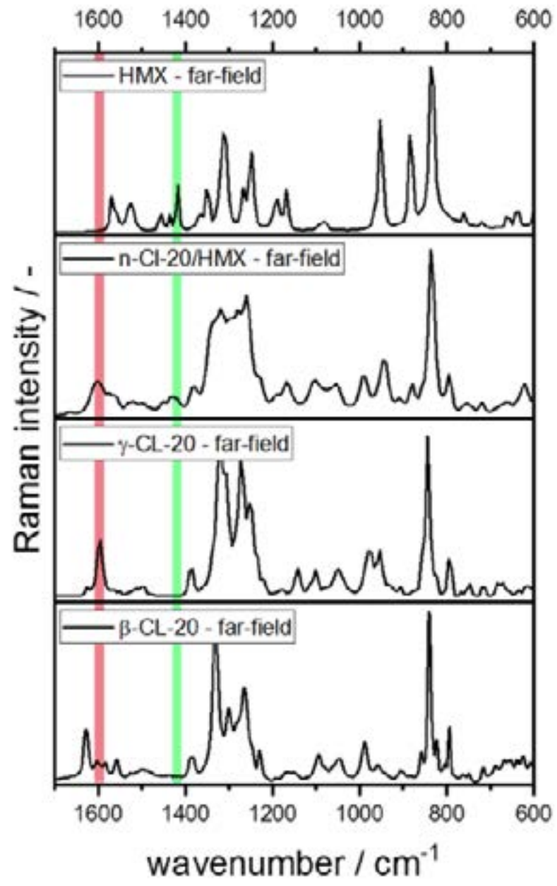

Figure 2: Far-field Raman spectra of *ß*-CL-20, *y*-CL-20, *n*-CL-20/HMX nano co-crystals, and *ß*-HMX between 1700 cm^{-1} and 600 cm^{-1}. Two Raman band markers are indicated: **Red stripe** is the NO2 asymetric stretching vibration of CL-20 at ~1600 cm^{-1}. **Green stripe** is the CH_2 out of plane wagging vibration of HMX at ~1416 cm^{-1}.

« *PREVIOUS*

NEXT »

Home Introduction Stories Scientific Papers Applications Multimedia Contact

HORIBA Scientific

TERS characterization of explosive nanoparticles, cont.

Prior to TERS, X-ray powder diffraction (XRPD) reveals the monoclinic structure of the nanosize co-crystals in which layers of HMX alternate with bilayers of CL-20. XRPD gives the information about the complete conversion of the precursor mixture into CL-20/HMX co-crystals.

AFM topographic images (typical example shown in Figure 1) of the nanoparticles acquired in non-contact mode confirm the crystalline morphology of the particle with flat surfaces and sharp angles. The height of the angular plates of 29 nm is in line with the XRPD calculated coherence length in the [300] direction.

The µRaman spectrum acquired from the nano-particles is comparable to the signature spectrum obtained in the literature [2]. µRaman spectra were also collected from individual pure HMX and CL-20 crystalline particles to compare with the specific signature of the co-crystals. Such spectra comparison (Figure 2) guides the selection of HMX and CL-20 marker bands, making sure that no signal appears at these wavenumbers in the other pure crystalline compounds to monitor their spatial distribution of their contribution at the µscale, but also at the nanoscale: The NO_2 asymmetric stretching vibration at 1602 cm^{-1} (1595-1615 cm^{-1} integration interval) for CL-20 and the CH_2 out of plane wagging vibration at 1416 cm^{-1} (1404-1434 cm^{-1} integration interval) for HMX. These bands are present in the co-crystal signature but are broadened and shifted compared to pure individual compounds as a result of different chemical environments. The areal CL-20:HMX band marker ratio is 2.5:1 in the spectrum of the CL-20/HMX nanoparticles.

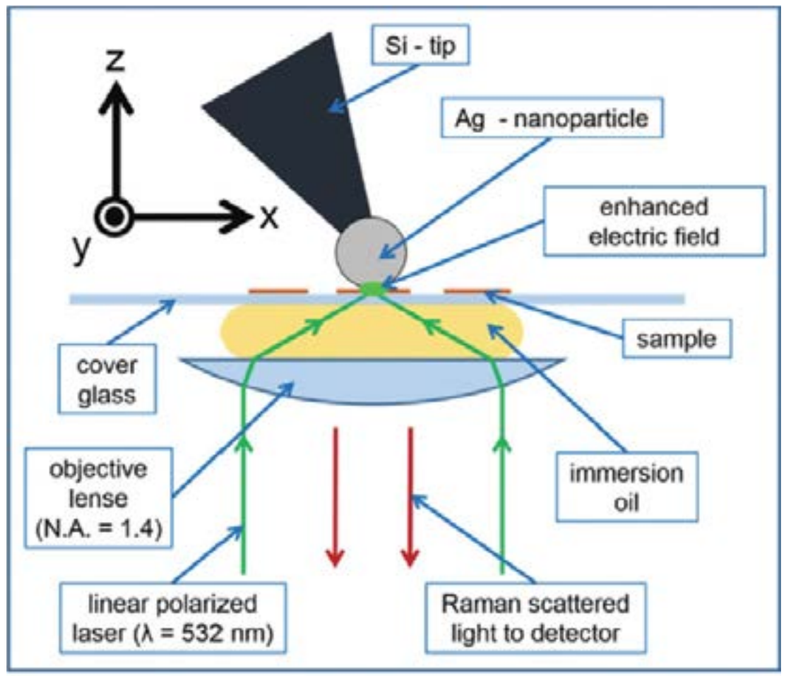

Figure 3: Schematic diagram of the TERS experimental setup.

TERS measurements were performed using a NanoRaman system from HORIBA Scientific integrating an atomic force microscope (CombiScope™ SPM - TRIOS platform) and a Raman microscope (LabRAM HR Evolution) in bottom illumination mode (transmission mode). The 532 nm linearly polarized laser is precisely focused onto the TERS tips by a 100× 1.4 NA oil immersion objective by means of the piezo movement of the scanner on which the objective is mounted (Figure 3). TERS maps are recorded in non-contact mode which means that the distance of the tip-sample surface varies constantly during the measurement. TERS images of two nanoparticles (with a pixel size of 50 nm) with their corresponding far-field and near-field spectra averaged over each entire particle are shown in Figure 4.

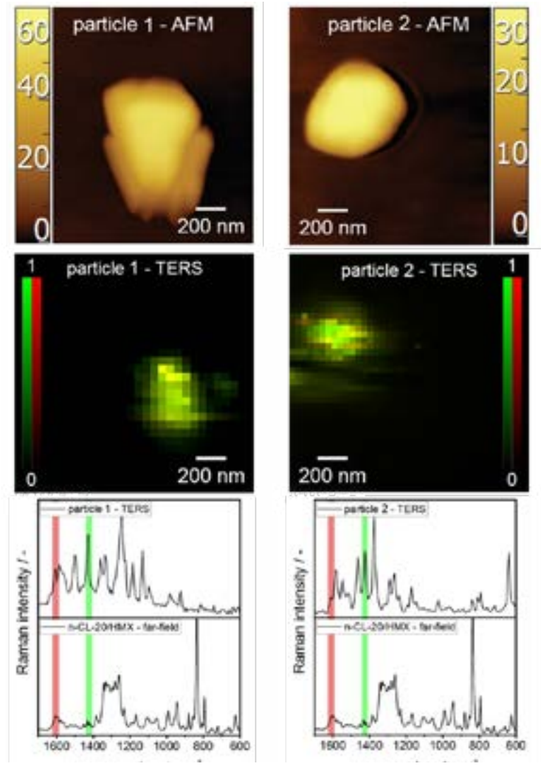

Figure 4: AFM topographic images of two n-CL-20/HMX nanoparticles and their corresponding TERS maps and spectra. TERS spectra represent the average over all TER spectra on the particle surfaces.

« PREVIOUS

NEXT »

TERS characterization of explosive nanoparticles, cont.

Each spectrum of the maps is recorded with an acquisition time of 0.2 s. A striking difference between the near-field and far-field spectra is the intensity inversion between the two CL-20:HMX markers: From a ratio of 2.5 to 1 in the far-field to about 1 to 1.5 in the near-field spectra. This inversion could arise from a special arrangement of the oriented nano co-crystal particles toward the Raman scattering system. Figure 5 shows additional data from three nanoparticles: The TERS maps have been acquired with higher resolution (20×20 nm² pixel area). Same observation can be made about the inversion ratio of the CL-20:HMX markers between far-field and near-field spectra.

However, some approximated normal coordinate analysis leads to the conclusion that the CL-20 contribution should be three times the HMX contribution. As a result the intensity inversion observed in the near-field Raman spectra is very likely arising from a molecular HMX layer terminated surface. The HMX cyclic nitroamine may be more deformable than the CL-20 cage and thus be energetically more favorable to accommodate and form a crystal free interface.

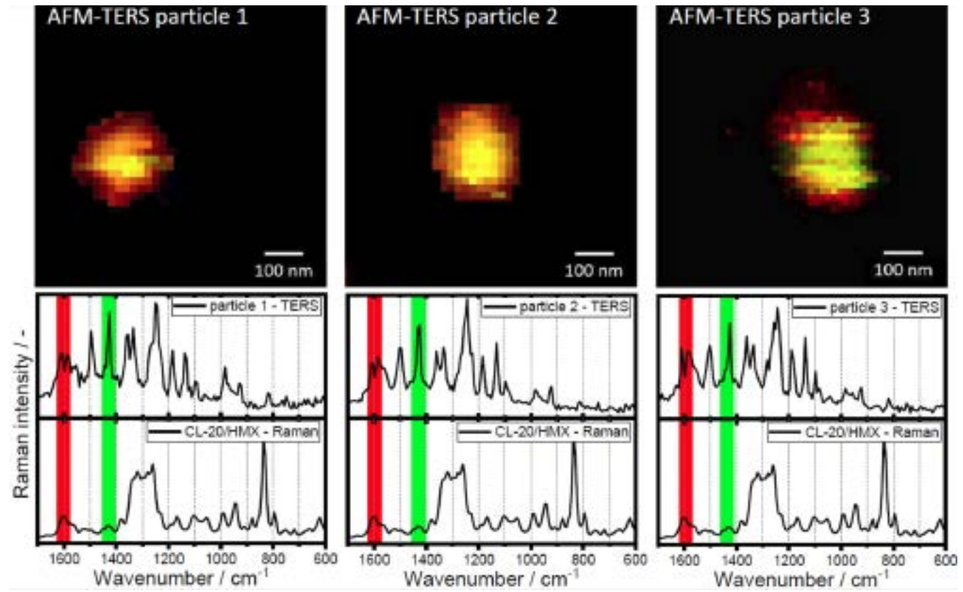

Figure 5: TERS maps of three n-CL-20/HMX nanoparticles and their µRaman (far-field) and TER spectra. TERS spectra represent the average over all TER spectra on the particle surfaces.

Conclusion and perspectives

This application note shows how TERS mapping is capable to characterize the crystalline nature, quality and orientation of single nano-particles prepared by co-crystallizing two explosive organic compounds (CL-20 and HMX) in a molar ratio of 2:1 under a spray evaporation process. Such sensitivity is appreciated when minute sample amount is available and other techniques like XRPD are limited.

Single nanoscale co-crystals imaged by AFM feature well-defined flat faces and edges with step height of 29 nm and size of 100-400 nm. TERS images of single CL-20/HMX nanocrystals are collected with a spatial resolution down to 20 nm. The TER spectra feature a HMX/CL-20 contribution intensity ratio that is inverse with respect to the µRaman spectra which reveals a HMX molecular layer terminated surface. This finding helps to explain the mechanical sensitivity value of the co-crystal nanoparticles that is close to that of HMX (and much lower that CL-20). The HMX terminated surface also yields an impact mechanism proposal where ignition is spread from surfaces.

In conclusion, data in this note perfectly illustrate the surface sensitivity of TERS and its subsequent potential to give insights in the formation mechanism of co-crystal formation and to engineer co-crystals for dedicated applications.

References

1. O. Bolton, L. R. Simke, P. F. Pagoria, A. J. Matzger, Cryst. Growth Des, 12, 4311-4314 (2012).
2. M. Ghosh, A. K. Sikder, S. Banerjee, R. G. Gonnade, Cryst. Growth Des, 18, 3781-3793, (2018).
3. C. An, H. Li, B. Ye, J. Wang, J. Nanomater., 2017, 3791320 (2017).
4 J. Hübner, T. Deckert-Gaudig, J. Glorian, V. Deckert, D. Spizter, Nanoscale, 12, 10306-10319, (2020).
5. T. Deckert-Gaudig, V. Pichot, D. Spitzer, V. Deckert, ChemPhysChem, 18, 175-178, (2017).

« PREVIOUS

Carbon nanotubes exhibit several strong Raman peaks...

Characterization of carbon nanotubes using Tip Enhanced Raman Spectroscopy (TERS)

Agnès Tempez, Marc Chaigneau
HORIBA Scientific, Avenue de la Vauve, Passage Jobin Yvon, 91120 Palaiseau, France

Keywords

Carbon nanotubes (CNTs) - Nanomaterials - Tip Enhanced Raman Spectroscopy

Context and issues

Carbon nanotubes are now manufactured in large volumes (several thousand tons per year) and are present in many daily life products ranging from car parts, batteries, and sports equipment, to water filtration systems and boat equipment.

Nevertheless, there is still a long way to go to produce SWCNTs (single wall carbon nanotubes) in large scale devices with exceptional theoretical electrical and thermal conductivities and mechanical resistance.

Additional knowledge is essential for boosting CNT integration into thin film microelectronics, optoelectronics, and medical devices.

Potential / Input from technique Raman spectroscopy is the technique of choice to characterize CNTs and related nano-objects in terms of chirality, diameter, density, length, and presence of defects. Because conventional Raman is a far-field optical technique (the spot size is diffraction-limited), its applications are restricted to the micro- and macro-worlds. TERS bridges the gap to NanoRaman and offers nanometric spatial resolution down to the single tube level for those characteristics provided by the rich Raman spectra.

Starting point, what is known?

Carbon nanotubes exhibit several strong Raman peaks: (i) the radial breathing mode in the range of 100-400 cm^{-1} has a frequency related to nanotube diameter and chirality through a simple known function; (ii) the G-band peak (at ~1590 cm^{-1}) can distinguish SWNT as metallic or semiconducting; and (iii) the disorder-induced D band (~1350 cm^{-1}) provides information about the presence of defects in the nanotube structure. The 2D band (a two-phonon band at ~2700 cm^{-1} associated with the disorder-induced D band) indicates changes in the electron energy dispersion of a CNT and thereby is informative about the presence of dopants in their 1D structure.

Description of sample and measurement

This application note presents TERS data obtained on CVD-grown SWCNTs deposited on Au substrate using spin-coating. TERS measurements were performed using a NanoRaman™ system from HORIBA Scientific combining an Atomic Force Microscope (SmartSPM, AIST-NT) with a Raman spectrometer (XploRA) with a ×100 LWD objective tilted at 60° with respect to the sample plane. A 638 nm p-polarized laser is focused onto the cantilever-based silver TERS tip with a 0.13 mW power on the sample. An AFM topography map is first recorded to locate one or several CNTs. Then a high resolution Raman map focusing on two SWCNTs (300 × 160 nm (100 × 60 points)) is collected with a 100 ms integration time for the Raman spectrum (200-3600 cm-1) of each pixel (3 nm step). The Raman image (Figure 1) is generated from the integration of the three D, G, 2D band intensities using blue, green, red color scales respectively. The integration windows for the D, G, 2D bands are visible in figure 1 (b) showing two TER spectra detected at two different locations in the CNT. The intensity of the D band (blue pixels) is showing the imperfection in the structure of the latter and thus the location of the defects. In contrast, the areas in red correspond to the pure graphitic arrangement of the CNT through the intensity of the 2D band.

NEXT »

Applications

Characterization of carbon nanotubes using Tip Enhanced Raman Spectroscopy (TERS), cont.

Prior to TERS, X-ray powder diffraction (XRPD) reveals the monoclinic structure of the nanosize co-crystalthe particle surfaces.

In order to push the limit of the optical resolution through TERS, Figure 2 presents a high resolution TERS hyperspectral image of an individual SWCNT, 100 x 100 nm scanning area, obtained with a pixel step size of 1.3 nm, in a total acquisition time < 9 min, 100 ms per pixel. The Full Width at Half Maximum (FWHM) of the TER intensity profile along the line across the CNT clearly demonstrates 8 nm spatial resolution. In addition, the TERS map (Figure 2a in which D band is shown in white and green pixels and 2D band in red) also demonstrates a chemical sensitivity down to the pixel size (1.3 nm): e.g. the intensity of the D peak in the red circle marked area close to the local lattice defects rises drastically from one pixel to the adjacent one (Figure 2 c).

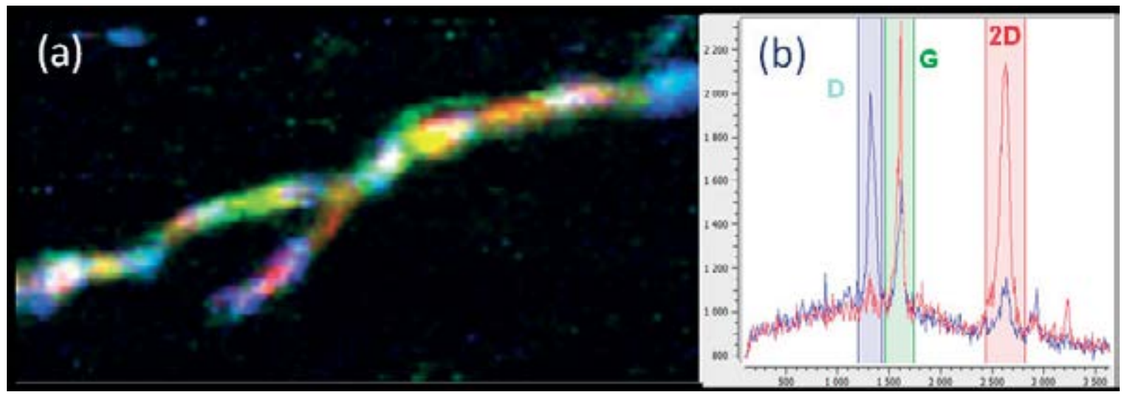

Figure 1: (a) TERS chemical mapping of two SWCNTs, (b) typical TER spectra from the tubes.

Conclusion and perspectives

The use of TERS to reveal the defects density in the structure of CNTs is of interest for a better understanding of the electrical properties of the devices made with such nano-objects. Not only defects concentration but also local chirality changes from the different radial breathing modes, pressure effect and strain distribution can be studied at the single carbon nanotube level through TERS. The TERS characterization of both 1D carbon nanotubes and 2D graphene (another very promising form of carbon for a wide range of applications) is likely to contribute to further deployment of these carbon materials into general consumer products.

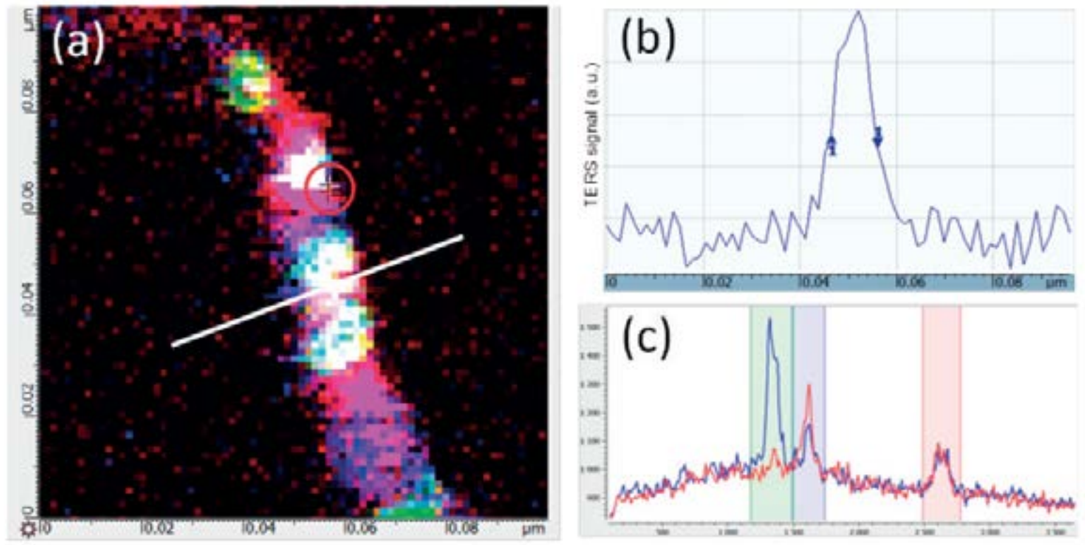

Figure 2: (a) Hyperspectral TERS map (100 nm x 100 nm, 1.3 nm step size) of an isolated CNT, (b) section analysis of the TERS signal (G band) showing <10 nm Raman resolution, (c) TER spectra from the area located by the red circle. The two Raman spectra are from two adjacent pixels (separated by only 1.3 nm).

Bibliography

«TERS Ready or Not» Barbara Foster, American Laboratory, September 2016. “Nanoscale imaging and identification of a four-component carbon sample,” E. Sheremet, R. D. Rodriguez, A. L. Agapov, A. P. Sokolov, M. Hietschold, D. R.T. Zahn, Carbon 96 (2016) 588-593.

« PREVIOUS

Memristive elements are believed to be one of the most promising components for the next generation of electronics for artificial intelligence (AI) and internet of things (IoT).

c-AFM and in operando TERS & µRaman characterization of molecular switching in organic memristors

Sreetosh Goswami[1], Sreebrata Goswami[2], Thirumalai Venkatesan[1], Agnès Tempez[3], Marc Chaigneau[3]
[1]National University of Singapore, Singapore, [2]Indian Association for the Cultivation of Science, Kolkata, [3]HORIBA FRANCE SAS, Palaiseau, France.

Abstract

Memristive elements are believed to be one of the most promising components for the next generation of electronics for artificial intelligence (AI) and internet of things (IoT). One of the biggest problems with existing memristors is that their switching is non-uniform (filamentary) and stochastic which accounts for their lack of reproducibility and device-to-device consistency. This application note reports on the demonstration of a 100% uniform molecular switching mechanism in memristors based on Ru-complexes of azo-aromatic ligands using concurrent nanoscale mapping of the conductance by c-AFM and of the chemical signature by in operando TERS.

Keywords

Conductive AFM, memristor, in operando Tip Enhanced Raman Spectroscopy, transition metal complex, uniformity.

Context and issues

The word memristor is the contraction of memory and resistance; a memristor is an electrical two-terminal device whose resistance depends on the history of the applied voltage. Memristors are non-volatile memories predicted to be the component of the future for high density data storage and brain inspired ultralow energy computing. Of different material systems used to realize memristive devices, oxide based devices are close to a commercial deployment. Among other genres, a lot of research effort has also been put in organic memristors because of their nonstochastic and more uniform switching, as well as their cheap fabrication cost. However, emergence of organic memristors has been hindered by poor reproducibility, endurance stability scalability and low switching speed. Knowing the primary driving mechanism at the molecular scale will be the key to improve the robustness and reliability of such organic based devices. Deterministic tracking of molecular mechanisms necessitates nanoscale in-situ spectroscopy in tandem with nanoscopic current measurement that can correlate molecular changes with the current response. Such a measurement remains long awaited yet elusive. The article by Goswami et.al., in Advanced Materials achieves this using a concurrent cAFM and TERS measurement [1].

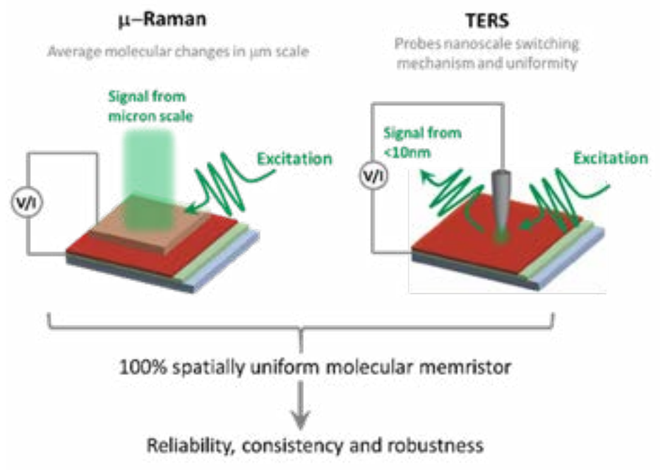

Figure 1: From microscale to molecular scale.

Potential/Input from technique

TERS has emerged as a powerful analytical technique providing high chemical sensitivity for surface molecular mapping with nanoscale spatial resolution. In operando TERS and concurrent conductive AFM will allow characterization of the chemical fingerprints of the molecular switching mechanism: As voltage across the memristive layer between the AFM tip and a bottom conductive layer is applied, Raman spectra are acquired and plasmonic enhancement permits nanoresolution at the contact point of the tip. In addition, µRaman comes in play to confirm the switching mechanism up to the microscale.

NEXT »

c-AFM and in operando TERS & µRaman characterization of molecular switching in organic memristors

Starting point, what is known?

A device based on a ruthenium complex with an azo-aromatic ligand has been reported as giving great performance: Stable (tested over hundreds of devices), enduring (≈10^{12} write/erase cycles), fast (<30 ns), and ultralow energy (≈1.5 fJ) memristive switching properties [2-5]. Its switching mechanism has been studied using in situ µRaman and UV-vis spectroscopies. The role of the ligand in the molecular redox transition has been determined and confirmed by quantum chemical calculations. As schematically depicted in Figure 1, chemical fingerprints obtained in µRaman will be compared with the molecular changes probed by in operando TERS to establish areal switching uniformity [1].

Description of sample and measurement

The memristive organic layers are prepared from solutions of the two precursor azo-aromatic complexes in acetonitrile (Figure 2): (i) system-A, $[Ru(L_1)_3](PF_6)_2$ (L_1 = 2(phenylazo)pyridine) and (ii) system-B, $[Ru(L_2)_2](PF_6)_2$ (L_2 = 2,6-bis(phenylazo)pyridine). The test devices comprise a layer of these materials off-centered spin-coated (thickness ≈15-70 nm) on an epitaxial indium tin oxide (ITO) film of ≈60 nm thickness grown via pulsed laser deposition (PLD) on an annealed yttria-stabilised zirconia (YSZ) substrate. The ITO thin film serves as the bottom electrode and the conductive c-AFM/TERS tip as the top electrode. The use of an atomically flat ITO bottom electrode (RMS roughness of ≈0.5 nm over 25 × 25 µm²) facilitates the formation of an ultrasmooth spin-coated film with RMS roughness ≈1.5 nm over 25 × 25 µm². After deposition, the samples were stored inside a vacuum chamber with a pressure of about 10^{-8} Torr for 12 h.

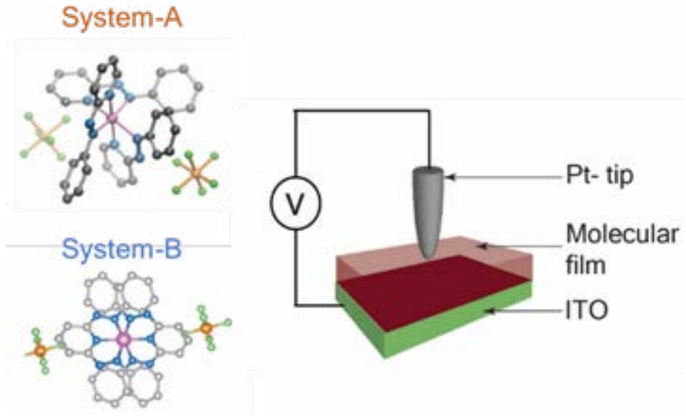

Figure 2: Left: Azo-aromatic molecules of system-A: $[Ru(L_1)_3](PF_6)_2$ (L_1 = 2(phenylazo)pyridine) and system-B:, $[Ru(L_2)_2](PF_6)2$ (L_2 = 2,6-bis(phenylazo)pyridine), Right: schematic diagram of the test device.

TERS measurements were performed using a NanoRaman system from HORIBA Scientific integrating an atomic force microscope (OmegaScope, based on SmartSPM) and a Raman microscope (XploRA) with a 100× WD objective tilted by 60° with respect to the sample plane. A 638 nm p-polarized laser (80 µW) was focused onto the cantilever-based gold coated AFM-TERS tip (OMNI TERS-SNC-Au, App Nano). This probe was conductive and thereby suitable to apply a voltage and acquire Raman spectra at any voltage. After recording an AFM topography image in AC mode (2 × 2 µm²), the tip was positioned on a spot of interest, potential voltage was applied on the tip, and a Raman spectrum was acquired for 50 s with the tip in contact with sample surface with a typical interaction of 2–10 nN. It had been checked that the spectrum acquired with the tip few nm away from the sample, which is the far-field or µRaman contribution, was background spectrum without Raman signature. As a result, the "in contact" spectrum was pure near-field contribution generated from the nanoregion under the tip.

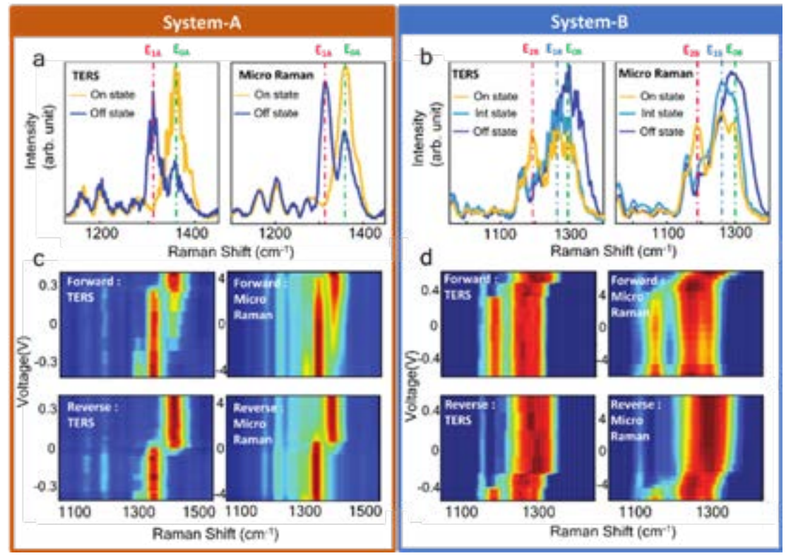

Figure 3: (a) System-A: TER (left) and µRaman (right) spectra measured in operando for two states (b) System-B: TER (left) and µRaman (right) spectra measured in operando for three conductance states. (c) and (d) Intensity color plots of spectral voltage dependence in TERS (left) and µRaman (right) of system-A and system-B for forward (top) and reverse (bottom) voltage sweeps.

Figure 3 compares the Raman spectra obtained in µRaman and in TERS for both systems A and B in their ON and OFF states and also in the intermediate state for system B. In both scale Raman spectroscopies, the changes in the azo-stretching modes are identical. The molecular redox process induces spectral weight transfer, from a dominant E_{0A} (unreduced) mode in the ON state to a dominant E_{1A} (singly reduced ligand) in the OFF state in the reduction process for system-A (Figure 3b).

« PREVIOUS

NEXT »

c-AFM and in operando TERS & µRaman characterization of molecular switching in organic memristors

For system-B, the Raman spectrum features a higher E_{2B} (triply reduced ligand state) mode in the ON state, higher E_{1B} (singly reduced ligand state) in the intermediate state and dominant E_{0B} (unreduced ligand state) in the OFF state (Figure 3c). The plots featuring color coded intensity µRaman and TERS spectra collected for voltages from -0.3 V to +0.3 V (forward sweep) and from +0.3 V to -0.3 V also indicate the very close voltage dependence behavior for both devices A & B at the micro and nanoscales. Another way to show the areal uniformity of the switching mechanism is to record TERS maps and monitor intensity of characteristic ON/Intermediate/OFF state Raman bands. Figures 4b and 4c show the variation of intensity in the range of 1330-1400 cm^{-1} for device A for scan area of 2 × 2 μm^2 (pixel size = 50 nm) and 200 × 200 nm^2 (pixel size = 7 nm), respectively in both ON and OFF conductance states of device A. Standard deviations (A(2σ)/Amean) in the spectral distributions in all states are <10%. In Figures 4d–f, we show uniform TERS response for device B. The integration spectral range is 1250–1380 cm^{-1} and the spectral weights in different states (i.e., OFF, intermediate and ON) are different but spatially uniform for each conductance state.

Conclusion and perspectives

This note shows how TERS mapping realized in operando in a memristive device brings the key demonstration of the homogeneity of the molecular redox transition mechanism between conductance states with a sub-10 nm spatial resolution. With the complementary µRaman study a uniform 100% switching of an entire device area has been proved. Knowing that the molecular switching process scales from nanoscale to macroscale is a significant and long awaited achievement in organic memristors and molecular resistance switches. This paves the way for robust devices and implementation in ultralow energy digital electronics. This in operando characterization method could be applied to a wide variety of molecule-enabled electronic devices and systems, such as molecular diodes, organic light emitters, and collectors.

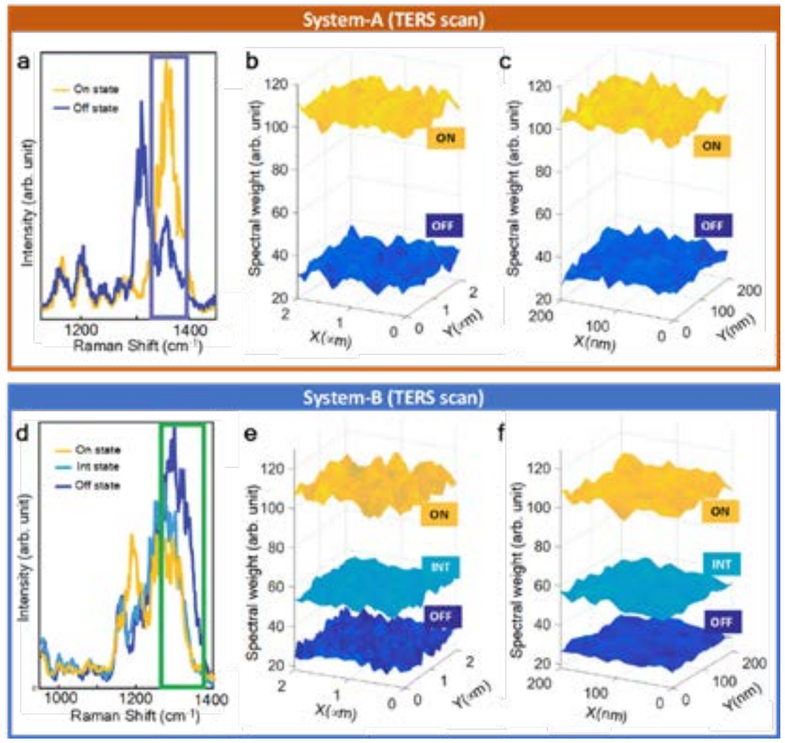

Figure 4: Areal uniformity in TERS mapping: a) In situ TER spectra measured in ON and OFF states of system-A. The blue frame in spectra (a) represents the range (1320–1400 cm^{-1}) integrated in the TERS maps presented in panels (b) and (c). b) A 2 × 2 μm^2 TERS map in the ON and OFF states. c) A 200 × 200 nm^2 TERS map of ON and OFF states with the same spectral range as in (b). d–f) Same as (a)–(c) for the three states of system-B.

References

1. S. Goswami, D. Deb, A. Tempez, M. Chaigneau, S. Prasad Rath, M. Lal, A. R. Stanley Williams, S. Goswami, T. Venkatesan, Adv. Mat., 2020, 2004370
2. S. Goswami, A. J. Matula, S. P. Rath, S. Hedström, S. Saha, M. Annamalai, D. Sengupta, A. Patra, S. Ghosh, H. Jani, Nat. Mater. 2017, 16, 1216.
3. S. Goswami, S. P. Rath, D. Thompson, S. Hedström, M. Annamalai, R. Pramanick, B. R. Ilic, S. Sarkar, S. Hooda, C. A. Nijhuis, J. Martin, R. S. Williams, S. Goswami, T Venkatesan, Nat. Nanotechnol. 2020, 15, 380
4. Goswami, S., Thompson, D., Williams, R. S., Goswami, S., & Venkatesan, T. (2020). Colossal current and voltage tunability in an organic memristor via electrode engineering. Applied Materials Today, 19, 100626.
5. Goswami, Sreetosh, Sreebrata Goswami, and T. Venkatesan. “An organic approach to low energy memory and brain inspired electronics.” Applied Physics Reviews 7.2 (2020): 021303.

« *PREVIOUS*

Home Introduction Stories Scientific Papers Applications Multimedia Contact

Multimedia

Webinars:

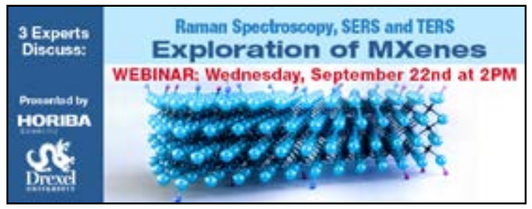

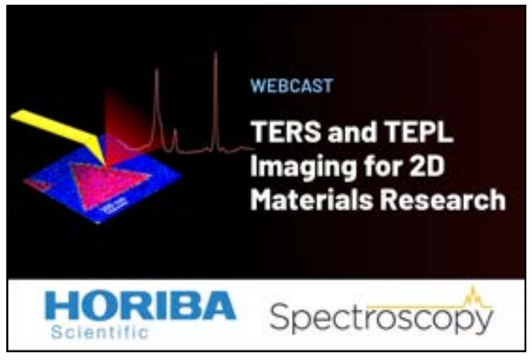

Video:

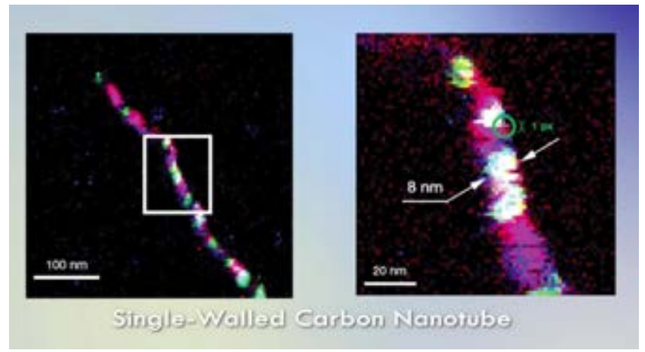

Find out about the power of our AFM/TERS solution for nanoscale chemical imaging.

Contact

horiba.com/scientific